4-20-2018 9:30 AM

Mechanical Characterization and Shear Test Comparison for Continuous-Fiber Polymer Composites

Matthew Crossan, *The University of Western Ontario*

Supervisor: Wood, Jeffrey T., *The University of Western Ontario*

A thesis submitted in partial fulfillment of the requirements for the Master of Engineering Science degree in Mechanical and Materials Engineering

Abstract

As fiber-reinforced composites continue to be used in a wide-range of high performance structures, more detailed understanding and accurate prediction of stress-strain behaviour is necessary to improving designs and reducing costs. This thesis compares the experimental behaviour of a continuous fiber polymer composite of carbon fiber and epoxy resin using Digital Image Correlation to analytical and theoretical predictions. Furthermore, an in-depth analysis of shear testing methods reveals the advantages and limitations of different testing standards. Finally, the limitations of the Iosipescu Shear test (ASTM 5379) fixture to break high-strain-to-failure composites in comparison to the V-notched Rail Shear Fixture (ASTM 7078) is conclusively shown.

Keywords

Carbon Fiber; Composite Laminate Theory; Digital Image Correlation; Epoxy Resin; Finite Element Analysis; Iosipescu Shear; Shear Testing of Continuous Fiber Composites; V-Notched Rail Shear

Acknowledgments

To Prof. Jeff Wood, for his wisdom and guidance

To Ying Fan, for her continuous support

To Prof. Takashi Kuboki for providing his insights from new perspectives

To the University Machine Services for, their support in fabricating the modified V-Notched Rail Shear fixture and help machining the test specimen

To Chris Vandelaar, for his time and instruction on how to best machine composite test specimens

To Ian Swentek, for his initial help in setting up the Digital Image Correlation system

To Yuchao Liu, for his help in a range of testing

To the Western Formula Racing Team, for their donation of carbon fiber and consumables for fabrication of the test specimens

Table of Contents

List of Tables

List of Figures

List of Appendices

Chapter 1

1 Introduction

Composite materials are becoming increasingly more prevalent because of their high specific strength and stiffness properties which allow for better lightweight solutions. The aerospace and automotive industries are particularly interested in composites as a light-weighting solution to improve fuel economy and reduce emissions. By embedding high strength fibers in a matrix, materials with high anisotropy can be made which outperform isotropic materials.

These non-homogenous, anisotropic materials however, provide a challenge when designing structures since it is more difficult to predict the stresses and strains present within the structure. There are many different standardized tests to characterize the properties of composite materials which are defined by the ASTM International. The most common tests needed to provide a material data card are tension, compression, and shear testing.

Both tension and compression tests are well understood and provide very agreeable results with theoretical models. However, obtaining inter-laminar shear properties are much more difficult and there is less agreement as to which type of test is the best. This lack of agreement is evident by the fact that there are eight different ASTM standards for shear testing as well as about six other non-ASTM standard tests in common use which all attempt to solve different problems faced when shear testing.

Properties of fiber reinforced composites also depend heavily on the method of manufacturing, especially when the final product differs from the design due to manufacturing deviations. Often, this means that a designer cannot rely on calculations or computer models, so a great amount of physical testing is needed to quantify the physical properties of the material or structure.

Moving towards more virtual testing can decrease both cost and design time to produce cheaper, higher volume parts often with improved performance. This is because designs do not have to be as conservative when there are fewer unknown variables. As computer models get closer to simulating real-world tests, the amount of mechanical testing can be reduced. This requires a more precise and complete analysis and understanding of the physical phenomenon taking place in the material being tested.

This study's aim was to better understand how a composite material responds to mechanical testing and then replicate these phenomena in virtual simulations. Specifically, it was determined that the Iosipescu Shear test method (ASTM D 5379) could not bring high-strength composite materials to failure since materials would strain too much and hit the fixture limits before breaking. An alternative testing method, the V-Notched Rail Shear test (ASTM D 7078), was investigated and the methodology was validated using our own materials, and measurement systems. Finite element models were also created to replicate and validate data provided by the ASTM standard's supplementary documentation. These models were then used for further development and understanding of the shear test method and deformation mechanisms.

Outline of Thesis

This thesis is divided into five chapters and follows the monograph format.

Chapter two starts with a broad description of the roles of composites in industry and general mechanical properties. The chapter then further describes the specific materials used in this study along with critical reviews of research relevant to determining the mechanical properties of continuous fiber carbon-epoxy composites, especially in shear. This is examined through various analytical, experimental, and numerical analysis.

Chapter three outlines the methods used in both the physical and numerical analysis including material preparation, tool manufacturing, sensor calibration, and physical setup. The first round of mechanical testing produces a material property card for two layup types. The second round of physical testing compares and characterizes shear properties obtained through two different experimental standards.

Chapter four summarizes the obtained data. Postprocessing analysis was done in Microsoft Excel to compare mechanical properties to theoretical values as well as between test methods. Finally, possible sources of error were investigated and the impact of these errors on the results was included.

Chapter five summarizes the findings throughout the paper and relates these findings back to the overarching purpose of this thesis. Furthermore, Chapter five identifies areas where this study could be improved, and proposes other studies which could expand on this work.

Chapter 2

2 Literature Review

This chapter provides an overview of composites, why they are an attractive material for light-weighting solutions and how they are classified. It then focuses on continuous fiber reinforced polymer arrangements consisting of carbon fiber reinforcements embedded in an epoxy resin matrix. Next a review of existing literature will outline techniques for characterizing the mechanical properties of fiber-reinforced composites. The three areas of focus are:

1. Analytical
2. Numerical
3. Experimental

Analytical methods for determining mechanical properties include classical laminate theory (CLT), experimental methods include ASTM standardized testing, and numerical methods include Finite Element Modelling (FEM). While examining literature on physical testing methods, various measurement techniques are briefly reviewed. Finally, the review will conclude by defining the opportunity seen and describe the importance of this thesis.

2.1 Composites

By definition, “[a] composite is a material made from two or more constituent materials with significantly different physical or chemical properties that, when combined, produce

a material with characteristics different from the individual components. The individual components remain separate and distinct within the finished structure" (Reviews, 2016). Composites have been an attractive area of research and development largely because of the high specific strength and specific stiffness properties, as can be seen in the material bubble plots of Figure 2.1 below.

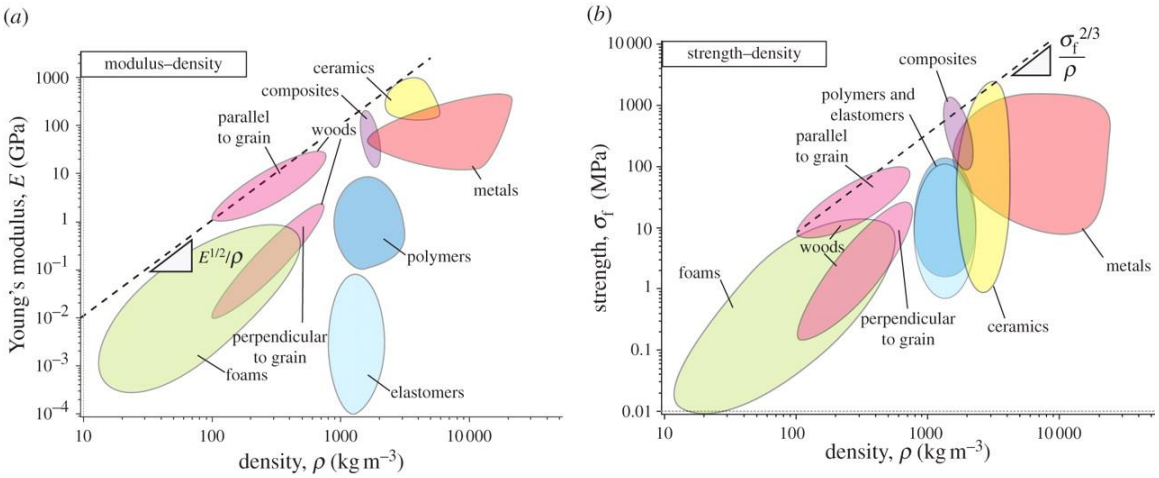

Figure 2.1 - Stiffness vs. Density and Strength vs. Density Material Plots (Gibson, 2012)

Composites usually consist of a reinforcement embedded in a matrix. The reinforcement is usually a strong, stiff material that bears the load in a structural application. While the purpose of the matrix is to evenly distribute and transfer load to the reinforcement as well as to retain the shape of the composite material and protect the reinforcement from environmental damage.

There are three main matrix material classifications of composites:

1) Polymer Matrix Composites (PMCs)
2) Metal Matrix Composites (MMCs)
3) Ceramic Matrix Composites (CMCs)

This study exclusively discusses Polymer Matrix Composites, specifically composites consisting of an epoxy resin matrix, because of their high performance as an adhesive over a wide range of objectives such as strength and durability (STAFF, 2015).

There are also different types of reinforcements which can be embedded in any of these matrices. A breakdown of the classification for the types of reinforcement can be seen in Figure 2.2. The specific types of reinforcement considered in this study are the Continuous Fiber Reinforcements with either woven or non-woven Fabrics. The specific material chosen is carbon fiber, which is further classified as a synthetic fiber. Synthetic fibres are created using chemical synthesis to specifically tailor the mechanical properties of the material, (Gorss, 2003).

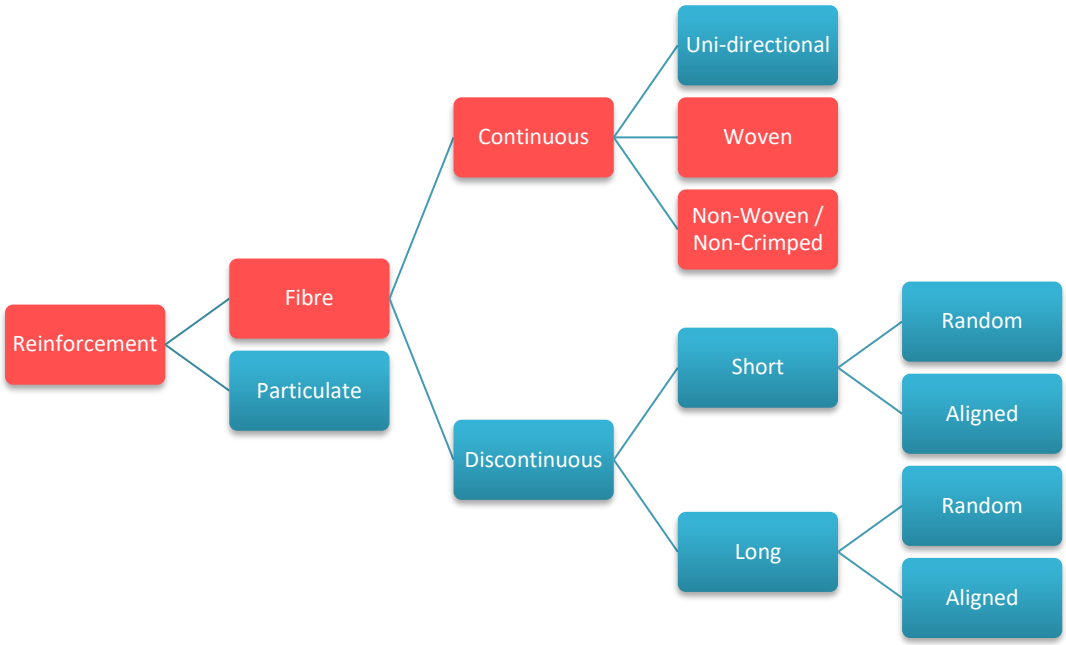

Figure 2.2 - Reinforcement Classification of Composite Materials

Continuous vs Discontinuous Fibres

Before discussing the properties of continuous carbon fiber reinforced polymers (CFRPs), it is important to understand the distinction between continuous and discontinuous fibres as well as fiber configuration. Fibres can either be; continuous or discontinuous, and randomly oriented or aligned, as shown in Figure 2.3. The longer a fibre is, the better it transfers load. Therefore, the better the mechanical properties of stiffness, strength, and toughness. The more aligned the fibres are, the more anisotropic the material becomes. This can be advantageous in some situations, whereas in other situations requiring more isotropic properties, a randomly oriented configuration may be more appropriate. The drawback to long fibers is they are difficult to process during manufacturing, or have poor processability. The trade-off is shown in Figure 2.4.

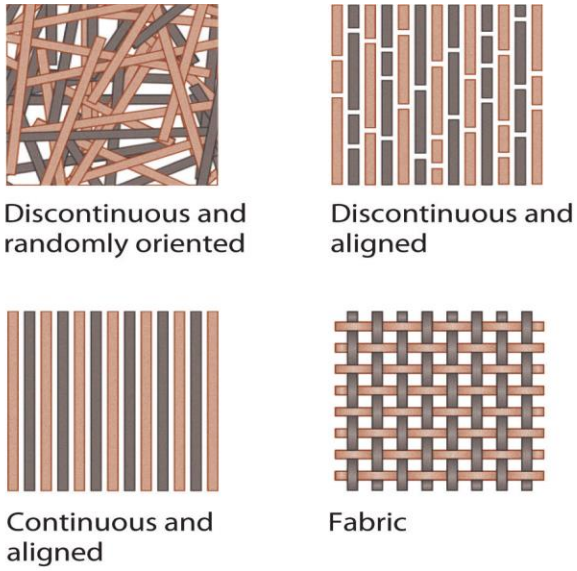

Figure 2.3 - Classifications of Fibre Reinforcements (Howard University, 2017)

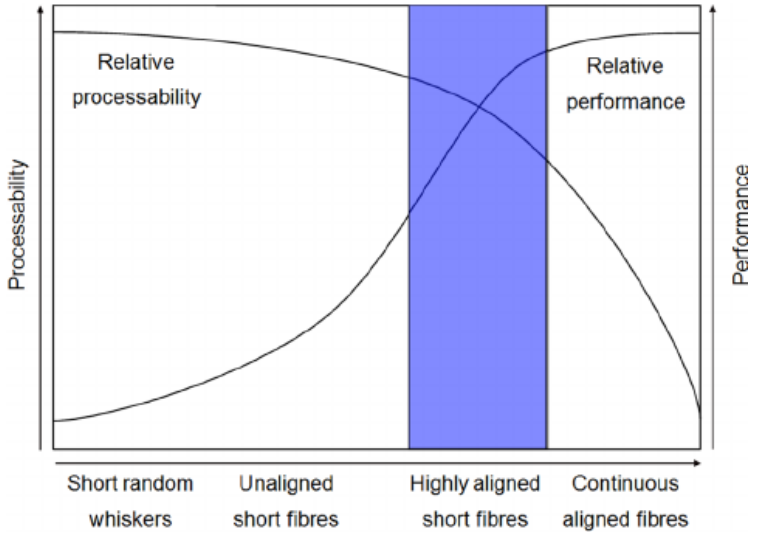

Figure 2.4 - Processability and Performance vs Fibre Length and Orientation (Such, Ward, & Potter, 2014)

2.2 Mechanical Properties of Continuous, Carbon Fiber Reinforced Polymer (CFRP) Composites

This study is constrained to studying continuous Carbon Fiber Reinforced Polymers (CFRPs). The polymer in the following pages is epoxy resin unless otherwise stated specifically. A chart of the expected material properties of the constituent materials and composite are outlined in Table 2.1. Composite properties were estimated using a 50% volume fraction of fibres and the rule of mixtures method to define properties in the axial (fibre) direction for reference.

Table 2.1 - Approximate Properties of Epoxy Resin (Hexion, 2017), Carbon Fiber (Toray Group) and 50%vf CFRP

	Epoxy resin	Carbon fiber	CFRP (50% vf)
Young's modulus [GPa]	3.0	240	121.5
Strength [GPa]	0.065	4.2	2.1
Density [g/cm^3]	1.15	1.8	1.475

There are various analytical models for predicting the mechanical properties of composites. Figure 2.5 shows an example comparison of experimental data of two models for predicting stiffness (E) in long/continuous fiber reinforced polymers. For stiffness in the axial directions (E_1), analytical models can give accurate predictions for experimental data in certain circumstances, and transverse stiffness

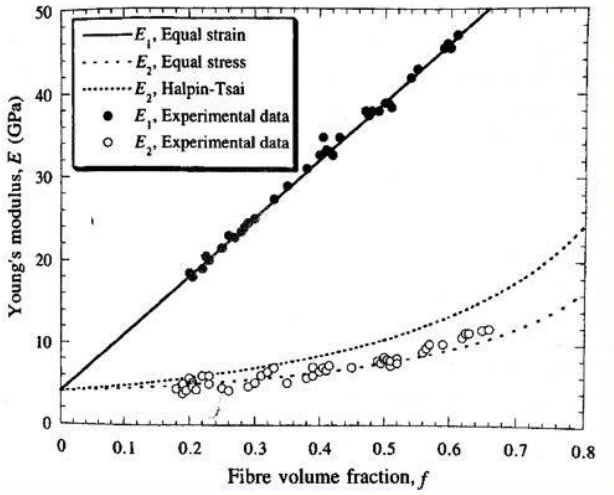

Figure 2.5 - Stiffness models vs. experimental data in the axial (1) and transverse (2) directions for a CFRP (Hull & Clyne, 1996)

(E_2) can be accurate as well. Conversely, this study will show that some properties (such as shear stiffness) are much more difficult to predict. Often with composites it is necessary to characterize the material properties through physical testing to generate a material property card. These material property cards are then given to the designer who makes design decisions based on the obtained material properties. Therefore, it is very important that the designer receives data that accurately reflects the physical phenomenon which occurred during a physical test.

2.3 Analytical Methods

Analytical methods aim to provide material property predictions through standard equations involving the properties of the constituent materials, as well as manufacturing characteristics such as fiber volume fraction. Occasionally, these analytical predictions deviate from empirical data. Therefore, predictions are sometimes used either as an upper or lower bound, or involve other "fitting" parameters to better align with observed phenomenon.

What follows is a description of the current analytical methods used to describe the physical properties of a long fiber composite laminate. The description will include predictive equations for measuring the modulus and strength for tensile, compressive, and shear properties of long fiber composites.

The following topics will be covered:

1. Elastic deformation of long fiber composites (laminae)
2. Elastic deformation of laminates (including off-axis loading)
3. Strength of composites (including failure criterion)

A majority of the review will sample the book, "An Introduction to Composite Materials" (Hull & Clyne, 1996) with supplementary research when necessary.

2.3.1 Elastic Deformation of Long Fiber Composites

This section will describe the characteristic equations for the elastic properties of long fiber composites with all the fibers in the same direction. The equations in Chapter 2.3 assume there is perfect bonding at the interface between the fiber and the surrounding matrix.

Axial Stiffness

The equation for describing axial stiffness is based on the Voigt model. The model describes that both the fiber and matrix undergo equal strain, with the provision that there is no sliding at the interface, since there is perfect bonding. This is modelled in Figure 2.6 and can be written as:

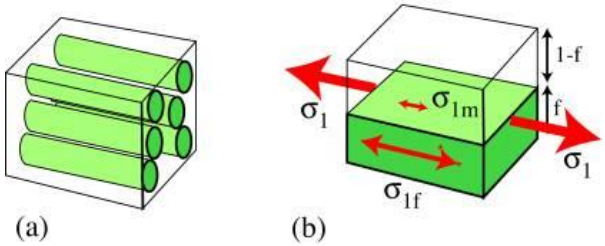

Figure 2.6 – Fibre (a) vs Slab (b) model for equal strain under axial loading (University of Cambridge, 2008)

$$\varepsilon_1 = \varepsilon_{1f} = \frac{\sigma_{1f}}{E_f} = \varepsilon_{1m} = \frac{\sigma_{1m}}{E_m}$$

For the general case where the fibers are much stiffer than the matrix, they will be subject to much higher stresses where:

$$\sigma_1 = (1-f)\sigma_{1m} + f\sigma_{1f}$$

The above equation simplifies to describe what is known as the “Rule of Mixtures”:

$$E_1 = (1-f)E_m + fE_f$$

The composite’s stiffness in the axial direction is therefore a weighted mean between the Young’s moduli of the constituent material based only on the volume fraction of fibers in the overall composite. Very minor deviations can occur if the Poisson’s ratios of the two materials differ significantly as stresses will develop in the transverse direction at different rates.

Transverse Stiffness:

In the transverse direction, theoretical and empirical values are more difficult to obtain. The common method of determining transverse stiffness is the "Slab model", as shown in Figure 2.7. The model describes equal stresses in the constituent materials as follows:

$$\sigma_2 = \sigma_{2f} = \varepsilon_{2f}E_f = \sigma_{2m} = \varepsilon_{2m}E_m$$

$$\varepsilon_2 = f\varepsilon_{2f} + (1-f)\varepsilon_{2m}$$

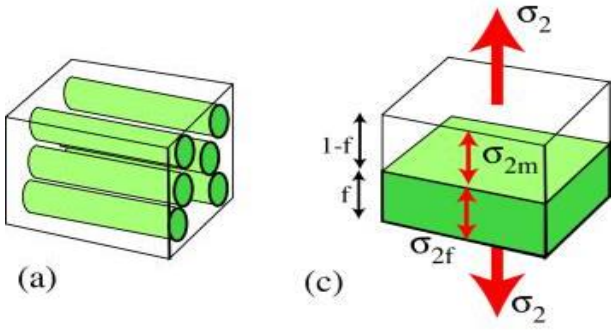

Figure 2.7 – Fibre (a) vs Slab (c) model for equal stress under transverse loading (University of Cambridge, 2008)

By representing the above two equations in terms of the Young's modulus, we get the following equation, often referred to as the "Reuss Model":

$$E_2 = \left[\frac{1}{E_f} + \frac{(1-f)}{E_m}\right]^{-1}$$

This model however is a poor approximation as the matrix can creep under even small loads, taking more stress. In addition, stress concentrations can occur when the "slab" is represented instead by fibers to more accurately represent a physical specimen. Figure 2.8 and Figure 2.9 show these stress concentrations around the fiber perimeter more clearly. Stress concentrations mean that a material is more likely to fail earlier than expected.

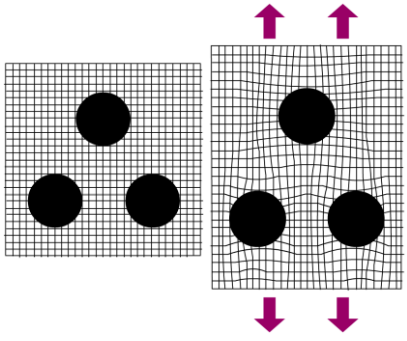

Figure 2.8 – Stress concentrations around fibers when loaded transversely (Hull & Clyne, 1996)

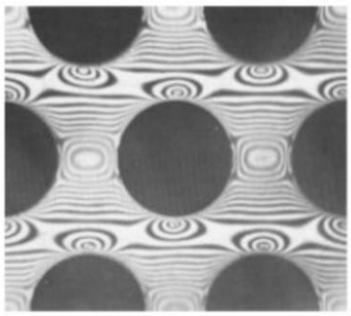

Figure 2.9 – Stress concentrations visible under transverse loading - photoelastic material (Hull & Clyne, 1996)

This means that the Reuss model underestimates the stiffness of the material and so provides a lower-bound estimate. Figure 2.5 shows how the Equal stress model can under-predict experimental data depending on factors such as fiber volume fraction and fiber aspect ratio. To more accurately describe the material, an equation developed by Halpin and Tsai (1967) was proposed, which is based on semi-empirical evidence:

$$\eta = \frac{\left(\frac{E_f}{E_m} - 1\right)}{\left(\frac{E_f}{E_m} + \xi\right)}, \text{where } \xi \sim 1$$

$$E_2 = \frac{E_m(1 + \xi\eta f)}{(1 - \eta f)},$$

A third model for the elastic deformation of long fibre composites is the Eshelby inclusion. It is based off a thought experiment from Eshelby in the 1950's (Hull & Clyne, 1996, p. 121). The model involves constraining an ellipsoid inclusion into an infinitely sized matrix. However, it can be seen graphically in Figure 2.11 that the Halpin Tsai and Eshelby methods produce nearly identical results. For these analyses, it is not necessary to use the more complex Eshelby method for the prediction of elastic deformation of long-fibre composites.

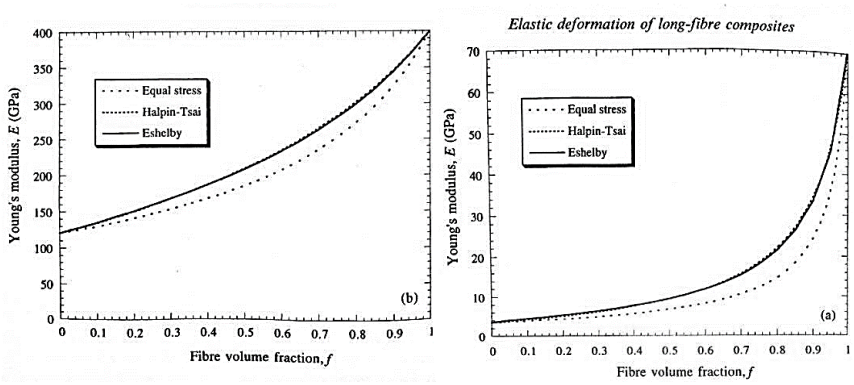

Figure 2.10 - Comparison of Eshelby Inclusion to the Equal Stress and Halpin Tsai methods (Hull & Clyne, 1996)

Shear Stiffness

Shear stiffness predictions can also be made using the slab model and an equal shear stress method. It is important to note that the equalities in the actual model are not the same as the equalities in the slab model as shown in Figure 2.12.

Since the 2 and 3 directions are equivalent, the following relationships are observed:

$$G_{12} = G_{21} = G_{13} = G_{31} \neq G_{23} = G_{32}$$

$$\tau_{12} = \tau_{12f} = \gamma_{12f} G_f = \tau_{12m} = \gamma_{12m} G_m$$

By summing the contribution of the constituent shear properties to the shear displacement (Equal Stress), the following equations result:

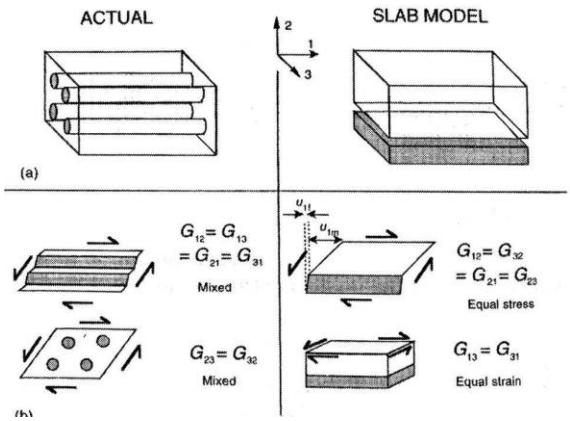

Figure 2.11 - Comparison of actual vs slab models in shear (Hull & Clyne, 1996)

$$\gamma_{12} = f\gamma_{12f} + (1-f)\gamma_{12m}$$

$$G_{12} = \left[\frac{1}{G_f} + \frac{(1-f)}{G_m}\right]^{-1}$$

The above equation may be a significant underestimation for the 12 direction. Alternatively, for the 13 direction, the following equation results from an equal strain condition like for axial tension:

$$G_{13} = fG_f + (1-f)G_m$$

This may be an overestimate because of fiber interaction. Therefore, Halpin and Tsai further developed another semi-empirical expression to describe the shear properties in the 12 direction with respect to volume fraction:

$$G_{12} = \frac{G_m(1+\xi\eta f)}{(1-\eta f)}$$

$$\eta = \frac{\left(\frac{G_f}{G_m} - 1\right)}{\left(\frac{G_f}{G_m} + \xi\right)}, where\ \xi \sim 1$$

For a composite with a 40% volume fraction of fibres, G_f of 10 [GPa] an G_m of 1.2 [GPa] (similar to the properties of materials used in this study), the differences in the above three calculations can be seen in real terms in Table 2.2:

Table 2.2 – Results from different methods for calculating shear stress of a long-fiber composite:

Equal Stress	1.85	GPa
Equal Strain	4.72	GPa
Halpin Tsai	2.3	GPa

For the case of glass fibres in epoxy, the shear modulus is very close to the shear modulus of neat epoxy until larger volume fractions. In contrast, for Silicon Carbide fibres in Titanium, the shear modulus diverges further from the matrix modulus with the addition of reinforcement. Both trends are shown in Figure 2.12

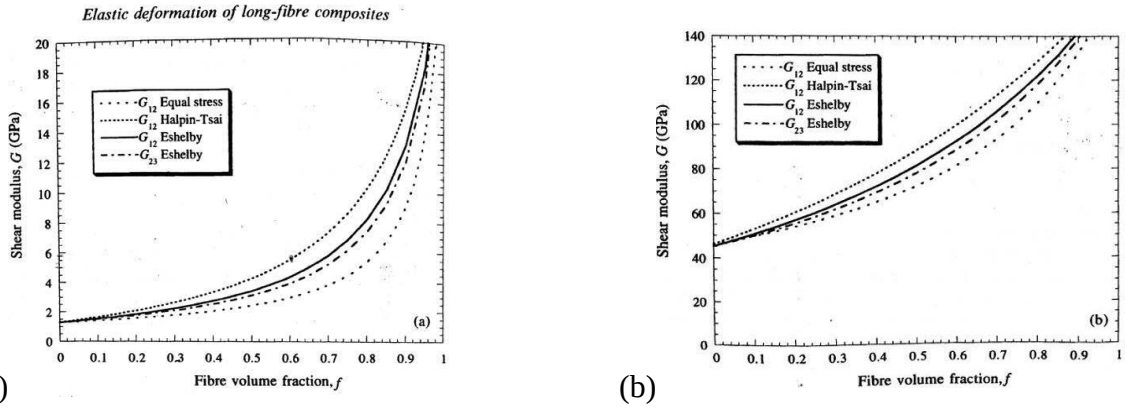

Figure 2.12 - Comparison of analytical models for predicting the shear modulus of long-fiber composites vs fiber volume fraction for (a) Glass Fiber-Epoxy and (b) Silicon Carbide-Titanium composites (Hull & Clyne, 1996)

Poisson's Ratio

Poisson's ratio describes the ratio of the change in transverse strain to the axial strain relative to the load: $v_{ij} = -e_j/e_i$. Inter-relationships can be seen in Figure 2.13, where

$v_{12}=v_{13}$, $v_{21}=v_{31}$ and $v_{23}=v_{32}$.

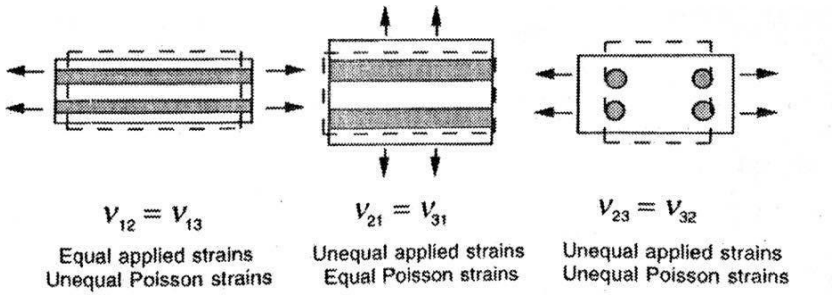

Figure 2.13 - Relationship between Poisson's ratios (Hull & Clyne, 1996)

Therefore, there are only 3 unique Poisson's ratios. The first, $v_{12}=v_{13}$ can be defined using the equal strain criteria and represented by a rule of mixtures:

$$v_{12} = fv_f + (1-f)v_m$$

Additionally, the reciprocal can be true for v_{21},

$$v_{21} = \left[fv_f + (1-f)v_m\right]\frac{E_2}{E_1}$$

The value for v_{21} is smaller than for v_{12} because the fibres do not contract much when subjected to a transverse tensile stress. This information can be used to calculate v_{23}, which is then defined by the change in the materials volume:

$$\Delta = \epsilon_1+\epsilon_1+\epsilon_1 = \frac{\sigma_H}{K}, \qquad where\ K\ is\ the\ bulk\ modulus$$

Which by further inspection describes v_{23} as,

$$v_{23} = 1 - v_{21} - \frac{E_2}{3K}, \qquad where\ K_f = \frac{E_f}{3(1-2v_f)}$$

Graphically, when plotted against fibre volume fraction, the Poisson's ratio curves take the shapes seen in Figure 2.14

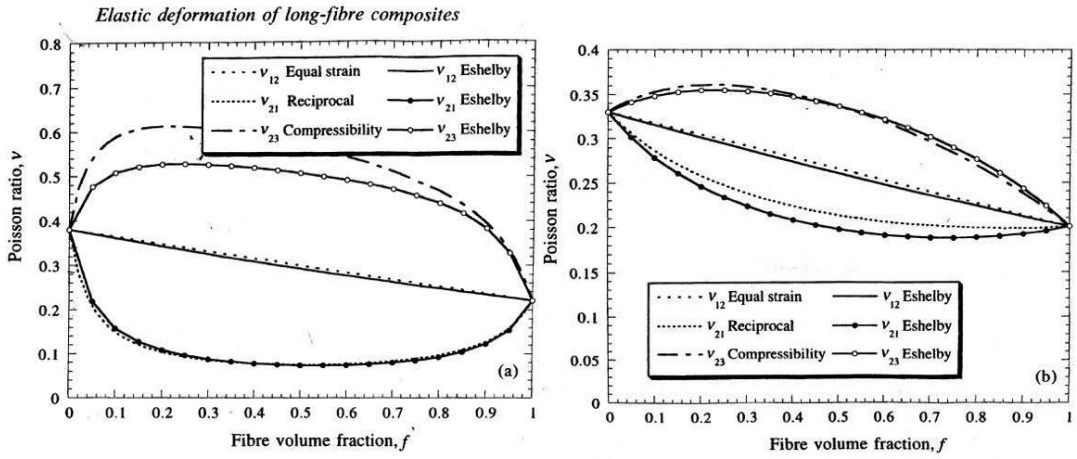

Figure 2.14 - Comparison of various models for predicting Poisson's ratio vs fiber volume fraction (Hull & Clyne, 1996)

2.3.2 Elastic Deformation of Laminates

With the knowledge that a lamina of continuous fibers are anisotropic in that they are stiff in its axial direction but not very stiff transversely, it is often necessary to stack laminae in various orientations to provide material properties which behave more isotropically, or are "quasi-isotropic". Figure 2.16 shows change in tensile strength with increasing fiber orientation angles. At a 45-degree load angle, the tensile strength is about 25% of the 0-degree strength. Figure 2.16 shows the material properties for different layups with increasing isotropy. The [0/45/90/135] laminate shows properties that allow it to be considered "quasi-isotropic", meaning it behaves as if it were isotropic.

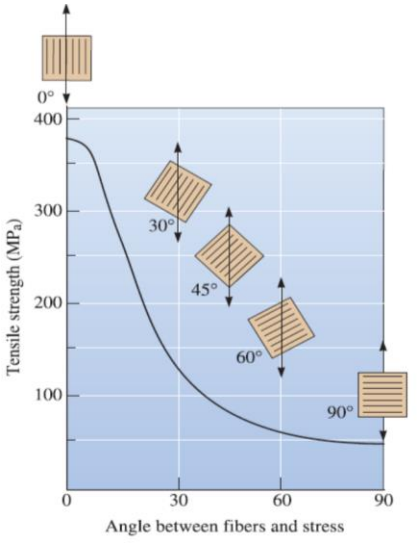

Figure 2.15- Tensile Strength vs fiber orientation angle (Hull & Clyne, 1996)

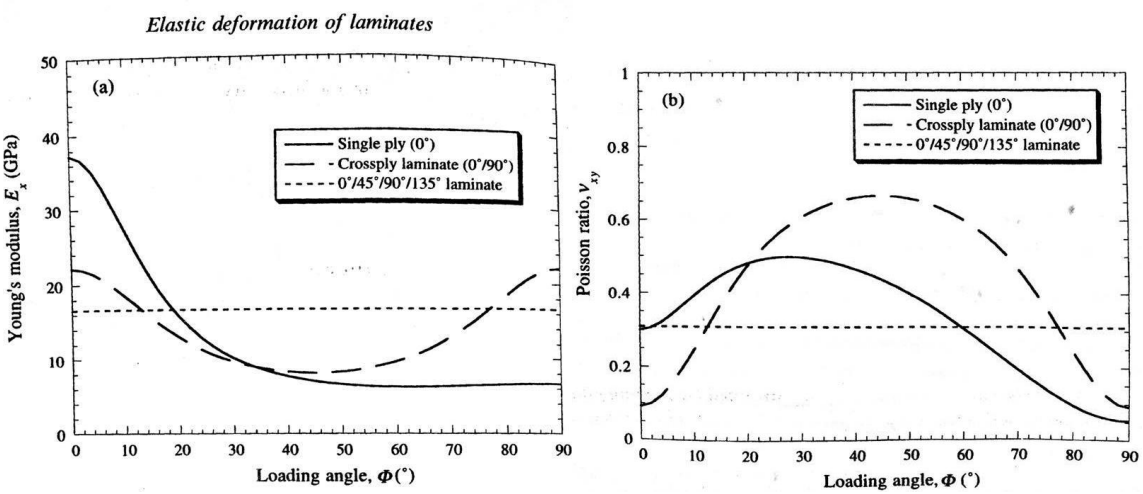

Figure 2.16 - Young's modulus and Poisson's ratio of a laminate with varying degrees of isotropy compared to loading angle (Hull & Clyne, 1996)

To determine the off-axis constants of a lamina, it is assumed that each ply is in a plane stress state, meaning there are no through thickness stresses. Each ply is transversely isotropic, and therefore has only four unique constants by which it's stress tensor can be fully defined as shown below.

$$\begin{bmatrix} \varepsilon_1 \\ \varepsilon_2 \\ \gamma_{12} \end{bmatrix} = [\,S\,] \begin{bmatrix} \sigma_1 \\ \sigma_2 \\ \tau_{12} \end{bmatrix} = \begin{bmatrix} S_{11} & S_{12} & 0 \\ S_{12} & S_{22} & 0 \\ 0 & 0 & S_{66} \end{bmatrix} \begin{bmatrix} \sigma_1 \\ \sigma_2 \\ \tau_{12} \end{bmatrix}$$

where σ_1, σ_2 and τ_{12} are the principle stresses. This results in the following independent equations in relation to the elastic constants:

$$S_{11} = \frac{1}{E_1} \qquad S_{22} = \frac{1}{E_2}$$

$$S_{12} = -\frac{\nu_{12}}{E_1} = -\frac{\nu_{21}}{E_2} \qquad S_{66} = \frac{1}{G_{12}}$$

Forces are then resolved geometrically:

$$\begin{bmatrix} \sigma_1 \\ \sigma_2 \\ \tau_{12} \end{bmatrix} = [\,T\,] \begin{bmatrix} \sigma_x \\ y \\ \tau_{xy} \end{bmatrix} \qquad \text{with:} \quad [\,T\,] = \begin{bmatrix} c^2 & s^2 & 2cs \\ s^2 & c^2 & -2cs \\ -cs & cs & c^2 - s^2 \end{bmatrix}$$

The variable c represents (cos Φ) and s represents (sin Φ) where Φ is the angle between the fiber axis (1) and the stress axis (x). Then similarly to above:

$$\begin{bmatrix} \varepsilon_x \\ \varepsilon_y \\ \gamma_{xy} \end{bmatrix} = [\,\bar{S}\,] \begin{bmatrix} \sigma_x \\ \sigma_y \\ \tau_{xy} \end{bmatrix}$$

Where:

$$\overline{S_{11}} = S_{11}c^4 + S_{22}s^4 + (2S_{12} + S_{66})c^2s^2$$

$$\overline{S_{12}} = S_{12}(c^4+s^4) + (S_{11} + S_{22} + S_{66})c^2s^2$$

$$\overline{S_{22}} = S_{11}s^4 + S_{22}c^4 + (2S_{12} + S_{66})c^2s^2$$

$$\overline{S_{12}} = (4S_{11} + 4S_{22} - 8S_{66} - 2S_{66})c^2s^2+S_{66}(c^4+s^4)$$

$$E_x = \frac{1}{\overline{S_{11}}} \qquad G_{xy} = \frac{1}{\overline{S_{66}}}$$

$$E_y = \frac{1}{\overline{S_{22}}} \qquad v_{xy} = -E_x\overline{S_{12}}, \qquad v_{yx} = -E_y\overline{S_{12}}$$

From these transformations, we can graph material properties vs load angles as shown in Figure 2.17. Of interest is the large increase in the shear modulus at the 45° load angle.

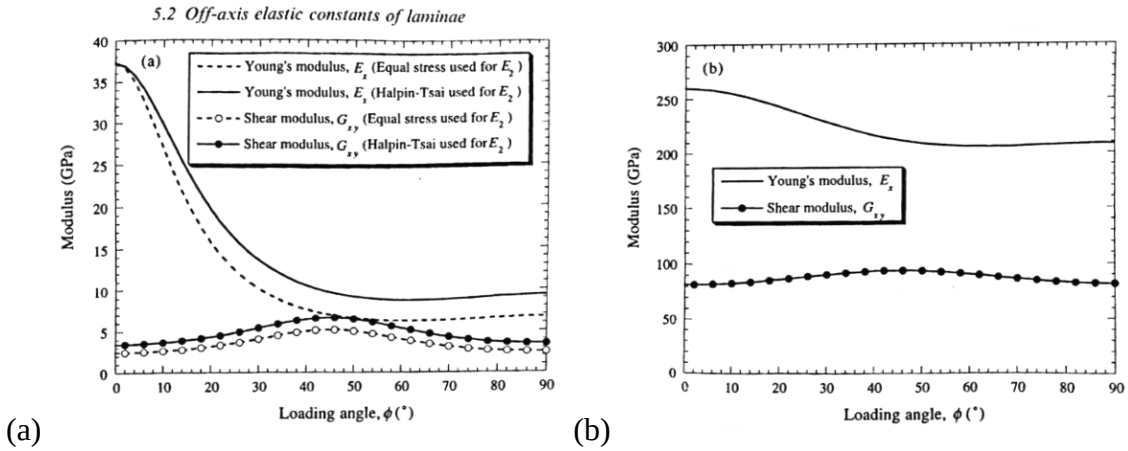

(a) (b)

Figure 2.17 - Young's and Shear Modulus vs Load angle for (a) glass fibre epoxy and (b) silicon carbide titanium composites (Hull & Clyne, 1996)

2.3.3 Strength of Composites

A composite lamina under plane stress can fail in three ways, as shown in Figure 2.18:

1. Axial Tensile Failure
2. Transverse Tensile Failure
3. Shear Failure

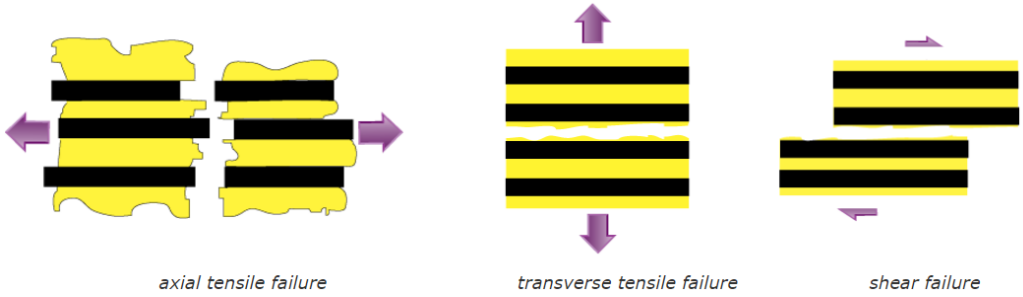

Figure 2.18 - Failure modes of long fiber composites: Axial tensile, Transverse tensile and Shear (University of Cambridge, 2008)

2.3.3.1 Axial Tensile Failure

In axial tension, it is assumed that both the fibers and matrix experience equal strain. There are two possible stress strain curves which can occur and depend on whether the fibers or matrix has a higher strain to failure. These two curves are shown in Figure 2.19

Case 1 deals with circumstances when the matrix has a lower failure strain than the fiber. Case 2 deals with circumstances when the matrix has a higher failure strain than the fiber. Case 2 is more suited to a CFRP material. Figure 2.19 shows the ideal curves for brittle materials. As seen in Figure 2.19 for case 1, if the fibres break before matrix cracking allows for full load transfer to the fibres, the axial tensile strength can be described as:

$$\sigma_{1u} = f\sigma_f \qquad \text{or} \qquad \sigma_{1u} = f\sigma_{fmu} + (1-f)\sigma_{mu},$$

A critical fibre volume fraction determines which of these two formulas should be used. A fibre volume fraction above the critical fraction means a failure strength represented by $\sigma_{1u} = f\sigma_f$. A lower fraction follows $\sigma_{1u} = f\sigma_{fmu} + (1-f)\sigma_{mu}$. The critical volume fraction is found by equating these to formulas and simplified to:

$$f' = \frac{\sigma_{mu}}{\sigma_{fu} - \sigma_{fmu} + \sigma_{mu}}$$

Similarly, for Case 2, the failure strength could be:

$$\sigma_{1u} = (1-f)\sigma_{mu} \qquad \text{or} \qquad \sigma_{1u} = f\sigma_{fu} + (1-f)\sigma_{mfu}$$

The critical fibre volume fraction determines which equation to use. A lower than critical volume fraction means the use of $\sigma_{1u} = (1-f)\sigma_{mu}$, while a higher than critical fraction means the use of $\sigma_{1u} = f\sigma_{fu} + (1-f)\sigma_{mfu}$. By equating and simplifying these two formulas the relationship for the critical fibre volume fraction is obtained:

$$f' = \frac{\sigma_{mu} - \sigma_{mfu}}{\sigma_{fu} - \sigma_{mfu} + \sigma_{mu}}$$

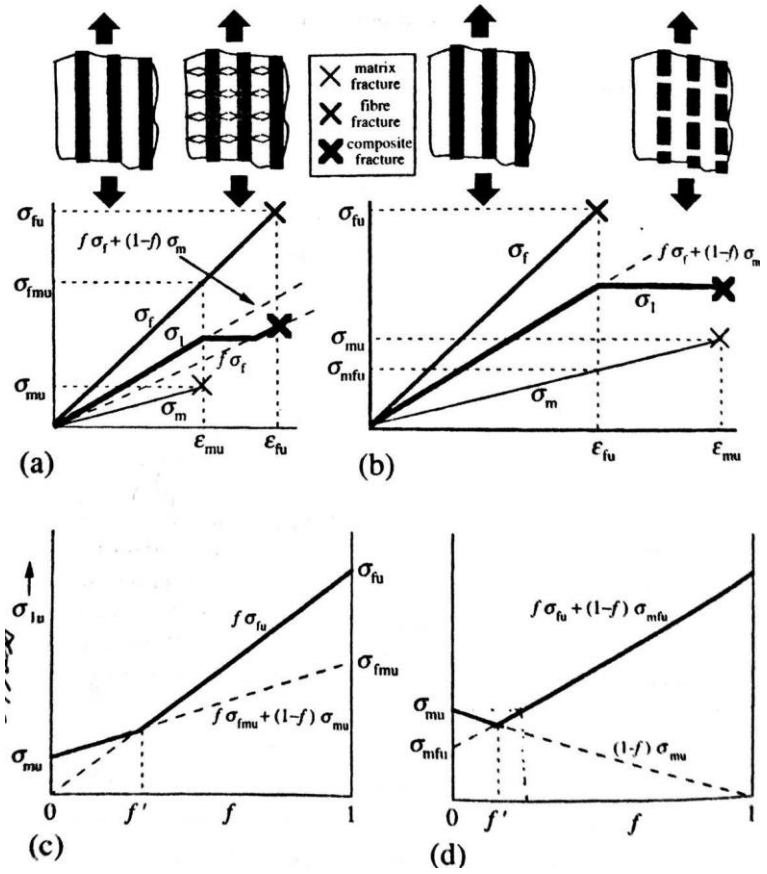

Figure 2.19 - Axial Tensile Strength of Long-Fibre composite depending on failure strain of the fiber and matrix. Case 1: (a) and (c). Case 2 (b) and (d) (Hull & Clyne, 1996)

2.3.3.2 Transverse Tensile Failure

Transverse tensile failure is very difficult to predict. It is often lower than the matrix tensile strength on its own since the fibres introduce stress concentrations and can fail at the bonded interface. The only equation to represent this value attempted to describe the phenomenon by considering the reduction in cross sectional area, due to the presence of the fibres, and represents them as holes:

$$\sigma_{2u} = \sigma_{mu}\left[1 - 2\left(\frac{f}{\pi}\right)^{0.5}\right]$$

2.3.3.3 Shear Failure

There are three pairs of possible failure orientations due to shear loading, as demonstrated in Figure 2.21. Failure in the 21 and 31 directions are not likely to occur because the fibers are much stronger than the matrix and so will not fail first. Stresses of type 32 and 23 are also non-existent in a lamina since they are the interlaminar planes, leaving only the 12 and 13 directions as possible failure modes.

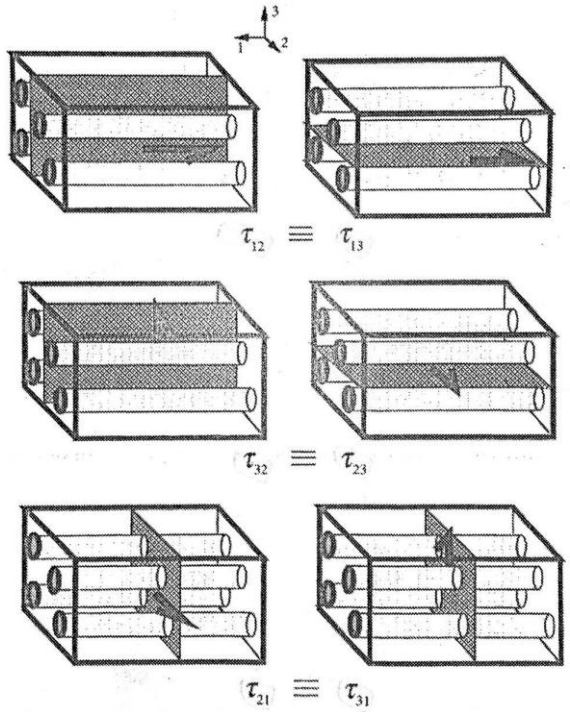

Figure 2.20 - Shear failure planes for long fiber composites (Hull & Clyne, 1996)

No simple analytical expression is available to predict the effect of fibre content on ultimate shear strength t_{12u}. Finite difference methods used by Adams and Dormer (1967) describe how the shear stress concentration factor should vary with fiber volume fraction, shown graphically in Figure 2.22. Of note, the shear strength of a long fiber composite is very close to the shear strength of the matrix until high-volume fractions or for high strength fibres.

For the material used in this study, the tensile strength of the fibres is quite high and the volume fraction is close to 50% therefore the shear strength may be much higher than the shear strength of the matrix. Additionally, some ASTM standard tests are designed in such a way that for the specimen to fail, there must be failure of the fibers and not only the matrix.

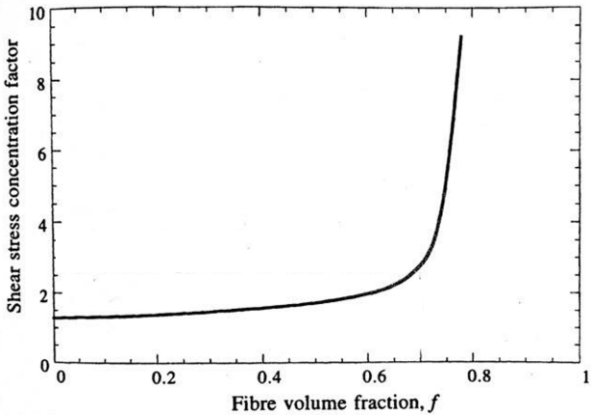

Figure 2.21 - Shear Strength Concentration Factor versus fiber volume fraction (Hull & Clyne, 1996)

Furthermore, it is possible that a pure shear load case does not result in a shear failure, but as discussed in section 2.3.3.6 on Failure Criterion, could result in an axial or transverse tensile failure in the principal stress directions. Failure prediction is important in determining at what stress a material will ultimately fail. It is complex because all three xyz normal stresses and three shear stresses must be known, and a material may fail because of any of these stress states.

2.3.3.4 Compressive Failure

Compressive failure of continuous fiber composite laminates are difficult to determine. The article “Effect of Stacking Sequence on the Compressive Strength of Composite Laminates” (Halverson & Tuttle, 2000), examines the compressive strength of quasi-isotropic laminates at various load angle and ply schedules. One proposal was that compressive strength would relate to the proximity of the 0-degree layer to the center of the laminate. However, it was found that this was not always the case, and that some failures were initiated by the fibers, and some by the matrix. Halverson and Tuttle concluded that “no one particular guideline or rule of thumb is applicable to the compressive strength of all quasi-isotropic laminates” (Halverson & Tuttle, 2000).

2.3.3.5 Flexural Failure

Flexural failure can be approximated when the flexural load causes the tensile or compressive load in a lamina to reach the ultimate tensile or compressive strength or if the interfacial shear strength is exceeded. An approximation can be made by assuming that the last layer to fail would be any 0-degree fibers and proportional to their distance from the neutral axis. This is analogous to an I-beam where the 90-degree fibers act only as the shear web and do not contribute significantly to the ultimate failure of the specimen. If the 90-degree layers fail, a stress concentration could build up in the 0-degree layers where they are no longer supported, thus making strength difficult to estimate, similar to the case of compressive failure.

2.3.3.6 Failure Criterion

A unit element in a material can undergo tri-axial normal stress states at orthogonal angles relative to the x-y-z axis, as well as orthogonal shear stresses. By rotating this unit element in 3-dimensions, these stress states can be resolved into 3 orthogonal principal stresses in which no shear stresses exist. For a specimen subjected to plane-stress, this can be simplified to an x-y and 12 coordinates as shown in Figure 2.23.

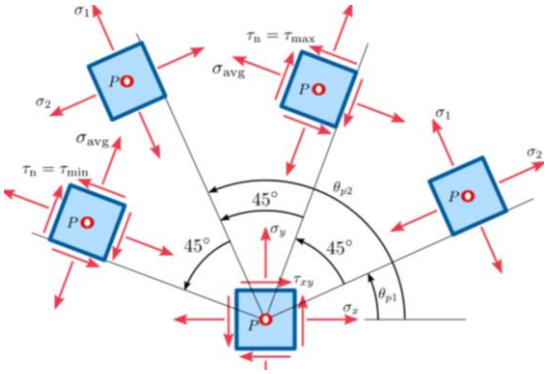

Figure 2.22 – X-y stress components vs. principal stress state (Sanpaz, 2016)

When a material is subjected to a combined load case or loaded at off-axis angles, it is important to consider the failure criteria used to predict the theoretical ultimate strength. The following is a review of the more popular failure criterion.

Maximum Normal Stress Criterion

The simplest of all failure criterion is defined such that if any normal stress exceeds the ultimate normal strength (tensile or compressive, and axial or transverse), then the material will fail, otherwise no failure will occur. This criterion gives a quick and simple idea of whether a material would fail. However, because of it's simplicity, this stress criterion may not accurately describe the actual phenomenon of failure when a material undergoes shear, or experiences a multi-axial stress state.

Von Mises Stress Criterion

The Von Mises theory states that a ductile material starts to yield at a location when the Von Mises stress becomes equal to the stress limit, and is calculated using the following equations for the x-y-z normal and shear stresses or converted to the principal stresses.

$$\sigma_{VonMises} = \sqrt{0.5 \cdot \left[\left(\sigma_x - \sigma_y\right)^2 + \left(\sigma_y - \sigma_z\right)^2 + (\sigma_z - \sigma_x)^2\right] + 3 \cdot \left({\tau_{xy}}^2 + {\tau_{yz}}^2 + {\tau_{zx}}^2\right)}$$

Individual stress limits are combined to create an elliptical failure envelope. If the actual combined stress state exceeds this ellipse, the material is expected to fail. Notably, the first and third quadrants depict that a material that experiences biaxial (or triaxial) tension, can reach a greater limit. In shear, quadrants two and four, the material experiences a much lower failure strength than the axial tension limits.

The largest drawback to this failure criteria is that it is meant for isotropic, ductile material, while many composites are brittle, and anisotropic. Therefore, alternate failure criteria are usually necessary.

Maximum Shear Stress Criterion (Tresca Yield)

Another method of failure prediction is the maximum shear stress criterion, or Tresca Yield. The criterion predicts yield to occur when the shear stress causes the material to yield from simple tension. For isotropic materials, it would be defined as the greatest of the three orthotropic shear stress states. However, as discussed in section 2.3.3.3 Shear Failure, τ_{12} is the only likely failure mode, where:

$$\tau_{12} = (\sigma_1 - \sigma_2)/2, \quad \text{and the Factor of Safety (FOS)} = \sigma_{limit}/(2 \cdot \tau_{max})$$

For a pure shear stress situation, the normal stresses are equal but opposite, so

$$\sigma_1 = -\sigma_2, \text{ then } (\sigma_1 - \sigma_2) = 2\sigma, \text{ and } \tau_{12} = \sigma, \text{ leaving (FOS)} = \sigma_{limit}/(2 \cdot \sigma)$$

Summary

A comparison of these criterion can be seen visually in Figure 2.24. For the evaluation of shear strength of a long fibre composite, the Maximum Shear Stress Criterion (Tresca) is the most conservative and should be best suited to a pure shear loading case. There are also more failure-mode based theories which are tailored to specific load cases such as from Puck and Hashim-Rotem.

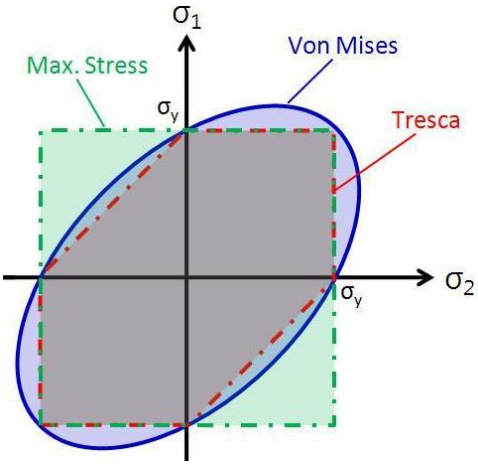

Figure 2.23 - Failure Criterion Comparison (Jeong, 2010)

2.4 Numerical Methods

In this context, the purpose of numerical solving methods, also known as finite element analysis (FEA), is to understand the physical behaviors of complex objects. The method is used most notably for determining the stresses and strains present in a structure, as a response to a given load. Analytical solutions such as those discussed above can sometimes over simplify physical phenomenon, or cannot be used for more complex structures. Often large factors of safety are necessary when predicting physical properties though analytical methods. Numerical methods aim to better predict the properties of a structure to optimize the use of materials or structure design with various goals such as lighter, cheaper, stiffer, or stronger. Figure 2.24 orients Numerical methods amongst other analysis techniques.

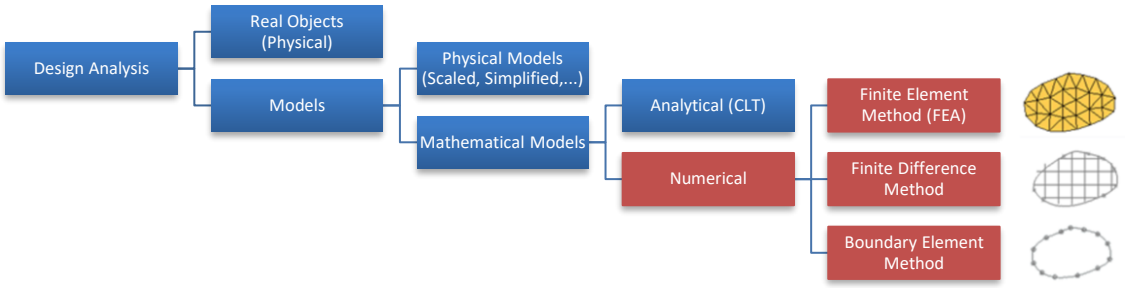

Figure 2.24 – Design Analysis Classifications (Kurowski, 2012)

FEA begins with a process called discretization, which converts a complex object into smaller manageable elements to simplify individual analyses. Discretization can also be referred to as “meshing”. The FEA work flow can be seen in Figure 2.25.

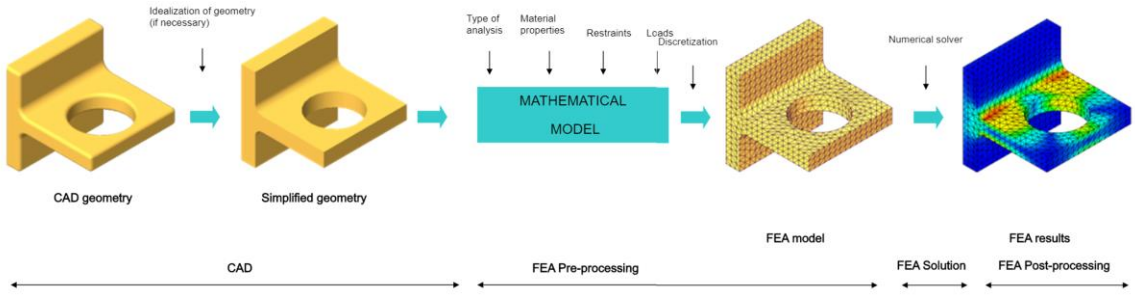

Figure 2.25 - FEA Work Flow (Kurowski, 2012)

2.4.1 Discretization Error

During numerical analysis, error can arise from different areas. The most common and easily avoidable is discretization error. Discretization involves creating a simplified mesh of nodes and elements. If the resolution of the model is too low, error can occur. The example in Figure 2.27 shows how much error can arise from a simple cantilever beam study. Even model #4 has a stress error of 10%. If a beam was then designed with these numbers in mind, the beam would be 10% heavier, stiffer, or costlier. It is important to minimize known errors such as this that can be mitigated, since there are many more areas where error can arise during testing and analysis.

Although accuracy is important, if the resolution is too high it can be impractical in terms of processing power and analysis time. Ideally, the lowest resolution which provides the maximum acceptable error should be chosen. To find this compromise, a convergence study is carried out. The components of a convergence study are identified in Figure 2.27.

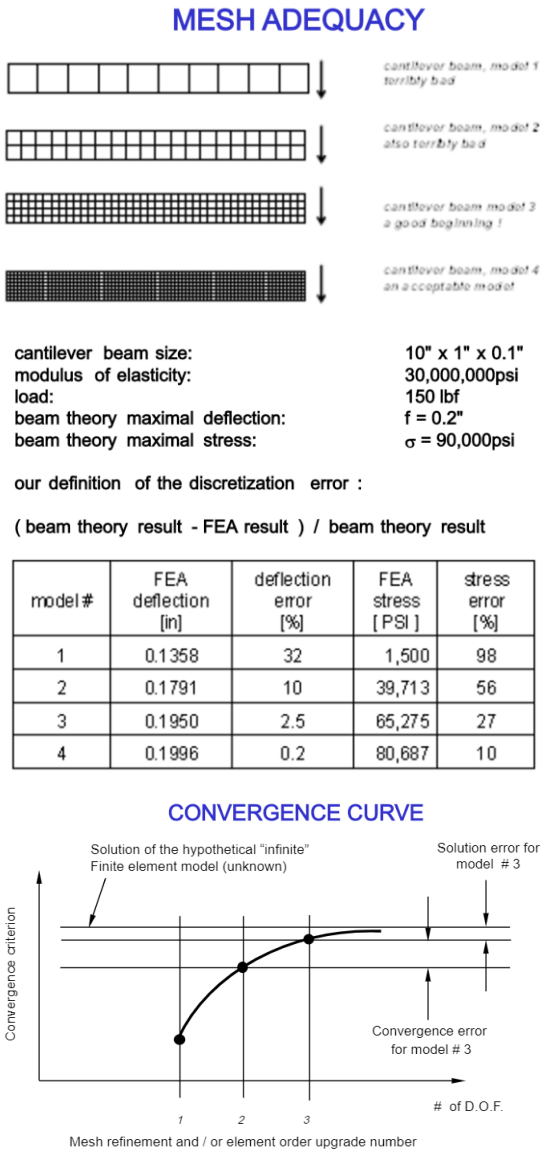

Figure 2.26 - Effect of mesh size on Discretization Error and Components of a Convergence study (Kurowski, 2012)

Convergence

Most FEA programs allow the user to run a test which automatically increases the mesh size to approach the solution until a maximum convergence error is reached. The two sub-types of discretization error are convergence error and solution error. Convergence error is the difference in the stress value between consecutive steps in the convergence study. Solution error is the difference between the model and the theoretical solution. This is estimated by extrapolating the convergence curve as if it were approaching an asymptotic value. The process of progressive mesh refinement is called “h convergence”, where “h” defines the characteristic element size.

2.4.2 Linear vs. Non-Linear Modelling

During the initial elastic loading phase of a material, some materials do not deform in a linear manner. This could be due to the inherent microstructure of the material as in Figure 2.28, or the design or interface of the structure as in Figure 2.28. Such materials require a non-linear analysis which is much more complex. Most ductile materials will exhibit non-linear behaviour after the yield point and begin plastic deformation, but this is now permanent plastic deformation, rather than a non-linear elastic deformation. For the case of continuous-fiber composites, which are brittle, the use of linear modelling often can be appropriate.

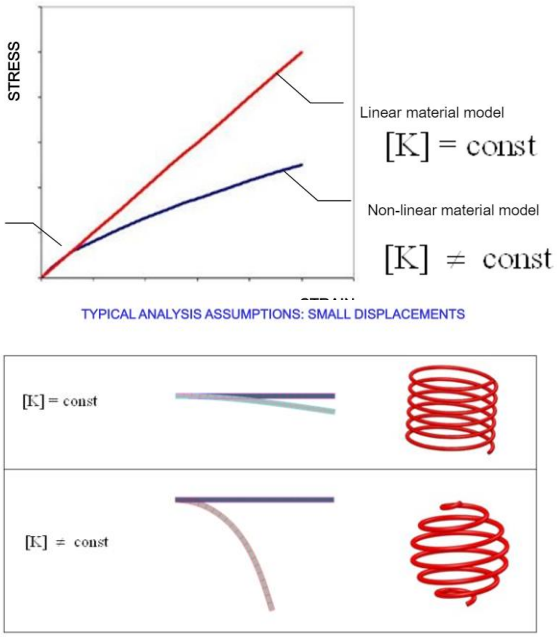

Figure 2.27 - Comparison of linear vs non-linear analysis material property and material shape effect on linearity (Kurowski, 2012)

2.5 Experimental Methods

Experimental methods for determining the mechanical properties of composite materials involve physically testing simple representative specimens. This data is then used in the design of more complex composite structures. Experimental testing has the advantage of being able to provide real-world data and can consider deviations due to manufacturing methods. Types of deviations include; voids, stretching and bunching of fibers, and resin rich or lean areas which may be difficult to predict through analytical methods.

Issues arise with experimental methods because physical testing can be expensive, time consuming, and may not accurately reproduce the stresses which will be seen in the design cases. ASTM lists guidelines for testing through "ASTM D4762 – 16: Standard Guide for Testing Polymer Matrix Composite Materials". Other non-ASTM standards can be found in CMH-17 Composite Materials Handbook.

For obtaining tensile, compressive, and flexural properties, the choice of standard to use is straight forward and well understood. For tensile properties, the recommend standard to follow is "D3039/D3039M - Test Method for Tensile Properties of Polymer Matrix Composite Materials". For compressive properties, the recommended standard is "D3410/D3410M Test Method for Compressive Properties of Polymer Matrix Composite Materials with Unsupported Gage Section by Shear Loading". For flexural properties, "D7264/D7264M Test Method for Flexural Properties of Polymer Matrix Composite Materials". The parameters which have historically been more difficult to obtain accurately are the shear properties of continuous-fiber reinforced composites.

This study will look at the possible sources of error in all of the tests with a more in-depth review of current shear testing methods.

2.5.1 Tensile

ASTM standard D3039 is widely used for testing of polymer matrix composites. It involves manufacturing a long rectangular specimen and subjecting it to a tensile load by

gripping the ends of the specimen and pulling. Strain can be measured in many ways including: cross-head displacement, extensometers, strain gauges, and digital image correlation (DIC). The advantages and disadvantages of each system are outlined in Section 2.7 on Strain Measurement Techniques. If strain gauges or DIC are used, it is possible to also obtain values for Poisson's ratio quite easily.

The main sources of error in the ASTM 3039 tests are material and specimen preparation, gripping, and system alignment. Poor manufacturing techniques can cause defects such as fiber misalignment or damage can be introduced through coupon machining. Gripping is especially of concern. If the material continuously fails in or at the edge of the grips, it may be necessary to add tabs to the specimen to remove a stress concentration due to the grips. Finally, since materials are usually anisotropic, if the specimen is misaligned in the grips, data may be obtained at the wrong angle. From Figure 2.16, the relationship between tensile strength and fibre load angle can be observed. At a 15-degree load angle, the tensile strength can be reduced by approximately 25%.

2.5.2 Compression

The standard for determining compressive properties of composites is ASTM D3410. The specimen is similar to a tensile specimen, rectangular in shape but shorter. It is also loaded between two grips but the gauge length is much shorter to avoid bending and buckling from the unsupported specimen. It is suggested that if the material is susceptible to bending, strain gauges be placed on both sides of the specimen, at the top and bottom on the back and in the center in the front to capture any bending. Similar to the tensile test, tabs can be adhered to the specimen to distribute the load from the grips if failure repeatedly occurs in the grips instead of the gauge area.

2.5.3 Flexure

Flexural testing is done using a 3-point load on a bar of material as per ASTM D7624. For specimen with only a few laminae, the flexural modulus can be affected by the layup

order. For example a [0/90]s material will have stiffer flexural properties than a $[90/0]_S$ specimen. The flexural stress at the outer surface of the material is defined as:

$$\sigma = \frac{3PL}{4bh^2}$$

where P is the load, L is the fixture span, b is the specimen width, and h is the thickness.

2.5.4 Shear

There are many common test methods used in industry for determining the in-plane shear response of polymer matrix composite. Most of these methods are ASTM standard methods, although some non-standard tests are popular because the tests are easy or inexpensive to carry out. The challenge with shear testing is that it is difficult to produce a uniform and pure shear stress state in a specimen. Furthermore, producing a more pure and uniform stress state usually requires an expensive and complex fixture or tricky to manufacture specimen. A sample of shear tests area listed below and in Table 2.3

1. D2344 / D2344M – 16: Standard Test Method for Short-Beam Strength of Polymer Matrix Composite Materials and Their Laminates
2. D3518 / D3518M - 133: Standard Test Method for In-Plane Shear Response of Polymer Matrix Composite Materials by Tensile Test of a ±45° Laminate
3. D4255 / D4255M - 15a: Standard Test Method for In-Plane Shear Properties of Polymer Matrix Composite Materials by the Rail Shear Method
4. D5379 / D5379M - 12: Standard Test Method for Shear Properties of Composite Materials by the V-Notched Beam Method
5. D7078 / D7078M – 12: Standard Test Method for Shear Properties of Composite Materials by V-Notched Rail Shear Method
6. D3846 – 08 (2015): Standard Test Method for In-Plane Shear Strength of Reinforced Plastics
7. 10 Degree Off-Axis Tensile
8. Torsion of a thin tube
9. DIN SPEC 4885 – Shear Test Method using a Shear Frame

2.6 Critical Review of Current Shear Testing Methods

2.6.1 Overview

In the September 2005 issue of *High-Performance Composites*, Dr. Don Adams, owner and president of Wyoming Test Fixtures, compared various ASTM standard shear testing methods as well as other popular non-standard tests. The criteria used in his comparison were:

1. Uniformity of the shear stress state
2. Practicality of testing all three Stress states
3. Obtainability of Shear Strength
4. Obtainability of Shear Stiffness

An important detail to note here is that “uniformity” may or may not mean “purity”. This small but important difference clarifies that a test such as the 10-degree Off-Axis (Tensile) Test can produce a very uniform stress state, but not pure shear. The importance of a pure stress state is that at ultimate strength, the contribution of non-shear stress states to material failure does not need to be discerned because the material is purely in shear. For an impure stress state, the contribution from axial and transverse loads must be resolved.

For stiffness however, the shear stress at a given point is known, whether by FEA or analytical analysis. Then purity of the stress state is not as important because the strain from shear can be easily extracted. Uniformity is important because if the shear stress at the point of measurement is not known, the shear component of the strain at that point cannot be extracted, and therefore an artificially high or low stiffness could be recorded. Dr. Don Adams conclusions are summarized in Table 2.3.

Table 2.3 - Comparison of popular shear testing methods in approximately decreasing order of frequency of current use. (Adams D. D., 2009)

Test Method (with ASTM Std. No., if applicable)	Uniform Shear Stress State	All Three Stress States Practical	Shear Strength Obtained	Shear Stiffness Obtained
Short Beam Shear (D 2344)			■	
Iosipescu Shear (D 5379)	■	■	■	■
±45° Tensile Shear (D 3518)			■	■
Two-Rail Shear (D 4255)			■	■
Three-Rail Shear (D 4255)			■	■
Double-Notched Shear (D 3846)			■	■
Torsion of a Thin Tube (D 5448)	■		■	■
Cross-Beam Sandwich			■	■
Torsion of a Solid Rod			■	■
Four-Point Shear			■	
Picture Frame Shear			■	■
Plate Twist				■
10° Off-Axis (Tensile)			■	■
V-Notched Rail Shear (D 7078)	■	■	■	■

One of the notable tests left out from Adams' review is a new German shear test standard DIN SPEC 4885, pictured in Figure 2.29. Since there has been little review in literature about this test, limited testing, fixture complexity and since it is not an ASTM standard, it was decided not to investigate this test method further. It might still be an attractive shear testing method as it may be able to produce a pure shear stress state with no stress concentration to cause premature failure.

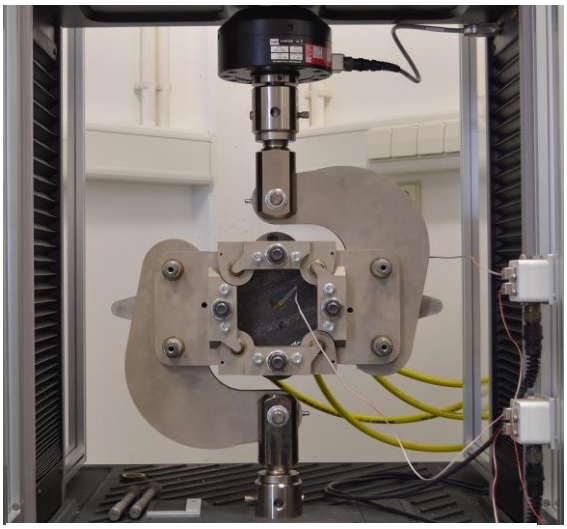

Figure 2.28 - DIN SPEC 4885 Picture Frame Shear Test Setup (GRASSE ZUR INGENIEURGESELLSCHAFT, 2015)

From Table 2.3 it appears that the best tests for obtaining shear properties of polymer matrix composites are ASTM 5279 – Iosipescu Shear, and ASTM 7078 – V-Notched Rail Shear, as these tests satisfy all the criteria. Of the two standards, Iosipescu Shear is more popular and is the current standard used at Western University. In comparison, the V-Notched Rail Shear test is relatively new but gaining in popularity.

Contrary to Dr. Adams' findings, during shear testing, and as outlined in the article "Development and Evaluation Of The V-Notched Rail Shear Fixture", it was found that the Iosipescu Shear test could not produce adequate ultimate shear strength values for high strain-to-failure composite specimen since the specimen would hit the limits of the fixture before breaking (Adams, Moriarty, Gallegos, & Adams, 2003).

It became necessary to find another shear testing standard which could bring a shear specimen to failure. Ideally, the test would provide the same functions as the Iosipescu Shear fixture to avoid doing multiple rounds of shear testing every time properties were needed.

Since the original challenge was that the Iosipescu shear fixture could not fracture certain specimens with a high strain at failure, the primary criteria for this research was to find a method that could provide shear strength data. The next most significant criterion was that a uniform shear stress state occurs throughout the test section. It is imperative to note that not only is uniformity important, but also the purity of the shear stress state, as additional stress states could cause premature failure, producing lower than expected shear strength values.

Having all three stress states being practical is not a necessary criterion for Western University's testing needs, and so the Torsion of a Thin Tube (ASTM D 5448) test could be used since it satisfies all the other criteria. However, based on reviews, it was common to introduce a bending moment into the specimen which would cause premature strength failure. Manufacturing of a thin tube is much more difficult than other tests which rely only on flat specimen. A final issue was the requirement of special fixtures for gripping.

Although the Short Beam Shear test only satisfies one criterion, it is listed as being used most frequently because the specimen is easy to make and the test is simple to run with little cost. Since the issue at Western University was that the specimen could not be brought to failure in the Iosipescu fixture, the short beam shear test could be a good addition. However, the lack of purity and uniformity of the stress state as well as the difficulty in obtaining in-plane shear test data discouraged further investigation.

A final note on Dr. Adams' analysis is that some tests, such as the 10-degree Off-Axis (Tensile) Test, which don't have a "uniform" stress state, could actually be good candidates because uniformity is not necessarily important if the stress at a given point can be known. For example, if the exact centre of the specimen can produce the same stress consistently, regardless of the orthotropy of the material, then this test could certainly be suitable for shear stiffness. As stated previously, because the stress state is not purely in shear, it would not be practical for obtaining a reliable strength value.

Partially based on Table 2.3, the V-Notched Rail Shear test was investigated in the greatest detail since it was the only test besides the Iosipescu Shear test which passed all criteria. The reason for the V-Notched Rail Shear test being at the bottom of the list in terms of frequency of use, is likely due to it having been only introduced as an ASTM standard in 2005. The lack of popularity is not due to other reasons such as the difficulty of creating the specimen.

Summary

Existing shear testing methods are not capable of accurately capturing shear property values of composites. The goal of this thesis was to determine an appropriate shear test which can more accurately provide shear strength and shear modulus values. For an accurate shear strength to be obtained, three conditions must be met. For an accurate shear stiffness to be obtained, only criterion number three must be met:

1. The fixture must be capable of a high enough strain-to-failure
2. The stress state must be purely in shear
3. The stress state must be uniform

A uniform stress state guarantees that measurement can be taken anywhere in the gauge section and no premature failure will occur due to a stress concentration.

This report will go into further detail reviewing the Iosipescu Shear standard and the V-Notched Rail Shear standard. It then briefly examines the 10-degree Off-Axis Tensile test and ±45-degree tensile test because of the applicability of the Off-Axis test to the tensile tests completed for material cards at various load angles, such as 22.5 and 45-degrees.

2.6.2 Iosipescu Shear

During initial testing with an industry partner, and as part of the inspiration for part of this thesis, the Iosipescu Shear test was incapable of bringing high strain-to-failure specimens to failure. Thus, shear strength values could not be determined for those specimens. The Iosipescu fixture is pictured in Figure 2.30 showing the issue of the fixture bottoming out on the specimen if the axial travel is too great. A modification could be made to the fixture so that bottoming out would not occur, such as a slot in the centre of the fixture, or by modifying the fixture for tension instead of compression. However, there are other issues with the test, desribed below, which discourage further investigation into fixture improvements.

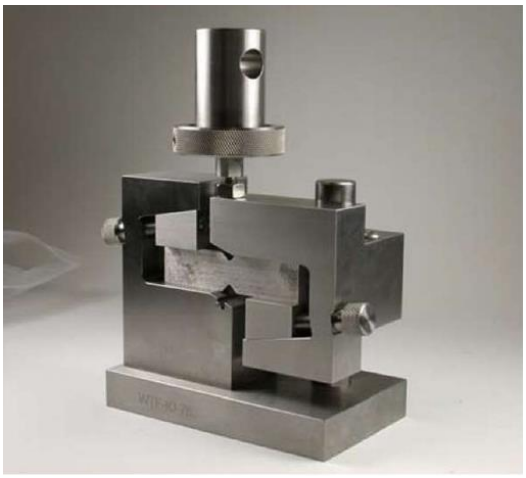

Figure 2.29 - Iosipescu shear fixture

The stress state in the specimen is not purely in shear, nor uniform, as noted by deformation cause by edge loading and concentrations at the notch tips. This means that even for lower strain-to-failure specimen, premature failure could occur such as a “notch root axial split”. Figure 2.30 shows such possible failure modes.

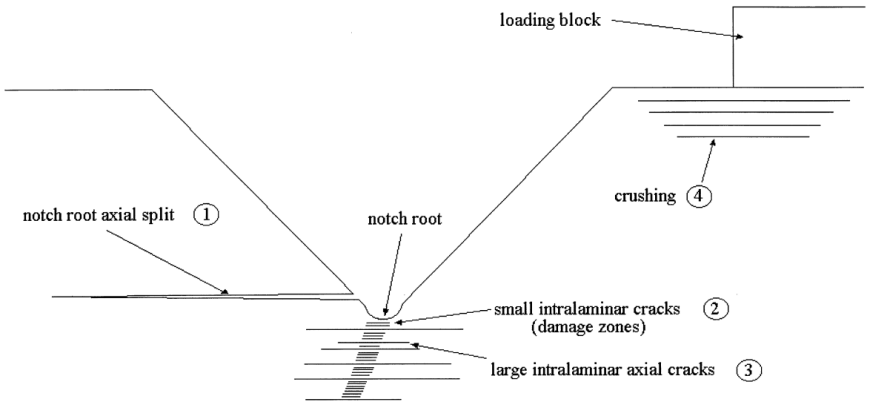

Figure 2.30 - Iosipescu Shear Test Failure Modes (Odegard & Kumosa, 2000)

These conclusions on the viability of the Iosipescu shear test standard for obtaining strength and stiffness values have been corroborated by others such as Odegard and Kumosa (2000). The authors stated that the method could only be successfully used if "fully non-linear finite element computations of the tests are performed which take into account the actual non-linear behaviour" (Odegard & Kumosa, 2000).

Furthermore, the computation requires non-linearity not only in material properties, but also geometric non-linearities, and boundary contact non-linearity. For these reasons and the reasons already stated, they concluded: "Owing to the difficulties associated with the measurement of the shear strength of the composite using the Iosipescu test, and in particular, with the interpretation of the experimental data, this test was found to be almost impractical for the determination of shear strength." (Odegard & Kumosa, 2000)

Figure 2.31 shows a typical Iosipescu shear specimen under load at the maximum deflection without "bottoming-out" on the fixture. The colour scale represents the strain contour in the specimen, with purple denoting areas of high shear strain and red areas of low shear strain.

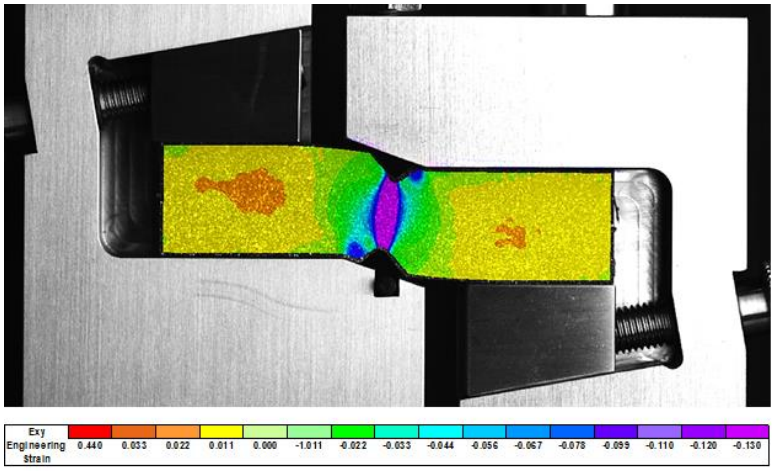

Figure 2.31 - Strain Contour plot overlay from Digital Image Correlation on a polyurethane material (Veryst, 2017)

The set of pictures in Figure 2.33 show the progression of the shear strain distribution at constant intervals throughout a test of the specimen from unloaded to maximum deflection. Stress is not uniform through the entire specimen, especially with the stress concentration cause by the loading blocks. By the end of the test the gauge section is no longer vertical and the material has also deformed around the load blocks, highlighting the non-linearity of the geometry.

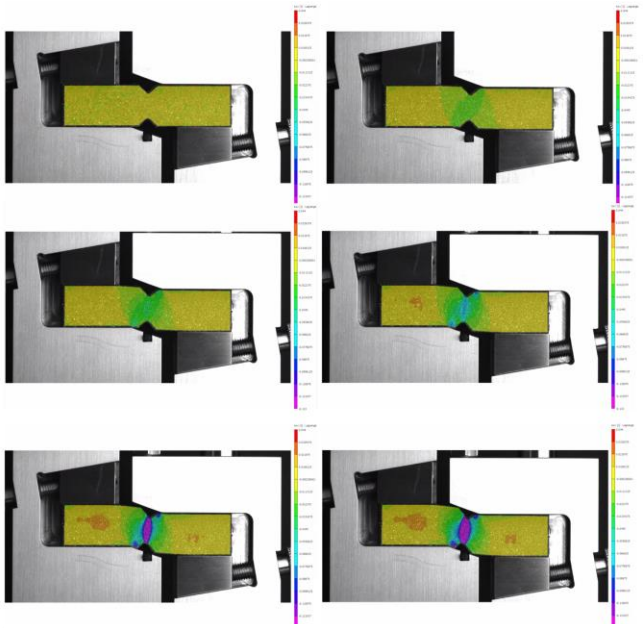

Figure 2.32- Shear Strain Distribution evolution throughout Iosipescu shear test (Veryst, 2017)

2.6.3 V-Notched Rail Shear

Shear testing began on anisotropic materials in the mid 1900's on plywood, originally with a four-rail shear test, however this quickly became a two-rail shear system. The uniformity of stress states in these tests were verified by experimenting on glass and using optical photoelastic analysis. The first modification was developed by Hussain and Adams by removing the drilled holes for the rail shear specimen, and instead gripping the faces by clamping. This eliminated premature failures and made specimen preparation simpler.

In July of 2005, Dr. Don Adams introduced the V-Notched Rail Shear test method which was approved as ASTM D 7078 in March of 2005. The V-Notched Rail Shear test combines the advantages of both the Iosipescu Shear test and the Two-Rail Shear test, eliminating the weaknesses of each. Design of the fixture and specimen can be seen in Figure 2.33. As was shown in Table 2.3, the V-Notched Rail Shear test satisfied all the criteria and is an attractive solution.

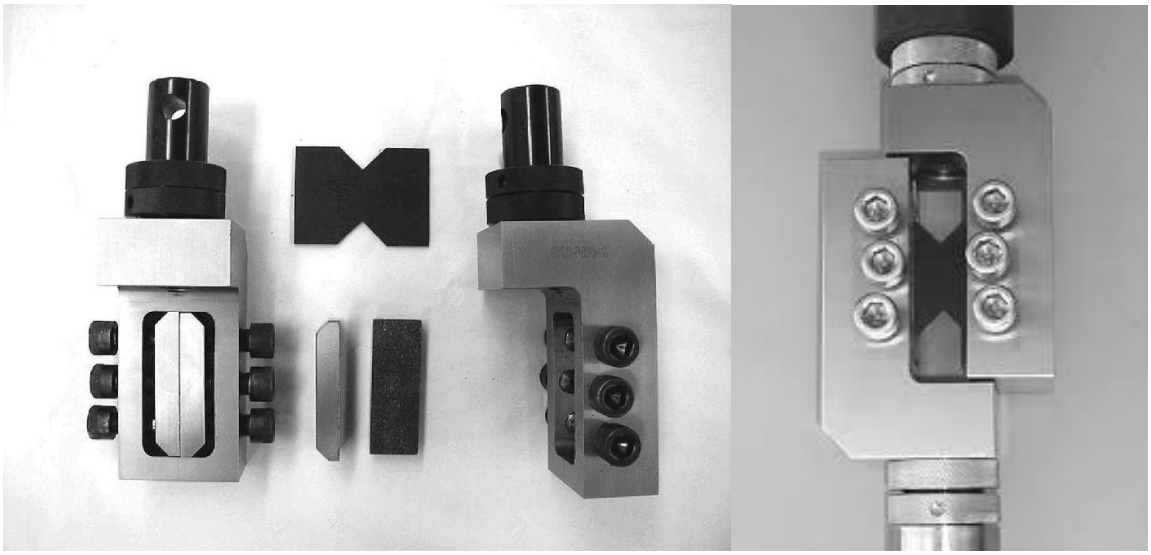

Figure 2.33 - V-Notched Rail Shear Fixture and Specimen (Adams, Moriarty, Gallegos, & Adams, 2003)

The V-Notched Rail Shear test was developed by combining other shear tests into a single test, while keeping the strengths and eliminating the weaknesses of each test. The main weaknesses of the Iosipescu Shear test are; a small specimen gauge section, edge loading which can cause edge crushing failure, and the inability to break high strain-to-failure materials. As seen in the chart in Figure 2.34, the main weakness of the Two-Rail Shear test is the stress concentrations where the specimen is bolted in. The V-Notched Rail Shear method solves these issues by clamp loading a specimen with v-notches like the Iosipescu shear test which gives a relatively uniform shear stress in the gauge area. Perhaps the greatest feature of the new V-Notched Rail Shear test method is that it has achieved shear strengths greater than 500 [MPa] which is much more than any other shear test could produce (Adams D. D., 2009).

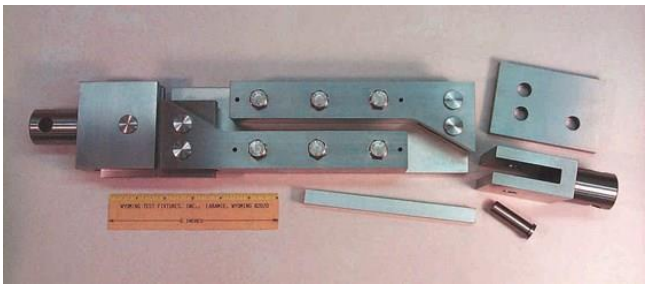

Figure 2.34 - Two Rail Shear Test Fixture (Adams D. D., 2009)

Comparing the “Development and Evaluation of the V-notched Rail Shear Test for Composite Laminates” (Adams, Moriarty, Gallegos, & Adams, 2003), to ASTM D7078, there is a discrepancy in the recommended bolt torque which could result in a high error reading for Ultimate Strength. ASTM D7078 recommends a bolt torque of 55 [N.m]. However, the shear strength appears to peak around a 41 [N.m] torque as seen in Figure 2.35. Running the test at 55 [N.m] could be causing the specimen to fail prematurely because of additional stresses. These failures are likely between 20% and 45% earlier than expected at a bolt torque of 55 [N.m] or higher, producing a lower apparent shear strength. This potentially large drop in Shear Strength will be investigated by testing at multiple bolt torques.

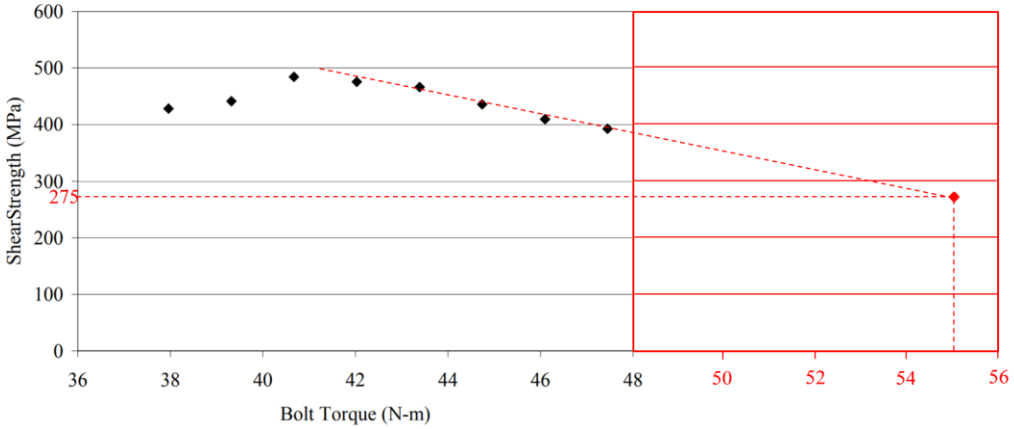

Figure 2.35 - Shear Strength vs. Bolt Torque for the V-Notched Rail Shear Fixture [edited] (Adams, Moriarty, Gallegos, & Adams, 2003)

In development of the V-Notched Rail Shear test standard ASTM 7078, FEA was carried out as a means of predicting and comparing the stress and strain contours in various specimen configurations. The FEA studies were used to settle on a design the produced the most uniform and pure shear stress state with minimum stress concentrations over multiple layups. The notches were added to satisfy this condition (Adams D. D., 2009).

The results were all normalized and can be seen in Figure 2.36. The white sections of the contour represent the normalized value for stress, where the normal stress value equals the applied force over the cross-sectional area. Contour areas in the red-yellow spectrum

represent higher than normal stresses, where green-purple represent lower than normal stresses.

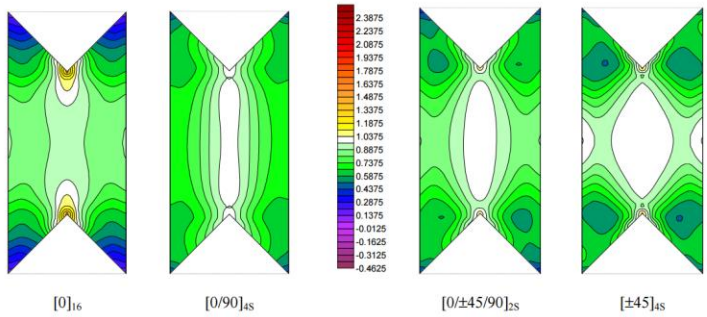

Figure 2.36 - Normalized Shear Stress distributions for multiple layups (Adams, Moriarty, Gallegos, & Adams, 2003)

Figure 2.38 shows the normalized shear modulus for these different layups and strain gauge types. One of the largest takeaways from this study is that the optimal place to place a strain gauge, or to choose as an Area of Interest (AOI) if using DIC, is any area in white as it would follow the expected average stress. The 0-degree specimen shows almost no white and are not a good option for shear testing This can be seen in Figure 2.38 showing the obtained shear modulus for various gage sizes on each layup.

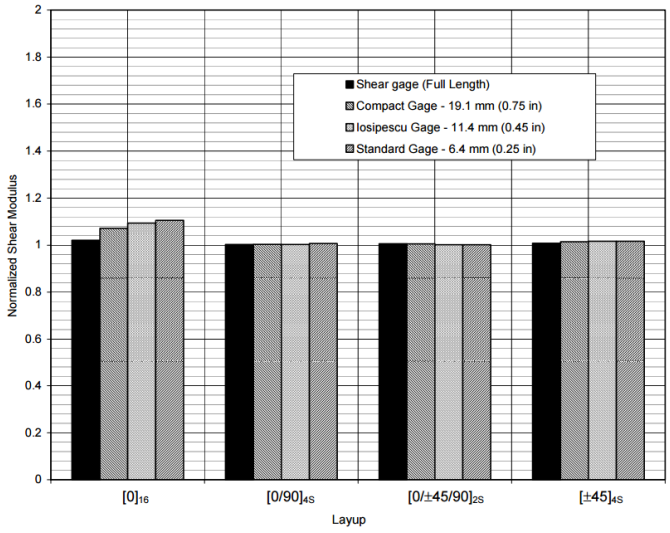

Figure 2.37 - Nondimensionalized shear moduli vs strain gauge size for each layup (Adams, Moriarty, Gallegos, & Adams, 2003)

However, this solution presents two problems. First, many of the layups show stress a concentration at the notch tips, and second, the axial and transverse stresses are not trivial (Figure 2.39). These are issues for the measurement of ultimate shear strength. This is because the concentrations at the notch tips could cause premature failure, and a reading would be taken in the white regions, therefore reporting a lower than expected ultimate strength.

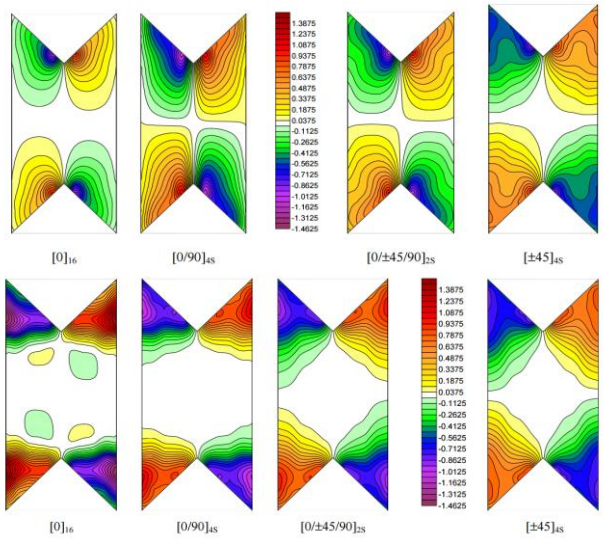

Figure 2.38 - Axial and Transverse Normal Stresses in the Gauge Area (Adams, Moriarty, Gallegos, & Adams, 2003)

The issue with having axial and transverse stresses is that they can contribute to a combined load case and again cause a lower apparent shear strength. The later phenomenon was discussed in Section 2.3.3.6 on Failure Criterion.

Lastly, the FEA development took place with no radius at the notch tips. When the authors (Adams, Moriarty, Gallegos, & Adams, 2003) added in 0.025in and 0.05in radii to their analysis, the central area where a strain gauge was recommended to be placed, saw up to a 10% decrease in shear stress, and more pronounced stress concentrations around the notch tip. A comparison is made in Figure 2.40. The result was that the specimen could fail at a lower load from the cross head, and a strain gauge would be reading a lower strain. Consequently, a lower ultimate strength and a lower ultimate failure strain would be obtained than the material could handle.

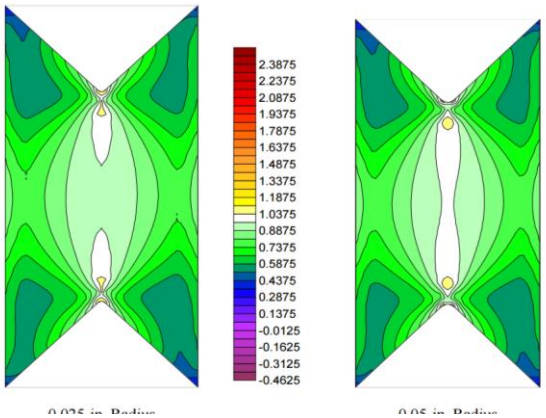

Figure 2.39- Shear stress distribution with added notch radii (0.025in and 0.05in) (Adams, Moriarty, Gallegos, & Adams, 2003)

A summary of the findings from the development of the V-Notched Rail Shear fixture can be found in Table 2.4. The most notable feature is that the strength value for the laminates with 45-degree laminae all bottomed-out on the Iosipescu fixture as previously discussed. Fixture failure also occurred for the Two-Rail Shear testing. From this information it was concluded that the the V-Notched Rail Shear test was the only one which could break high strain-to-failure materials.

Table 2.4 - V-Notched Rail Shear vs Two-Rail Shear vs Iosipescu Shear Strength Comparison (Adams, Moriarty, Gallegos, & Adams, 2003)

Laminate	Test Method	Average Shear Strength		Standard Deviation		Coefficient of Variation
		MPa	ksi	MPa	Ksi	%
$[0/90]_{4S}$	V-Notched Rail Shear	136	19.8	0.7	0.1	0.5
	Two-Rail Shear ASTM D 4255	Not Tested				
	Iosipescu Shear ASTM D 5379	148	21.4	3.4	0.5	2.3
$[0/90/\pm45]_{2S}$	V-Notched Rail Shear	418	60.6	32.8	4.8	7.8
	Two-Rail Shear ASTM D 4255	158*	22.8*	6.7	1.0	4.2
	Iosipescu Shear ASTM D 5379	195*	28.3*	13.9	2.0	7.1
$[\pm45]_{4S}$	V-Notched Rail Shear	530	76.9	26.2	3.8	4.9
	Two-Rail Shear ASTM D 4255	167*	24.2*	4.2	0.6	2.5
	Iosipescu Shear ASTM D 5379	164*	23.8*	9.9	1.4	6.0
Glass Fabric/ Vinylester	V-Notched Rail Shear	211	30.6	13.7	2.0	6.5
	Two-Rail Shear ASTM D 4255	111	16.1	8.9	1.3	8.0
	Iosipescu Shear ASTM D 5379	143	20.8	3.4	0.5	2.4

* fixture failure

Testing a 0-degree and a 90-degree specimen should produce the same results in terms of shear stiffness and strength, because they are lamina properties and the lamina are symmetric about the 45-degree plane. However, the 90-degree direction is not often used alone because any stress concentrations at

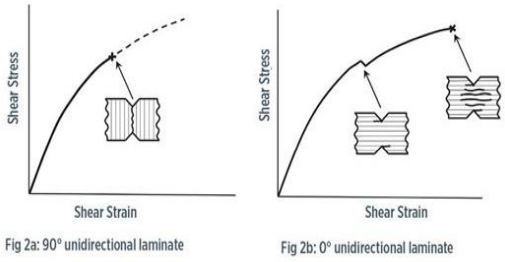

Figure 2.40 - Failure mechanics and Modulus or Damage vs Strain curves (Adams D. , 2017)

the notch tip, manufacturing defects, or transverse loads will produce a crack. The crack would easily propagate through the matrix along the fibre direction, causing a premature failure. In contrast, a 0-degree laminate will only fail once the fiber breaks because the fiber is constrained between the two fixtures.

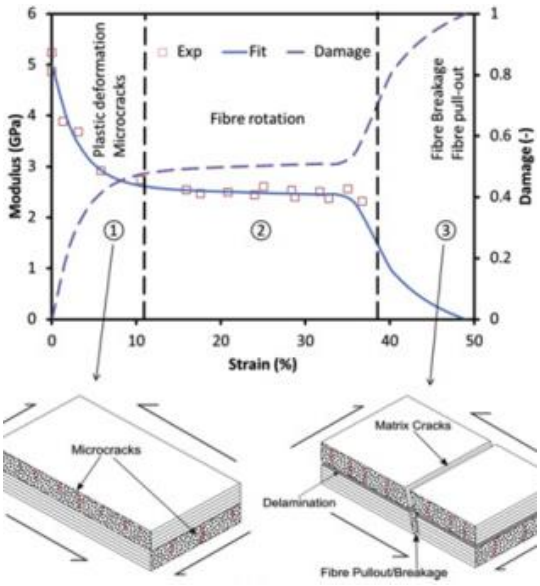

Figure 2.41 - Failure Mechanisms and Instantaneous Shear Modulus (Tan & Flazon, 2016)

Furthermore, an analysis of failure mechanisms can be seen in Figure 2.41 and with more detail in Figure 2.42. The figures show the development of failure as the fibers start to scissor after yielding to align with the principal stress axis. Figure 2.42 shows the areas where failure occurs, notably a thin fracture zone within a larger plastic deformation zone. This information suggests that calculation of shear strain should not use the full gauge width of the specimen.

The initial quick drop in the shear modulus indicates that the lower stiffness at higher strains is mostly associated with fibre deformation, and the shear modulus is controlled by matrix properties independent of fibre properties (Tan & Flazon, 2016).

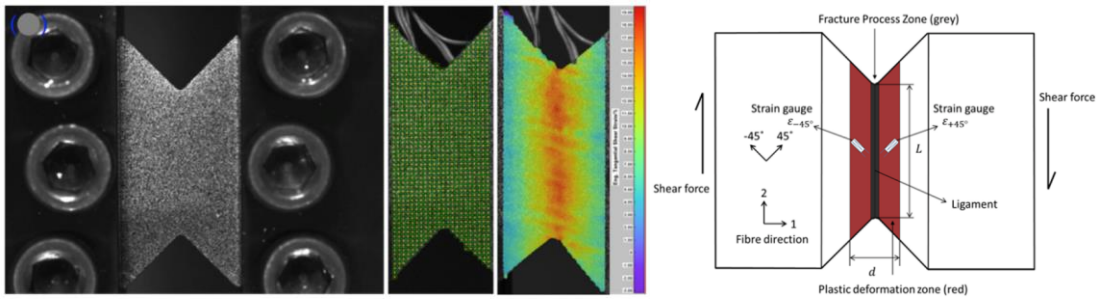

Figure 2.42 - Deformation zones and strain gauge locations (Tan & Flazon, 2016)

2.6.4 10-Degree Off-Axis Tensile

The 10-Degree Off-Axis test has no ASTM standard, does not have a uniform shear stress state, is not in pure shear, and not all three stress states are practical. However, it is popular because of the ease of specimen fabrication and there is no need for additional fixturing. Off-Axis Specimen are pictured in Figure 2.44. Although the specimens are easy to machine, microcracks can form along the edges from the machining and cause premature failure. Because of this, it is recommended to take the highest failure strength. (Chamis & Sinclair, 1976).

Figure 2.43 – Off-Axis tensile specimen (Chamis & Sinclair, 1976).

The 10-Degree, or any other Offset Tensile test, work by resolving the orthogonal normal stresses and shear stress and extracting the shear stress component. At approximately 7-degrees and to up to approximately 60-degrees load angle, a tensile stress should cause the material to fail from matrix shear as shown in Figure 2.44. Off-Axis tests are only successful if "fully non-linear finite element computations of the tests are performed which consider the actual non-linear behaviour" (Odegard & Kumosa, 2000). Because of this limitation, the 10-Degree Off-Axis test is used more to quickly validate other tests.

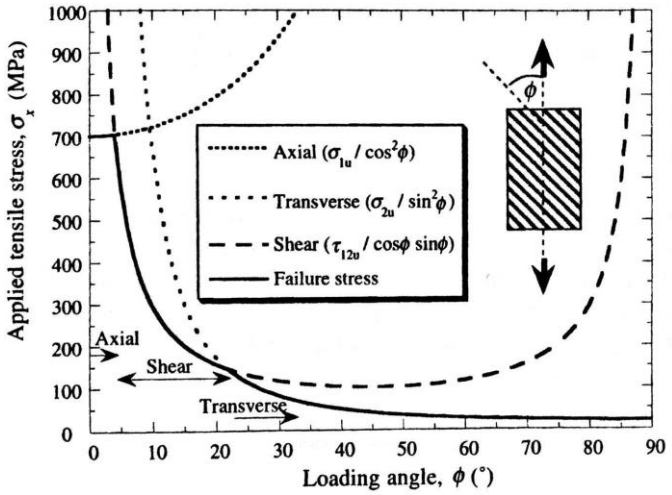

Figure 2.44 - Tensile Stress vs Load Angle, Failure mode (Hull & Clyne, 1996)

Although an Off-Axis Tensile specimen could fail in shear, it is possible that axial and transverse loads contribute to failure as discussed in Section 2.3.3.6 Failure Criterion. An article by NASA, *10-Degree Off Axis Test for Intralaminar Shear Characterization of Fiber Composites* (Chamis & Sinclair, 1976), critically reviews the 10-Degree Offset Tensile test failure on the specific issue of axial and transverse loads. The article concludes that failure is only represented by 88% shear, with the other 12% contributed by axial and transverse stresses. Therefore, an approximately 12% lower than expected ultimate shear strength will be obtained.

2.6.5 Summary of test Methods

The criteria for deciding on an improved shear testing method follow those proposed by Adams with two main changes. First, uniformity of a shear stress state is not necessary a guarantee of the stress being pure shear. Second, achieving all 3 stress states is not important, as long as in-plane shear can be achieved.

1. Uniformity of the shear stress state
2. Purity of shear stress state
3. Obtainability of Shear Strength
4. Obtainability of Shear Stiffness

This narrowed down the viable amount of shear testing to only the Iosipescu shear test, V-Notched Rail Shear test. At this point it is unclear if one of these two tests could produce a more uniform or pure shear stress state, and although Adams states that the Iosipescu Shear test could be used to obtain shear strength, it is uncertain and required further investigation.

2.7 Strain Measurement Techniques

There are many options for measurement techniques. Some standards lend themselves better to certain types of measurement techniques and options are available to provide a wide range of accuracy versus ease of use.

2.7.1 Crosshead Displacement

The simplest measurement for strain in a specimen is to measure the crosshead displacement during a tensile, compression, shear or flexure test, diagramed in Figure 2.46. However, this will not accurately represent the strain within the gauge length, and is seldom used.

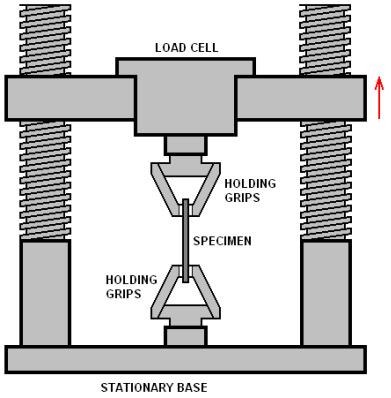

Figure 2.45 - Schematics of a Tensile Machine (Engineering Archives, 2012)

2.7.2 Extensometers

One of the common methods for measuring strain in a test specimen is the use of an extensometer. They are inexpensive, easy to use, and a fast way of measuring the strain in a specimen. The issue with extensometers is that the sensor can only properly be used for tensile specimen. Often the extensometer can slip during the testing and produce a curve which does not accurately describe the material.

Figure 2.46 - Extensometer on a tensile specimen (Epsilon Technology, 2017)

2.7.3 Strain Gauges

An alternative is the use of strain gauges. Strain gauges can be adhered to the surface of test specimens within the gauge area as pictured in Figure 2.47. The use of multiple strain gauges at an angle to one another, provides strain values in both x and y directions. Furthermore, placing a strain gauge on the backside of a specimen can detect any bending that arises during the test, such as for detecting buckling modes in a compression test.

The issue with strain gauges is the amount of time required for accurate application, and cannot be reused after testing. Additionally, with smaller specimens, a strain gauge may not be able to fit. Finally, for higher strain-to-failure materials, strain gauges can break before the specimen fails, causing a loss of data.

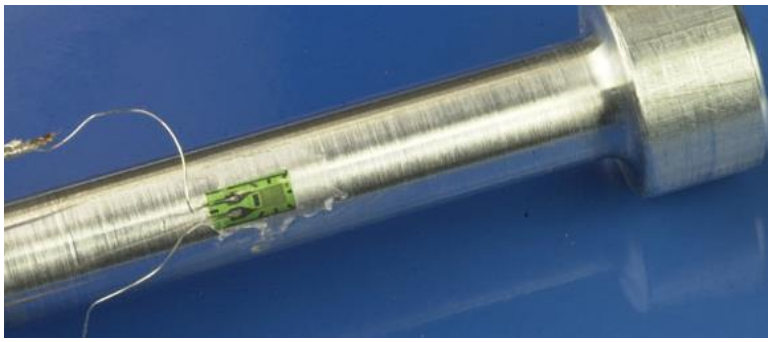

Figure 2.47 - Strain gauge epoxied to specimen with signal wires running to a data acquisition device (University of Cambridge, 2017)

2.7.4 Digital Image Correlation

Since the stress distribution within the gauge section of test specimen are not 100% uniform, it is important to be able to map the stress distribution in two-dimensions over the surface of the specimen. DIC can measure strain and deflection in 3 dimensions, which can be useful for the detection of an buckling. Strain gauges only capture what is happening at a single point and may not capture the entire strain field. By correlating the 2-D strain using a DIC system with FEA, optimal strain gauge placement can be used to obtain an accurate reading. Alternatively, the expected stress difference at various places along the part compared to the stress in the gauge section can be identified, i.e. at a stress concentration. It can also be used in determining Poisson's ratio. For example, the ASTM standard "Bonded Resistance Strain Gage Selection" recommends an active gage length of 1.5mm-3.175mm, and so the area of interest could be set to this size and compared to data collected from a strain gage.

DIC setups, including software, are an expensive initial purchase and can take some time to setup and post-process data. Therefore, the use of DIC may be more suitable as a

correlation technique to FEA. It could also be used to determine the best location to place a strain gauge rather than to characterize the strain in every test specimen. However, if the frontal area of the specimen is not flat, or is very thin, it can be impossible to measure the strain using DIC. An example of a difficult test for using DIC is a flexure test because the specimen is very thin. Figure 2.48 shows a typical DIC setup, depicting how the cameras measure the change in the speckle pattern to determine strain in the material.

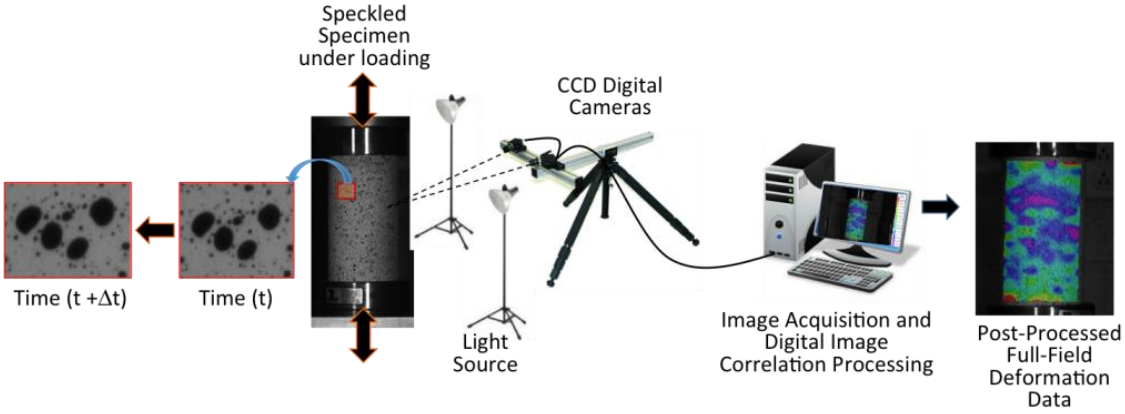

Figure 2.48 -Digital Image Correlation (DIC) Setup (Hansen, 2014)

Chapter 3

3 Experimental Methods

Two sets of physical testing were carried out on three different carbon fiber reinforced epoxy resin fabrics. The first set of tests were used to build material property cards for an industry partner, while the second set were to compare shear testing methods, and validate or calibrate finite element models. The studies are:

1) ASTM standard testing of two different continuous carbon fiber reinforced epoxy resin fabrics to characterize mechanical properties with material property cards
2) Iosipescu Shear Testing and V-Notched Rail Shear Testing on a different continuous carbon fiber reinforced epoxy resin fabric to evaluate the advantages and disadvantages of each test.

3.1 Study 1: Generating Material Property Cards

3.1.1 Fabrics

The first two tests of Study 1 were performed on two provided fabrics. The first fabric is Quasi-Isotropic (QI) and the second fabric is nearly Orthotropic (OR). The properties of each fabric are outlined below, and Fabric OR is modelled in Figure 3.1.

Quasi Isotropic (QI):

- 300 GSM Unidirectional / Multi-Directional (UD/MD)
- Fiber: Aksa 24K A42
- Layup: $[\pm 45_{300GSM}/90_{300GSM}/0_{300GSM}]_{sym}$

Orthotropic (OR):

- 2400 GSM 3D Woven (0 and 90 carbon fibers with small Z stitch in Z-direction)
- Fiber: Aksa 24K A42 (with Aksa 3K for the “Z stitch”)
- 5 Layers: 3 in X direction (52% by weight), 2 in Y direction (43% by weight) and Z Yarns (4.8% by weight)
- Layup: [0,90,0,90,0]

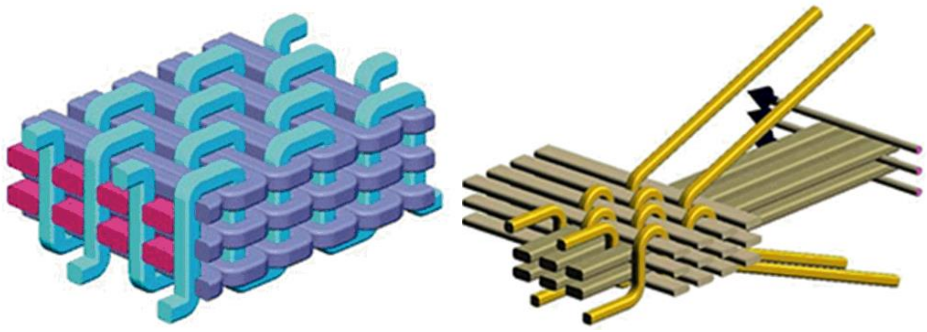

Figure 3.1 - Fabric Configuration OR showing Z Yarns (SAE International, 2008)

3.1.2 Specimen Layout

Both fabric panels were cut at University Machine Services within Western University using the same lay-out design as shown in Figure 3.2. Specimen sizes were in accordance with ASTM D3069, D5379, D790 and D3410 for tensile, shear, flexure and compression tests, respectively.

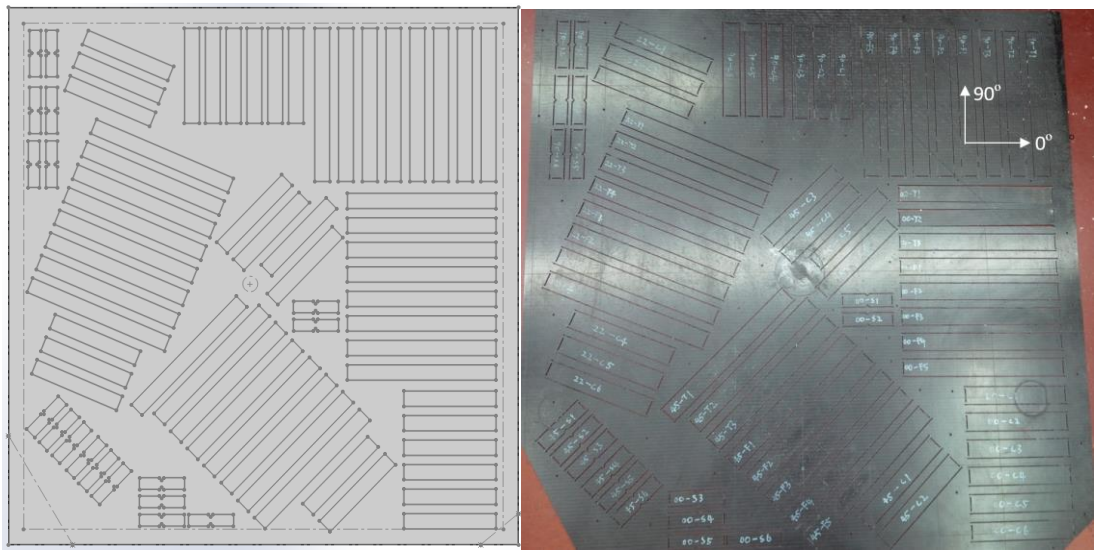

Figure 3.2 - Specimen layout showing orientations in CAD and after machining the sample plate

3.1.3 Apparatus

Tensile, shear, flexure and compression tests were conducted in Prof. Jeffrey Wood's lab at the Western University. The 8804 Servohydraulic Static Testing System from Instron was used for all tests. The Bluehill 2 v2.21 software was used for data acquisition in conjunction with a Digital Image Correlation (DIC) system by Correlated Solutions. The Vic-3D v7 software was used to process the DIC data. The DIC system was used to measure the strain distribution for calculation of strain and Poisson's ratio in the tensile and shear tests.

3.1.4 Procedure

3.1.4.1 Tensile Test

Tensile tests were conducted on both fabrics to determine: ultimate tensile strengths, tensile moduli, Poisson's ratios and failure strains. The tests followed ASTM Standard D3069 with a test speed of 2mm/min. Tests were carried out without added tabs. If a large percentage of grip failures occurred, tabs would have been added. Strain was measured both with a 25mm extensometer and a DIC system for comparison. Slippage occurred in some tests with the extensometer and so results include only DIC strain data. DIC was also used for determination of Poisson's ratio.

3.1.4.2 Compression Test

Compression tests were conducted to determine the ultimate compressive strength of the fabrics. ASTM Standard D3410 was followed at a test speed of 2mm/min with a gauge length of 12mm. This gauge length ensured the required minimum specimen thickness to prevent bending or buckling was satisfied. Strain was measured using crosshead displacement as compressive strength was the main parameter of concern, and the gauge length was too small for the DIC system to capture. Like the tensile testing, tabs were not to be used unless grip failure continuously occurred, which it did not.

3.1.4.3 Flexure Test

Flexure testing was conducted to obtain the flexural modulus and strength of each fabric. The test was carried out according to ASTM standard D790 at a test speed of 6.4mm/min. The support span was 96mm for the 3-pt bend test (40 times the specimen thickness). Flexural strain was measured using crosshead displacement.

3.1.4.4 Iosipescu Shear Test

Shear tests were conducted to obtain the shear modulus and ultimate shear strength of both fabrics. ASTM standard D5379 was followed with a test speed of 2mm/min. Strain was measured using a DIC system. Many of the tests bottomed out on the fixture, thus some results revealed a lower bound rather than the actual ultimate strength.

3.2 Study 2: Shear Testing Comparison

3.2.1 Fabrics

For comparison between the two shear test types, a non-woven ±45-degree multi-directional fabric was chosen: Zoltek PX35 MD, 300 GSM. Only one layup was done, however the specimens were cut along the 0-degree and 45-degree axis to produce the following two layups:

i. $[\pm 45\ 300GSM]_{2sym}$
ii. $[0/90\ 300GSM]_{2sym}$

3.2.2 Specimen Fabrication

Specimens were fabricated using a wet layup technique and set in a platen press during the curing period to consolidate the fiber layers and bring the fibre volume fraction up towards 40% by squeezing out excess resin. The press and cured laminate is pictured in Figure 3.3. Final volume fractions were calculated based on the mass of carbon fiber, final composite mass, and total composite volume.

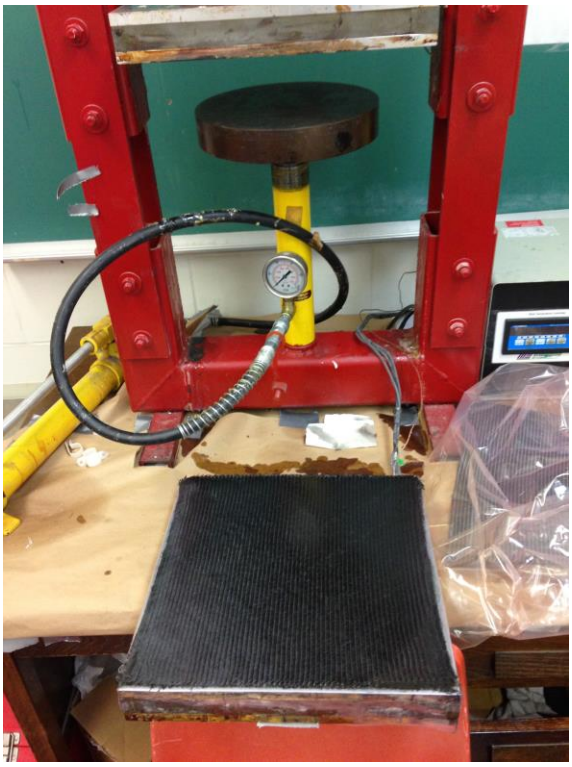

Figure 3.3 – Platen Press used to manufacture the test specimen, and cured composite plate (bottom)

The press was initially set to 400 PSI with a weight on the hydraulic handle which would sustain a compressive pressure on the plate while resin was squeezed out. Pressure was slowly let off to 0 PSI by the time the plate cured. Since testing is only comparative, post-curing was unnecessary.

Two composite plates were manufactured. The first was machined into Tensile, Iosipescu, and V-Notched Rail Shear specimens. It was used to check that the material properties of the plate were in the expected range, and to check fitment in the V-Notched Rail Shear fixture. These specimens were cut with a guide on a bandsaw since fiber alignment and dimensions were not critical for the proof

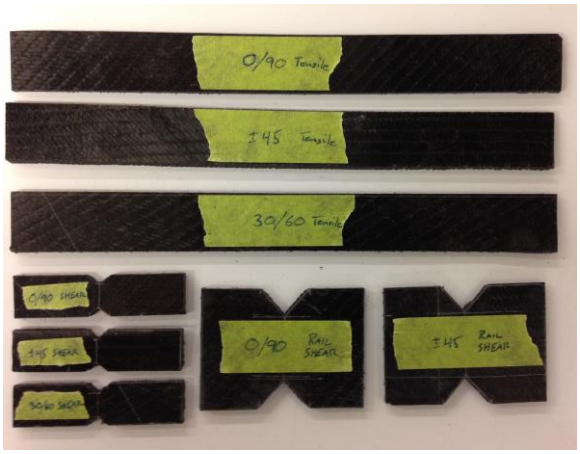

Figure 3.4 - Initial specimen cut for proof of concept testing

of concept. The proof-of concept specimen can be seen in Figure 3.4.

The second plate was manufactured in the same way, with the exception that one atmosphere of pressure was maintained throughout the full curing process. The resulting plates can be seen in Figure 3.5. Machining of these specimens were carried out in the Western Engineering Student Machine Shop on a 3-Axis Mill using a conventional, rather than climb, milling technique to preserve the specimen edges.

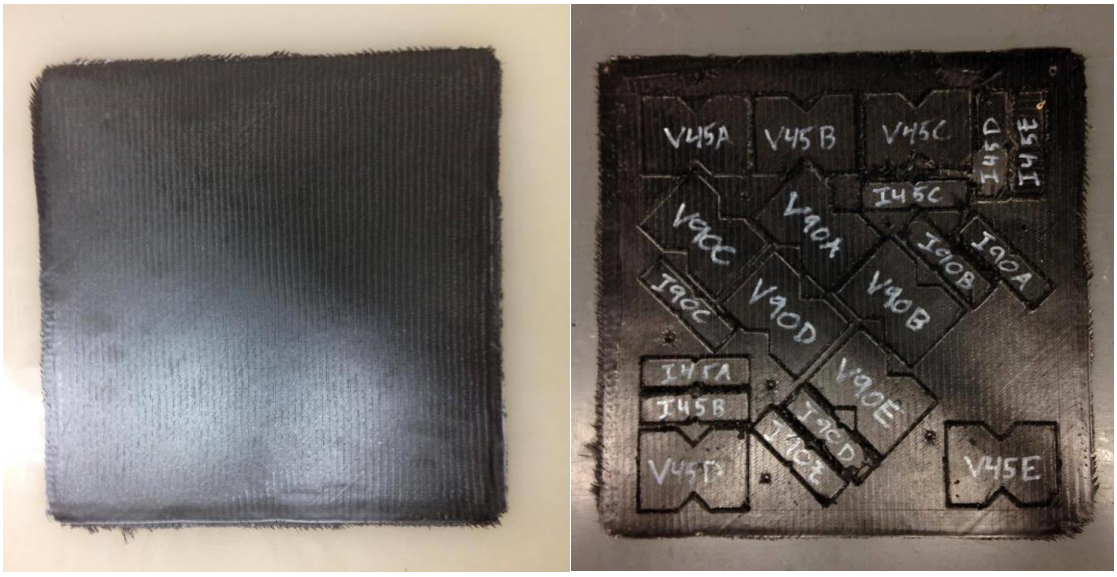

Figure 3.5 - Composite Plate before and after machining, showing specimen layout

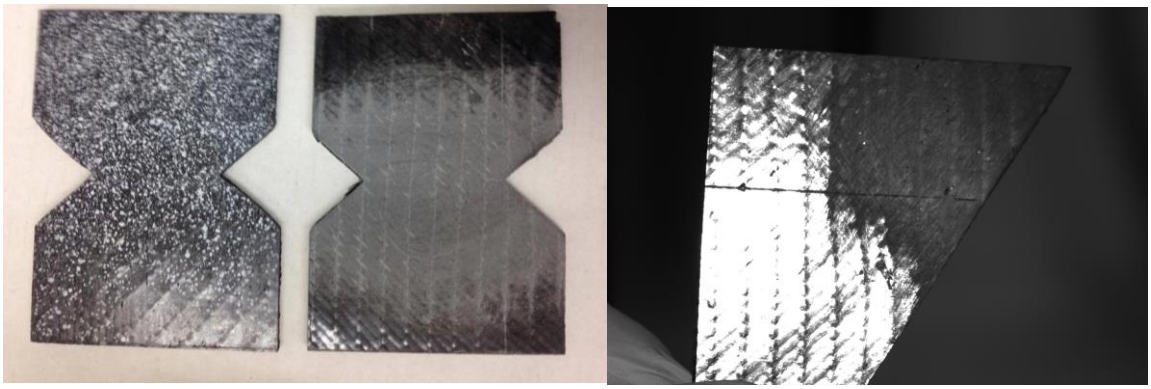

Figure 3.6 - Comparison of un-sanded (glossy) and sanded (glossy) surface finishes.

Initial tests showed data loss because of glare on the specimen from the z-stitching. It was determined that the data loss was more detrimental than the z-material removal with light wet-sanding because data could be obtained. The difference can be seen in Figure 3.6. Another possibility would be to apply a layer of matte black paint before speckling.

Speckling is necessary to provide contrasting points for the DIC system to register strain deformation. The random speckle patter was generated by a light coat of white spray paint to contrast the black specimen.

Final specimen volume fraction was determined using the mass of fibers, mass of the final composite, and volume of the composite plate. Ply orientations after manufacturing were checked with micro-CT scans done by Robarts Imaging at Western University on a finished sample of the composite plate.

3.2.3 Fixture

A fixture was designed according to the ASTM 7078 Standard with some minor differences to better suit the equipment available at Western University. The gripped ends were modified from cylindrical shafts to flat plates to suit the Western University Instron machine more easily. Plastic alignment inserts were given an extra feature to restrict specimen placement by an extra degree of freedom (up and down). Instead of a “flame sprayed surface”, a knurl-like pattern was machined into the specimen gripping plates for additional grip, pictured in Figure 3.8. A CAD model and fixture are pictured in Figure 3.7.

Figure 3.7 - Knurl pattern instead of flame-sprayed surface

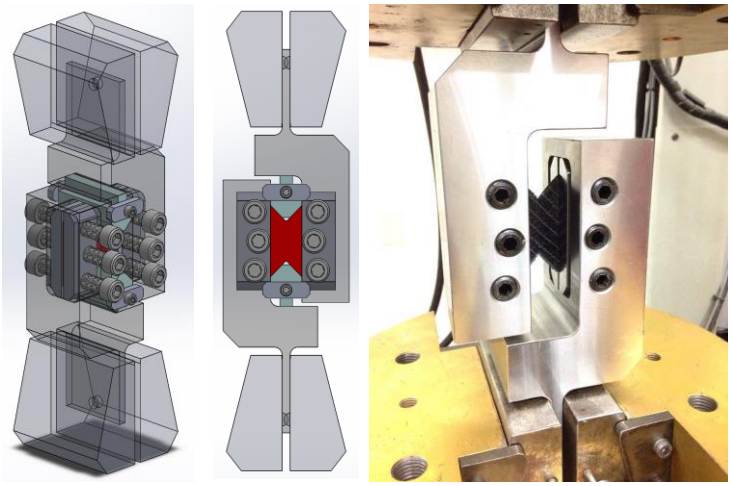

Figure 3.8- CAD Model and Finished Fixture holding a specimen

3.2.4 Apparatus

Digital Image Correlation (DIC) cameras were levelled to ensure the DIC axis matched the specimen axis. Flood lights, as shown in Figure 3.9, were used to ensure the speckle pattern of the specimen could be seen by the DIC cameras with high contrast.

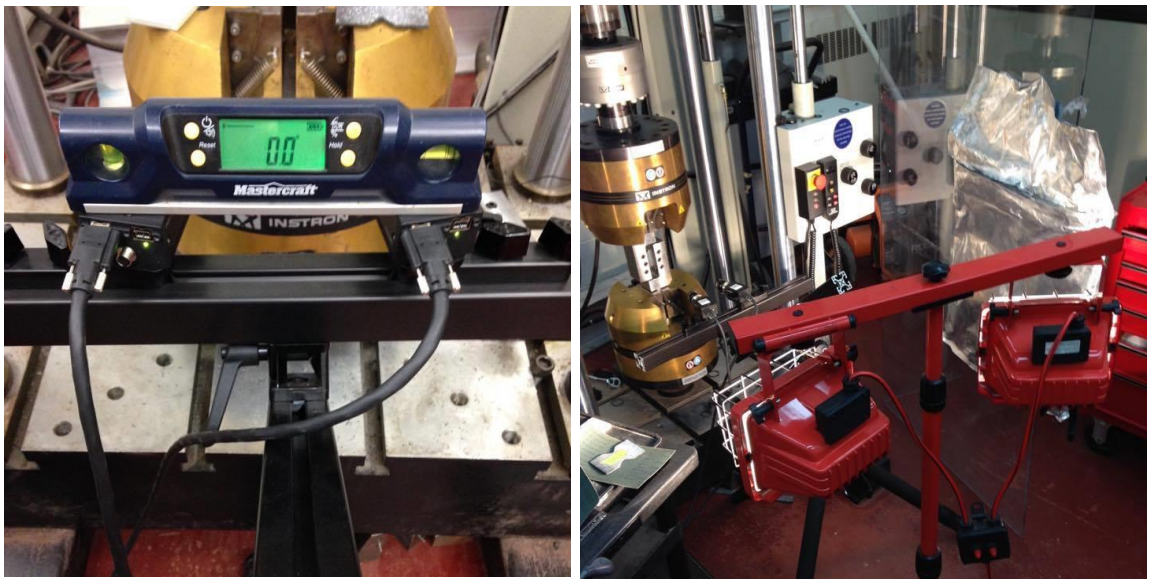

Figure 3.9 - Digital level used to align cameras and ensure the DIC axis match the fixture and specimen axis, and flood lights to highlight the speckle pattern

3.2.5 Procedure

The ASTM Standard D7078 was followed except for following the recommended bolt torques. The recommended 55 [N-m] bolt torque allowed the specimen to slip, so a higher bolt torque of 60 [ftl-lbs] or 81.33 [N-m] was necessary to completely stop specimen slippage. Iosipescu Shear tests were carried out as outlined in Section 3.1.4.4 This increase in bolt torque could cause a large error in the obtained shear strength value.

Chapter 4

4 Results and Discussion

The following chapter is broken into two sections: section 4.1 summarizes and discusses the results of the first set of experiments which classify the mechanical properties of two fabrics, while section 4.2 summarizes the findings from the shear test comparison experiment.

4.1 Mechanical Property Classification

Mechanical properties of two composite fiber materials defined in Section 3.1.1 were characterized through ASTM standardized coupon testing A full list of the obtained properties are in Appendix B and include: Tensile, Compressive, and Shear Moduli; Poisson's Ratios; Tensile and Shear Failure Strain; Tensile, Compressive, Shear and Flexural Strength. Properties are found through the following load angles: 0^o, 45^o and 90^o to see any load angle dependant trends. The 22.5^o load angle was also added for some tests where extra material allowed.

Classification required tensile, compressive, flexural and shear testing. The results of those tests and a discussion of these results are presented in the following sections. Notably, Fabric OR shows high orthotropy as expected, with a slightly stronger 90-degree direction. This is expected given that there are 50% more fibers in the 90-degree direction than the 0-degree direction (3 vs 2 layers). In comparison Fabric QI shows much higher isotropy having a quasi-isotropic layup.

4.1.1 Tensile Test

The results for each loading angle are shown graphically in

Figure 4.2 through Figure 4.5. For all tensile tests except for the 22.5-degree and 45-degree load angles on Fabric OR, the tensile specimens showed brittle stress-strain curves

where the yield strength and ultimate tensile strength were equivalent. In these cases, where the stress-strain curve is linear, the Young's modulus was determined not to significantly differ for a selection of modulus ranges. Therefore, only the 22.5-degree and 45-degree specimen for Fabric OR required choosing an appropriate range for deriving the tensile modulus, which is from 0.1% to 0.3% as defined by ASTM 3039. Examples of typical stress-strain curves for both fabrics are plotted in **Error! Reference source not found.** and **Error! Reference source not found.**.

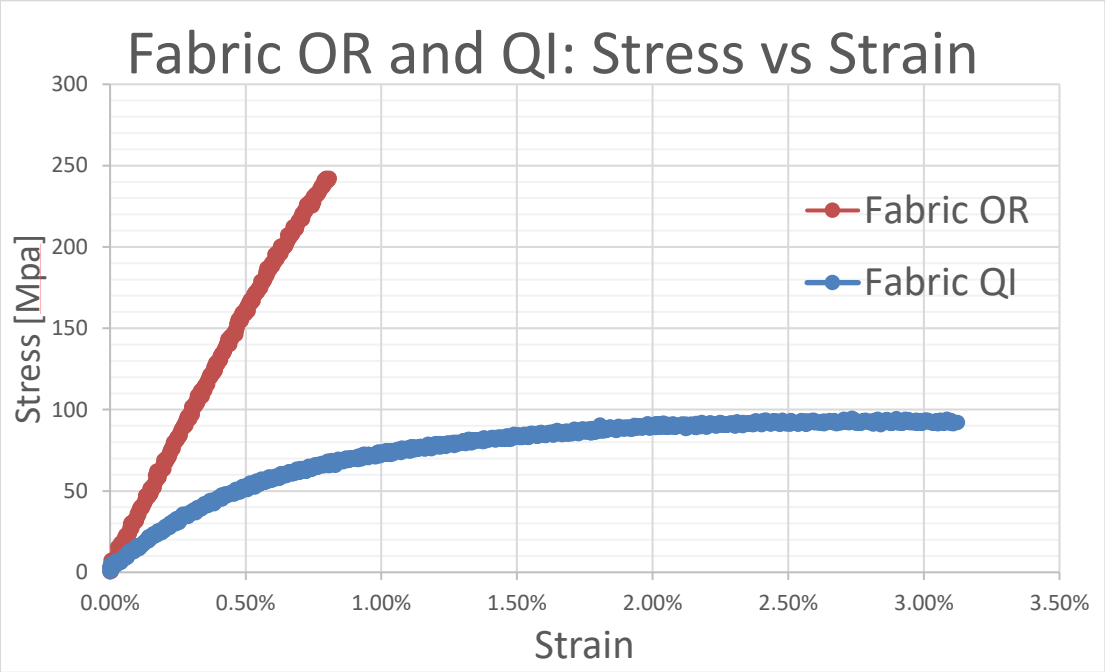

Figure 4.1 - Typical Stress-Strain curves for Tensile Specimen

Using classical laminate theory as outlined in section 2.3.1, the Young's modulus of Fabric QI was expected to be 40.39 GPa for all load angles. This value is agreeable for the 0-degree and 90-degree directions, however there is over 20% error for the 22.5-degree and 45-degree directions. A possible reason for this is in the 22.5-degree direction there are no fibers that reach both fixtures and so the specimens are subjected to end conditions which may allowed the fibers to have a high degree of rotation. For the 45-degree load direction, the outside layers of the fabric were perpendicular to the load path, and therefore may not have been able to transfer load efficiently to the inner layers of the

specimen. A similar phenomenon can be noted for the ultimate tensile strength of Fabric QI.

For Fabric OR, the results varied considerably by load angle as expected. For the 0-degree and 90-degree directions, the results follow predictions from classical laminate theory. For the 22.5-degree and 45-degree load angles though, the stiffness values are higher than expected. Poisson's ratio follows inversely where the lateral modulus resists the axial modulus. So, for example in Fabric OR, in the 0-degree and 90-degree directions, there are a high amount of lateral fibers to resist contraction in the lateral direction and therefore the Poisson's ratio is close to zero.

For Fabric QI, tensile strength was estimated as the force required to break the specimen, on the assumption that the 0-degree fibers would be the last to fail. This estimate proved to give reasonable results for the 0-degree and 90-degree direction but diverge for the 22.5-degree and 45-degree specimen by over 30%. A potential cause was where the 0-degree layers were in the layup.

For Fabric OR, a similar theory was applied for the 0-degree and 90-degree load cases which produced agreeable results. For the 45-degree load case, shear failure in the matrix occurred. Without the fibers terminating in the grips, the fibers did not need to fail for the specimen to fail, which is why the shear failure strength value was used as an estimate. A similar estimation was used for the 22.5-degree load case however the results were less accurate.

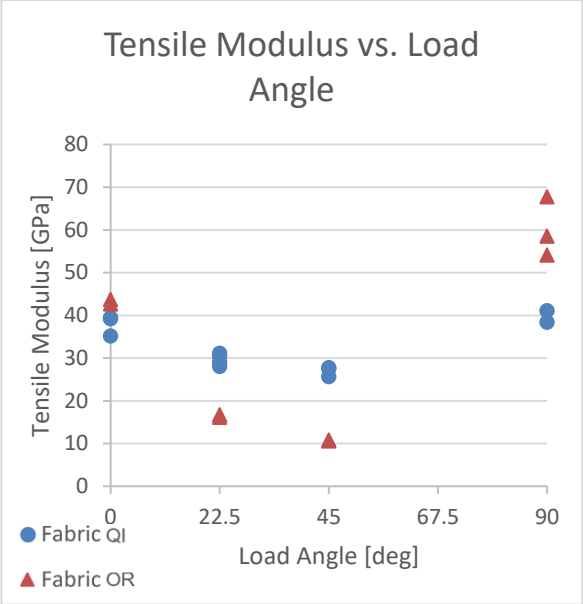

Figure 4.2 - Tensile Modulus vs. Load Angle

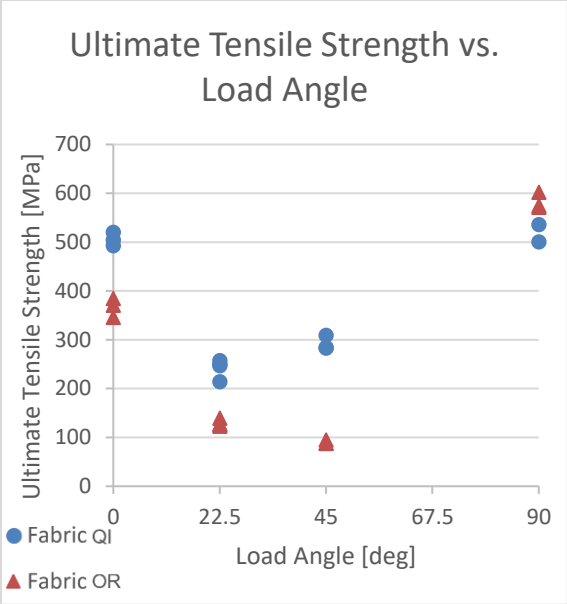

Figure 4.3 - Ultimate Tensile Strength vs. Load Angle

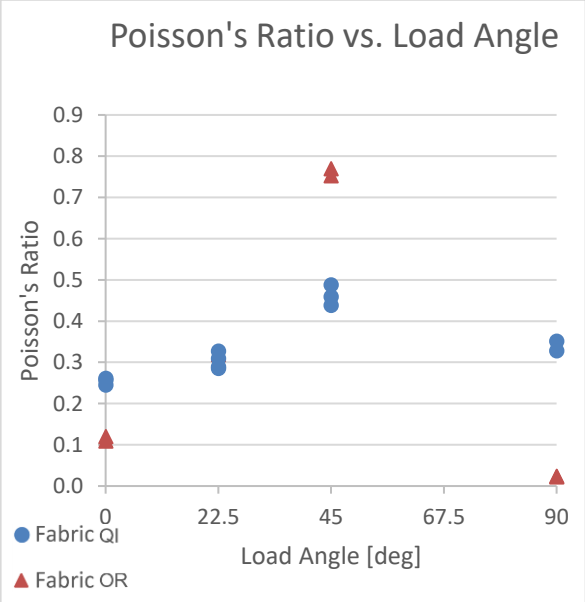

Figure 4.4 - Poisson's Ratio vs. Load Angle

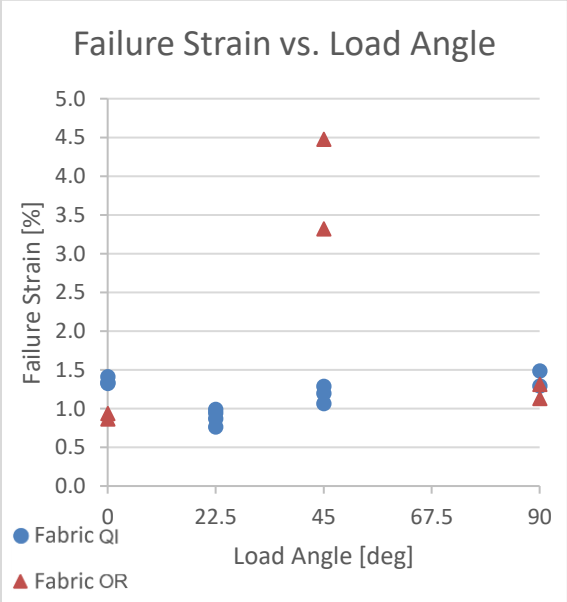

Figure 4.5 - Tensile Failure Strain vs. Load Angle

Figure 2.16 from the literature review describes the general trends for the Poisson's ratio of a single-ply, cross-ply or orthotropic (0/90) and quasi-isotropic laminate. A quasi-isotropic lamina is expected to have a constant Poisson's Ratio across al load angles of about 0.3, The crossply laminate follows an inverse cosine-like trend with a Poisson's

Ratio close to 0.1 at 0 and 90-degrees, and reaching a maximum of about 0.7 at 45-degrees. Poisson's Ratio was obtained through DIC measurement which simultaneously measure both axial and transverse strains.

For Fabric QI, the Poisson's ratio was estimated to be 0.317 for all load angles based on the CLT formula: $v_{xy} = -\underline{S}_{12g}E_x$. The value obtained for the 45-degree angle diverged the most from this theoretical value, but it is unclear why. For Fabric OR, Poisson's ratio was found to be agreeable for the 0, 45 and 90-degree load cases.

Failure strain was predicted by estimating the stress-strain curve to be completely linear for Fabric OR in the 0 and 90-degree directions since it should behave in an elastic brittle manner. It was also estimated to follow the predicted Young's modulus over the entire stress range, up to the estimated tensile strength. Error in these estimates could arise due to an error in the theoretical prediction of the Young's modulus or ultimate strength, or additionally with the knowledge that the stress strain curve is not perfectly linear. Predictions were therefore lower than the actual failure strain. An exception in the predictions was made for the 45-degree load case of Fabric OR since it was expected to haver a non-linear stress strain curve. In this case, failure strain was predicted through multiplying the volume fraction of resin and the failure strain of the neat resin, which assumed that failure ultimately occurs when the resin fails, long after fiber failure.

For physical testing, none of the materials had any negative local modulus, so failure was defined at the point of ultimate strength. Most of the specimens failed in the gauge area and therefore it was determined that adding tabs was not required, especially for non-unidirectional laminates. Table 4.1 classifies the type of failure. All but two failed in the gauge, and most failed at an angle except the 0-degree and 90-degree loads for Fabric OR which is to be expected. The specimen that failed at an angle usually followed then angle of one of the plies. Figure 4.6 on the following page shows the Typical Tensile Specimen after testing.

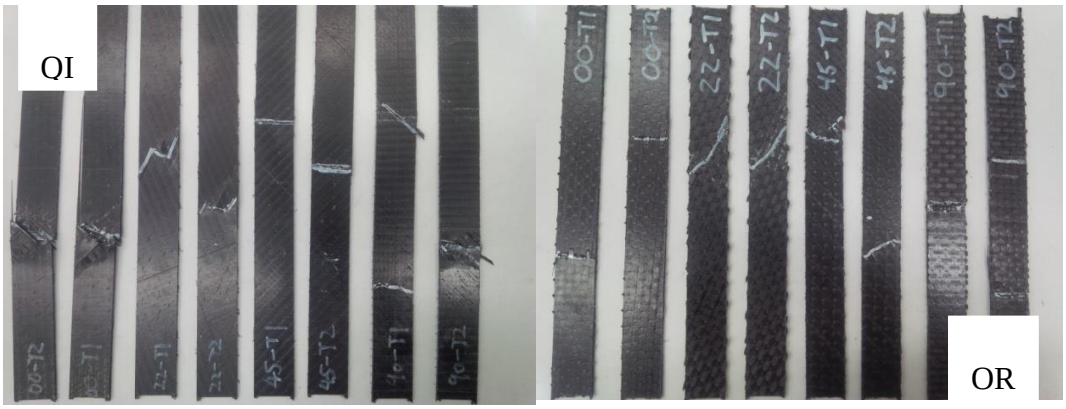

Figure 4.6 - Typical Tensile Specimens after testing

Table 4.1 - Tensile Specimen Failure Categorization

	0°		22.5°		45°		90°	
	T1	T2	T1	T2	T1	T2	T1	T2
Fabric QI	AGM	AGM	AGM	AGM	LAT	LGM	AAT	XGB
Fabric OR	LGB	LGT	AGT	AGT	AGT	AGM	LGM	LMV

Table 4.2 - Tensile Specimen Failure Categorization Legend

First Character

Failure Type	Code
Angled	A
edge Delamination	D
Grip/tab	G
Lateral	L
Multi-mode	M(xyz)
long. Splitting	S
eXplosive	X
Other	O

Second Character

Failure Area	Code
Inside grip/tab	I
At grip/tab	A
<1W from grip/tab	W
Gage	G
Multiple areas	M
Various	V
Unknown	U

Third Character

Failure Location	Code
Bottom	B
Top	T
Left	L
Right	R
Middle	M
Various	V
Unknown	U

Analysis of the tensile specimen using DIC shows that although the stress state is supposed to be perfectly uniform in tension, there are areas of higher and lower strain which can be seen in Figure 4.7. For the pictured specimen, A1-00-T2 was about to fail. The average strain in the image is 1.33%, however some small concentrations, shown in red, are at 1.51% strain and may have caused a premature failure. This means that if the concentrations were caused by a manufacturing error, the material may in fact be able to handle up to 1.51% strain with proper manufacturing or other applications. However, it will only r eport a failure strain of 1.33% (11.3% error). The reason for the stress concentration is of importance. If it is purely a result of post processing for the test specimen, then the 1.51% could provide a truer picture of the specimen ultimate failure strain. However, if it is a defect inherent to the materials or

manufacturing technique, then the 1.33% strain is more important as an overall failure strain.

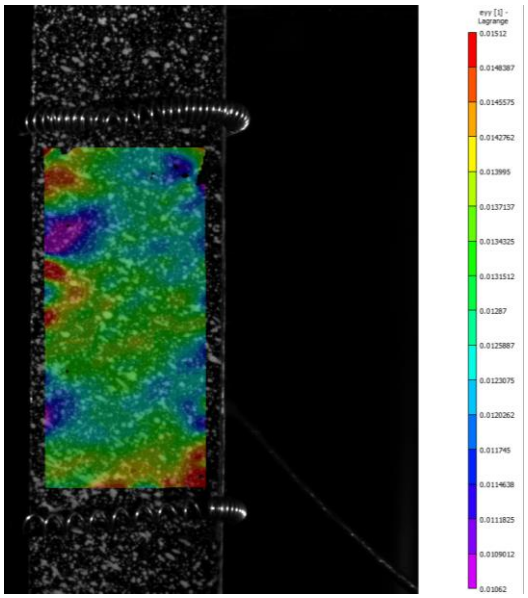

Figure 4.7 - Strain Distribution over tensile specimen A1-00-T2 under loading (Range shown: 1.062% in Purple to 1.512% in Red)

4.1.2 Shear Test

The results for each loading angle are shown in Figure 4.8 and Figure 4.9. All the shear tests bottomed out and therefore the strength values should be taken only as a lower limit to the achievable ultimate shear strength. The difficulty in bringing shear specimens to failure, coupled with the difficulty in shear strength prediction gave rise to high error between theoretical and actual values. As stated in section 2.3.3.3, a possible estimate for shear failure is based off a shear concentration factor to be applied to the shear strength of the matrix material. A concentration factor of 1.7 was used, coinciding with a 40% volume fraction. Estimates therefore ranged between 1% and 25% error. Values for Fabric QI should have been the same for all load angles, but had a 20% variation in error. A similar 25% range in error was found for Fabric OR which should have produced the same shear strength in the 12-plane and 21-plane.

For the shear modulus, results were consistent within reason for all but the 45-degree case for Fabric OR in comparison to theoretical predictions. The best predictor of shear modulus came from the equal shear strain equation, rather than equal shear stress or the Halpin-Tsai model. Both the equal stress and Halpin-Tsai model provided values that were too low by a factor of two in comparison to the obtained values through testing.

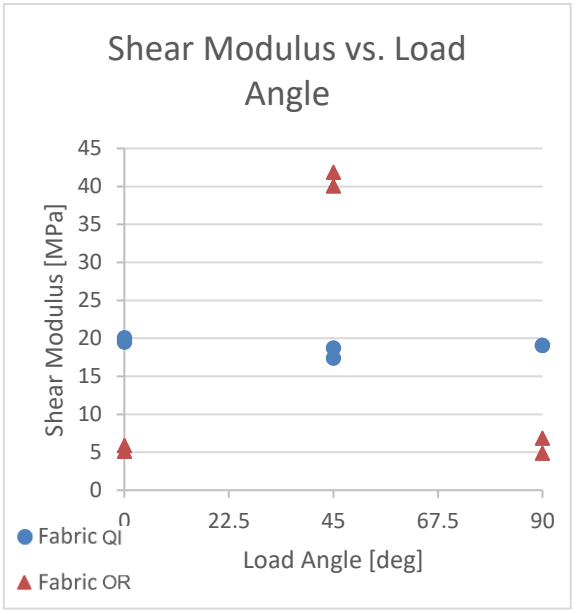

Figure 4.8 - Shear Modulus vs. Load Angle

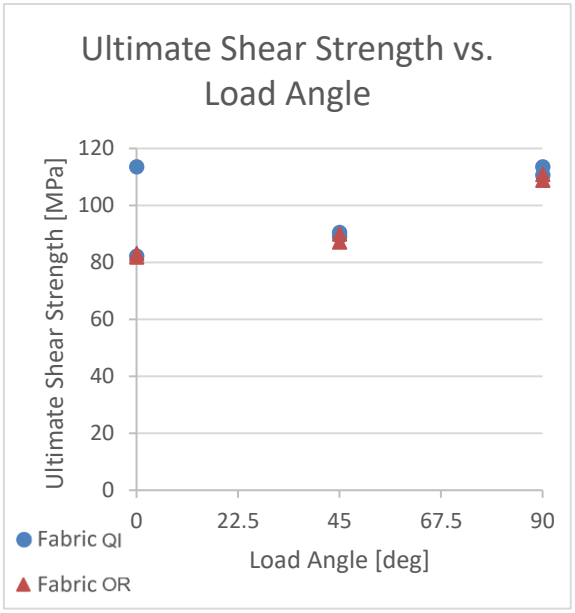

Figure 4.9 - Minimum Ultimate Shear Strength vs Load

Figure 4.10 depicts the specimen after loading. It is apparent that ultimate failure has not occurred in the specimen.

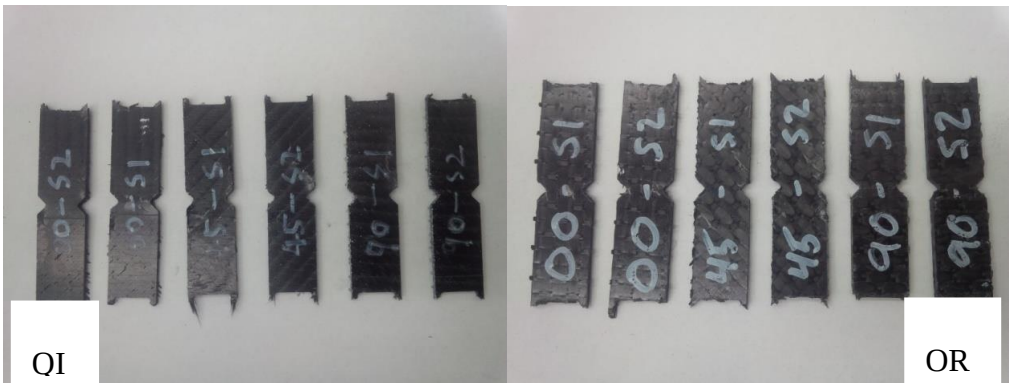

Figure 4.10 - Typical Shear Specimens after being loaded in shear

4.1.3 Compression Test:

The results for each loading angle are shown in Figure 4.11 below. Fabric QI should have produced the same results, however as stated in the literature review, it is difficult to predict compression strengths. This is because the failure mode relies on multiple interrelated characteristics including location of 0-degree plies. If this were the case, both 0-degree directions for Fabric QI and OR should have produced the highest strength but only produced the second highest strength. Figure 4.11 depicts the compression specimen after failure, all within the gauge area.

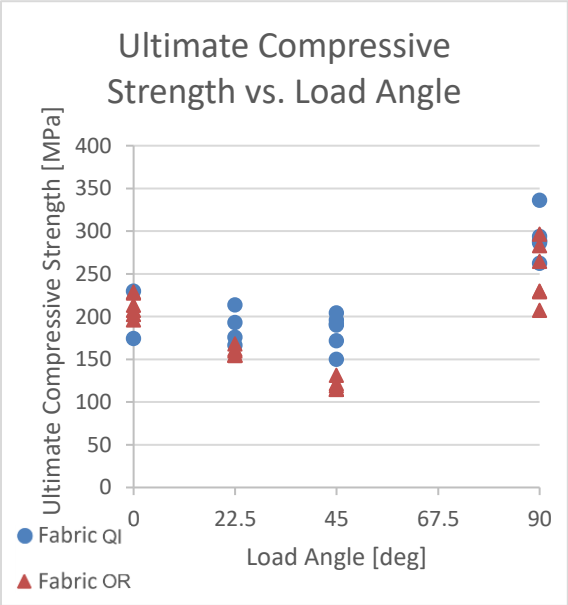

Figure 4.11 - Ultimate Compressive Strength vs. Load Angle

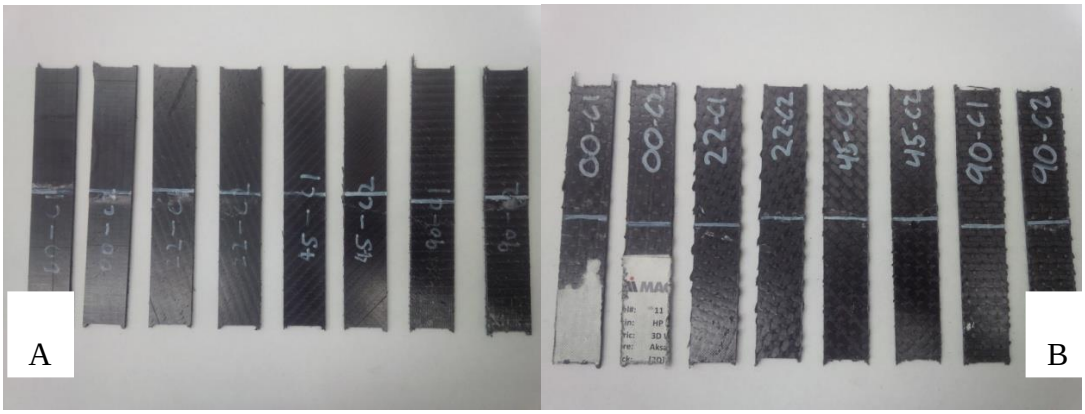

Figure 4.12 - Typical compression specimen after subjected to compression loading

4.1.4 Flexure Testing:

The results for each loading angle are shown in Figure 4.13 below. As with the compression testing, flexural results are difficult to predict, especially with such thin components. Theoretically, the specimen with the greatest number of 0-degree plies from the neutral axis should be the stiffest, but the strength could depend more on the compressive strength of the top layer. All the Fabric OR specimens tested at 45-degrees reached the limit of the fixture. Therefore, the shown strength is a lower bound of the ultimate flexure strength.

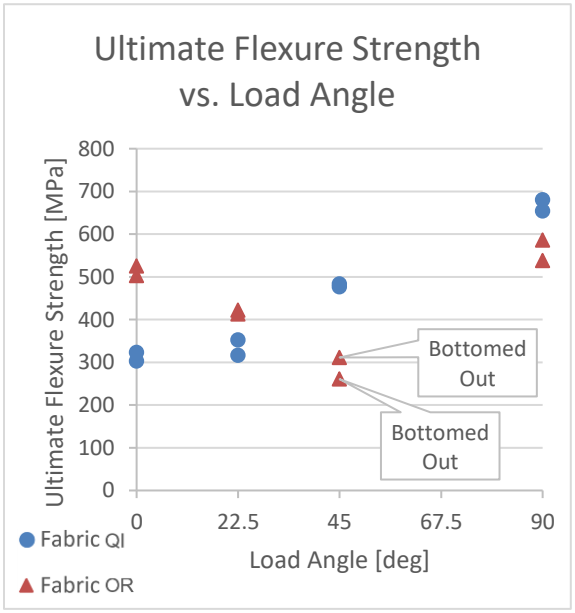

Figure 4.13 - Ultimate Flexural Strength vs. Load Angle

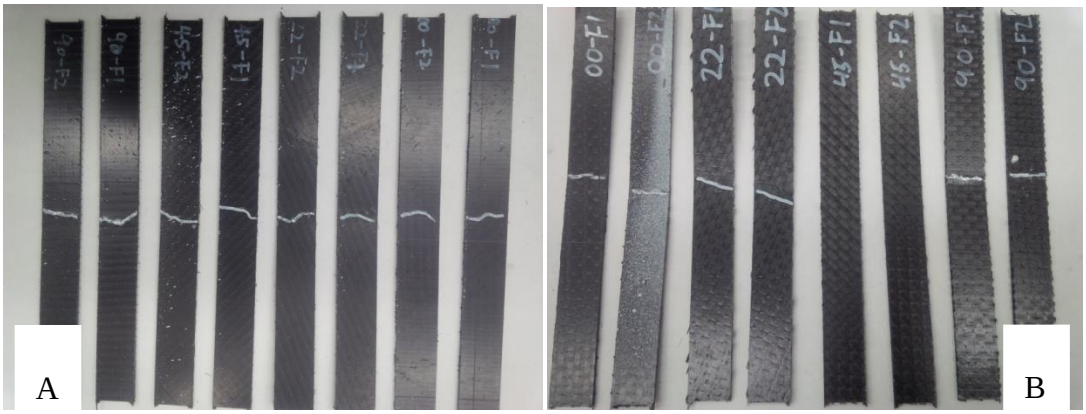

Figure 4.14 - Typical Flexure specimens after flexure loading

4.2 Shear Test Comparison

There are two components to this shear test comparison. First, a comparison is made between theoretical predictions and experimental results. Second, a comparison of the experimental results obtained through DIC to the FEA results generated in this thesis, as well as the numerical models created during the development of ASTM Standard 7078.

The purpose for the shear testing portion of this study was to understand the mechanisms involved with the deformation of composites in standard shear loading conditions. Since the Iosipescu Shear test method could not adequately bring high-strength composite specimens to failure, the V-Notched Rail Shear test method was implemented to investigate if an improvement existed over the Iosipescu Shear test. An improvement would consist of meeting any the following three goals:

1. Increase in maximum applied load without unwanted deformation
2. Increase in purity of shear stress
3. Increase in uniformity of shear stress

Typical stress-strain curves are shown in Figure 4.15 and Figure 4.16, with a complete set of stress strain curves for both the 0/90-degree and ±45-degree laminates from the V-Notched Rail Shear and Iosipescu Shear fixtures included in Figure 4.17 and Figure 4.18.

Initial tests using the V-Notched Rail Shear fixture were attempted at 41[Nm] of bolt torque, which would produce the highest shear strength value based on Figure 2.35. However, the 0/90 specimens rotated in the fixtures and needed to be reset. The test was attempted again at the 55 [Nm] torque recommended by the standard. Initial DIC analysis showed that some of the specimens slipped at high loads. The two specimens where this occurred can be seen in Figure 4.17 reaching a near constant force up to 6% strain before the test was stopped. Bolt torque was then further increased to the next available torque setting of 60 [ftl-lbs] or 81.33 [N-m] for the remaining 0/90-degree and ±45-degree tests.

The remaining 0/90-degree specimens did not slip in the grips and failed closer to 3% strain but also at a lower ultimate strength value.

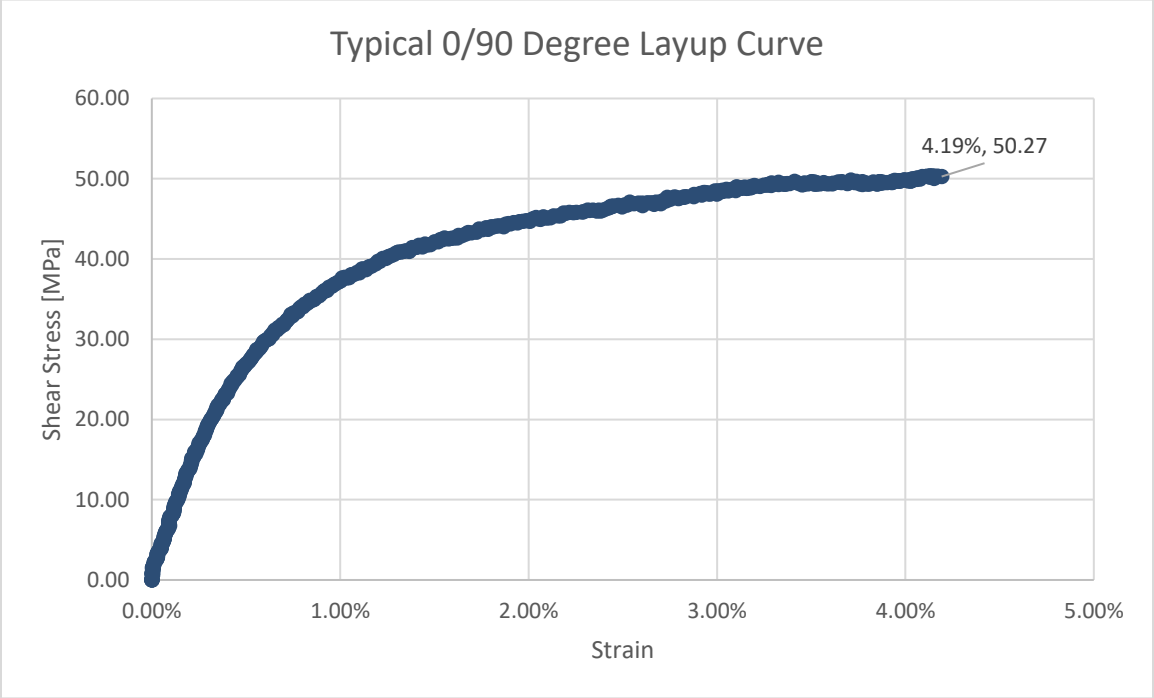

Figure 4.15 - Typical 0/90-Degree Layup Stress Strain Curve (Specimen I90E)

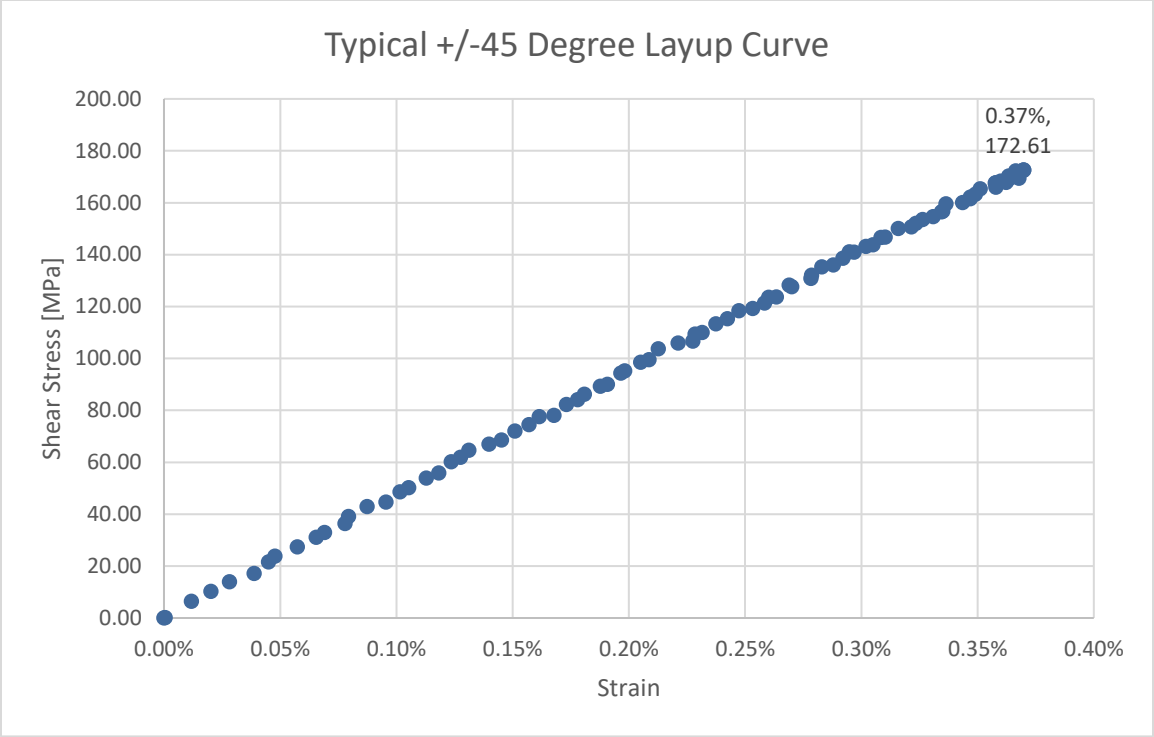

Figure 4.16 - Typical ±45-Degree Layup Stress-Strain Curve (Specimen V45D)

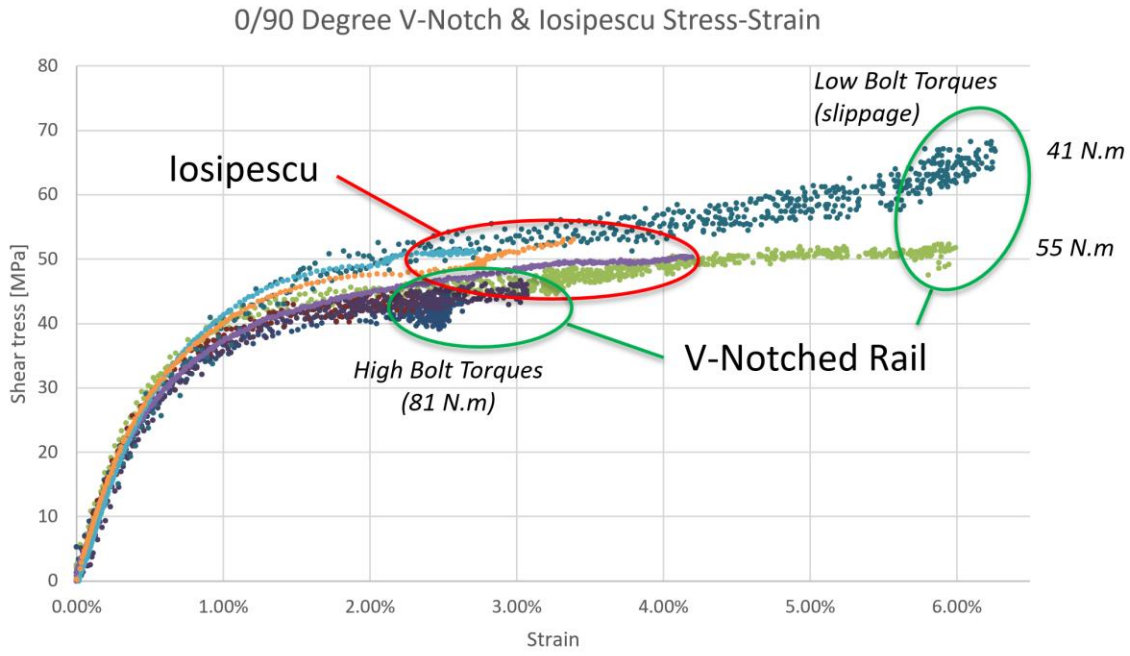

Figure 4.17 - All 0/90-degree Stress-Strain Curves for the V-Notch & Iosipescu Tests

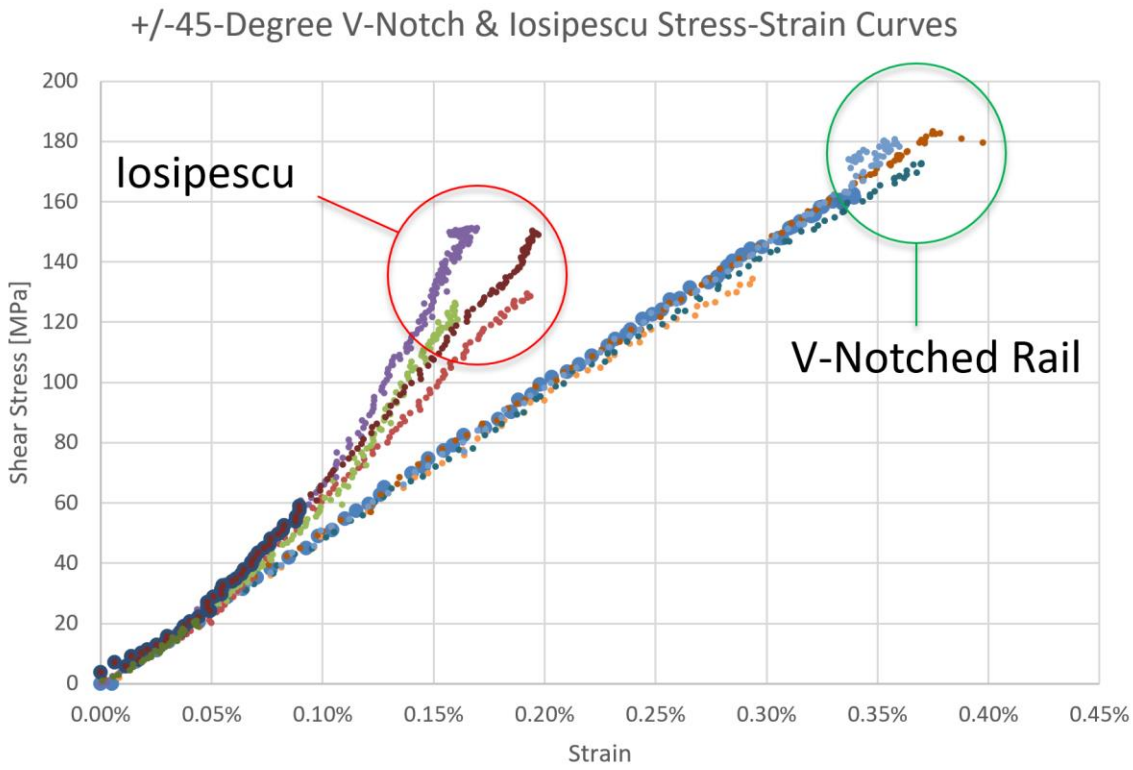

Figure 4.18 - All ±45-degree Stress Strain curves for V-notch & Iosipescu Tests

The data in Table 4.3**Error! Not a valid bookmark self-reference.** was generated following the standards set out by ASTM standard 7078 for the ±45-degree specimen and 0/90-degree specimen labelled V45 and V90 respectively. The results from the tests which following ASTM standard 5379 are similarly labelled I45 and I90. The table includes the averages, standard deviations, and coefficients of variation as well as a theoretical prediction and the error between the theoretical and actual values obtained.

Table 4.3 - Comparison of results between V-Notched Rail Shear and Iosipescu Shear tests for ±45 degree and 0/90-degree layups

		V45	I45	V90	I90
Samples (n)		5	5	5	5
Shear Modulus [GPa]	Theoretical*	51.04	51.04	4.72	4.72
	Average	47.97	48.48	4.68	4.73
	Error	-6%	-5%	-1%	0%
	Standard Deviation	1.63	1.96	0.31	0.37
	Coefficient of Variation	3.39	4.03	6.61	7.76
0.2% Offset Strength (Yield) [MPa]	Theoretical*	-	-	31.30	31.30
	Average	-	-	29.38	32.24
	Error			-6%	3%
	Standard Deviation	-	-	7.27	5.63
	Coefficient of Variation	-	-	24.75	17.45
Ultimate Strength [MPa]	Theoretical*	217.20	73.88	52.24	52.24
	Average	167.49	76.22	51.76	52.86
	Error	-23%	3%	-1%	1%
	Standard Deviation	18.09	5.78	10.07	0.69
	Coefficient of Variation	10.80	7.58	19.46	1.31
Failure Strain	Theoretical*	0.328%	0.145%	3.990%	3.990%
	Average	0.361%	0.175%	4.636%	4.217%
	Error	10%	21%	16%	6%
	Standard Deviation	0.02%	0.02%	2.05%	2.02%
	Coefficient of Variation	6.88	8.89	44.22	47.91
Load Cell		250KN	5KN	250KN	5KN

* Derivation of theoretical results described in 4.2.1 Discussion of Experimental Results

4.2.1 Discussion of Experimental Results

From Table 4.3 the following conclusions have been made.

Shear Modulus Comparison

The 0/90-degree specimen results agreed with the theoretical value calculated using the rule of mixtures for the shear modulus G_{13}.

The ±45-degree specimen differed from the predicted value slightly. Both the V-Notched and Iosipescu values for Young's modulus were 3 to 4% lower than predicted. Both standards called for taking the modulus measurement between 0.15% and 0.55% strain, however all the specimens failed before 0.55% and most of the Iosipescu specimens failed around 0.15%. For the ±45-degree specimens, the 0.05% to 0.20% range was used for the calculation of Young's modulus. For the Iosipescu specimens, the 0% to 0.05% range was used since the modulus increased quite rapidly during the +/-45-degree Iosipescu tests.

Possible sources for the discrepancy between predicted and obtained values could be from the strain range chosen. But a more likely cause was the inaccuracy of the volume fraction used in the theoretical calculation. Fiber volume fraction was calculated using the fibre and matrix densities, fibre weight, and final composite density. The calculation for composite density included measurement of the plate thickness. For instance, a 0.125mm discrepancy in thickness results in a 5.1% error, or 2.12% in absolute percentage, in volume fraction and consequently an 4.6% error in the theoretical Young's modulus. These results are summarized in Table 4.4.

Table 4.4 - Sensitivity of Shear Modulus to Volume Fraction

Measured Thickness (mm)	Volume Fraction	Calculated Shear Modulus [MPa]	% error in Shear Modulus
2.375	42.43%	26.82	5.1%
2.500	40.31%	25.52	-
2.625	38.39%	24.35	4.6%

It is also possible that the predicted stress distribution was different than expected and that the Area of Interest (AoI) chosen for DIC strain measurement was inappropriate.

The rapid increase in modulus for the Iosipescu test may be due to the non-linearity of the test. As shown in Figure 4.20 and discussed below, the Iosipescu Shear specimen undergoes simple shear, rather than pure shear, which may lead to the exponentially increasing stress vs strain. Results for the shear modulus of both layups with both test methods were quite consistent.

0.2% Offset (Yield) Strength

The ±45-degree specimens exhibited no signs of plastic deformation having failed in a completely brittle manner, and therefore the yield strength and the ultimate strength were the same.

For the 0/90-degree specimens, yield occurred at roughly half the ultimate shear strength. The obtained value has a relatively large standard deviation due to varied shear moduli and differences in the knee in the stress strain curve. Furthermore, since the V90 tests were carried out using the 250KN load cell, it was difficult to minimize zero offset error. This error is easy to see in the large coefficient of variations in the yield strength as well as ultimate shear strength in comparison to the Iosipescu tests. This study recommends that specimens with a low percentage of ±45 fibres should be tested with the 5KN load cell to reduce noise in the results.

Ultimate Strength

The ultimate strengths obtained through testing are off by a considerable amount. For the 45-degree Iosipescu testing, it is important to note that none of the specimens reached failure because of fixture limitations. Therefore the 76.22 [MPa] strength value only represents a lower bound.

From the numerical analysis shown in Figure 4.19 that stress concentrations form at the notch tips which can be in the range of 10%-20% greater than the normal shear stress in the gauge area. This means that a crack could begin to develop at a stress which is 20%

lower than expected and propagate through the specimen. Stress concentrations such as these make it difficult to predict what the actual stress might be at their location. Additionally, any differences in the manufacturing of the area around the notch tip, such as a reduced radius, could have caused even larger stress concentrations.

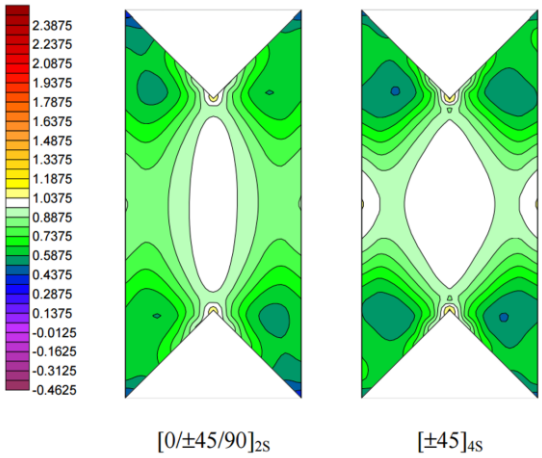

Figure 4.19 - Stress Concentration at Notch Tips (Adams, Moriarty, Gallegos, & Adams, 2003)

Further examination of the failure modes was necessary to better understand and predict the failure stress. The mechanism that dictates failure for the ±45-degree specimen was very different from the 0/90-degree specimen.

For the ±45-degree specimen, the fibers perpendicular to the principal tensile axis failed from a transverse load to the fiber direction. At this point, the layers in the axial tensile direction carried 100% of the load in simple tension. Consequently, the shear strength was simply the resolution of forces in the 45-degree direction to the load direction.

For the 0/90-degree specimens, the fibers in the 0-degree direction failed first since they were unbounded at their edges. The 90-degree fibers were clamped between the fixtures and although the matrix between the fibers may fail, the fibers themselves simply rotated to align themselves with the principal tensile direction. Because of the fixture geometry, as the fixtures moved apart, the specimen began to shear into a parallelogram. This means that instead of a pure shear stress state, the final stress state also involved rigid body

rotation, as well as tension and compression as shown in Figure 4.20. In pure shear, the total gauge area would remain the same. For simple shear, the specimen also experiences tension and compression as it is constrained by the fixture geometry. As shown in the Mohr's circle diagram of Figure 4.20, simple shear has a lower strength for a given shear load because of the additional tension and compression.

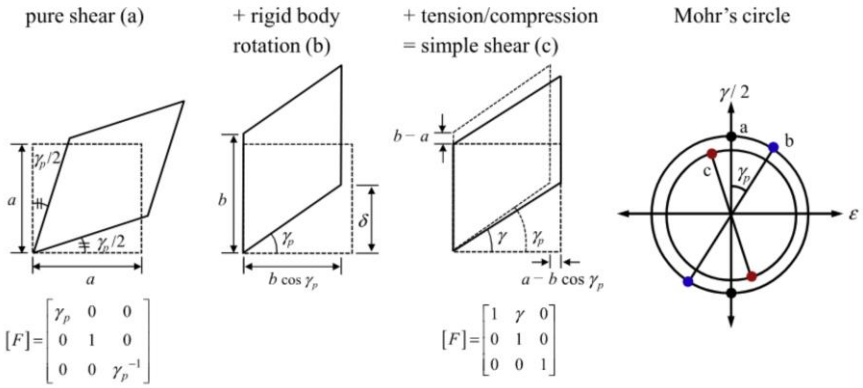

Figure 4.20 – Comparison of pure shear vs simple shear (Rickhey, Kim, Lee, & Kim, 2014)

The simple shear caused the 90-degree fibers to lengthen, inducing a tensile stress as shown in Figure 4.21. When this stress reached the axial limit of the fibers, the specimen ultimately failed in tension. This tensile strain can be represented by:

$$\varepsilon = \frac{l_2 - l}{l} \text{ where } l_2 = \sqrt{l^2 + \Delta l^2}$$

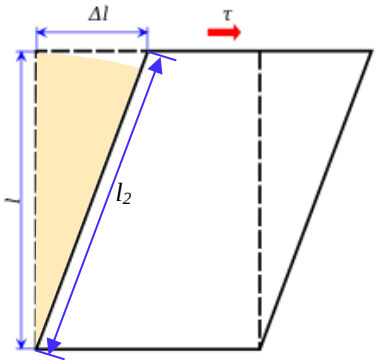

Figure 4.21 – Simple shear within failure area [edited] (Krishnavedala, 2012)

Here, 'l' represents the specimen gauge width, and 'Δl' represents the cross-head displacement. This conclusion should lead to a simple formula where the ultimate shear

strength for this test is simply defined by the axial strength of the fibers knowing the length change is from the crosshead displacement. However, this shearing effect only occurs in the fiber area where the 0-degree fibers failed. Figure 4.22(a) shows an overlay of the specimen at the start and end of the test. The red outlines show the movement of the specimen over the test. Particularly, the only part of the specimen which deformed is highlighted in red. This is the same section as the area in Figure 4.22(b) which shows the top layers peeled back off a 0/90-degree specimen to reveal the broken 0-degree fibers. Three tows were pulled back and it is evident in Figure 4.22(c) that the fibers failed at the edges of the middle tow. The unbroken 0-degree fibers held the 90-degree fibers in place and stopped them from rotating. This means that it is possible that the change in fiber length only occurred in the small width represented by the red area.

The width of the area of broken fibers is approximately 6 mm. The failure strain of carbon fiber is 1.7% which means that if the fixture extended 0.102 mm, this ultimate failure strain would be reached, and the fibers would have failed. However, it is possible the fixture itself could bend in response to this force. It is also clear that the crosshead moved more than 0.102 mm, it is likely that the fibers did not only move in the red area.

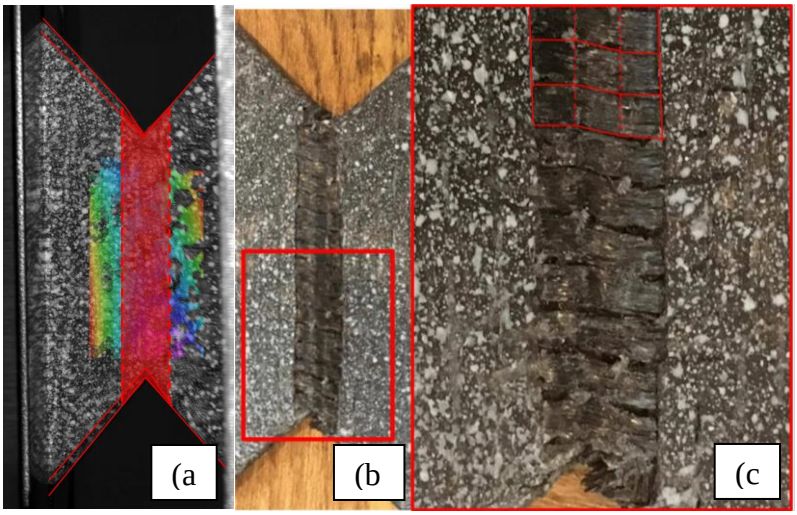

Figure 4.22 - Broken fibers in section where parallelogram effect occurs

4.2.2 FEA and DIC Analysis

The objective for the finite element simulations in this study was to determine the stress-strain contours present within the test specimen and compare to both the values provided by the standard, in addition to experimental data obtained through DIC images in physical testing. These comparisons aided in validating the mechanical testing. The goal was not to provide absolute value predictions over the entire stress-strain curve, but rather general trends and comparisons between different test methods.

Simulations were undertaken using the built in FEA component of SOLIDWORKS by Dassault Systemes. First, an isotropic material model was created to ensure that the FEA parameters were representative of the physical testing, and that the software would provide the expected property values. Both the Iosipescu and V-Notched specimens were represented as half specimens with the middle plane along the loading axis modelled as a symmetry plane to simplify the model. This symmetry plane was constrained to only deform along the loading axis.

Based on the isotropic results, the model was then converted to a simplified 2D composite laminate with the same layups as the tested fabrics. Each layer was made to be anisotropic by assigning appropriate E_1 and E_2 value as predicted from calculations. Mesh optimization was done manually. A convergence study was not utilized since the FEA study was only of a comparative nature between test methods.

For the V-Notched FEA model, the faces which would be gripped by the Instron tabs were fixed, and a pressure was applied to simulate the gripping load, in case this introduced significant stresses into the gauge area. A load was applied parallel to the symmetry face to simulate the load transferred through the specimen from the Instron machine.

After running the model, the purity and uniformity of the through-thickness strain field was checked and displayed in Figure 4.23. Analysis showed that there was variation in the through-thickness direction. Further analysis was carried out using the 2D approximation method for composites and did not reveal the exact extent of this through-thickness effect. It is possible that the through-thickness effect could have produced stress concentrations. These stress concentrations could have caused premature failure and may have not been detected by strain gauges or a DIC system.

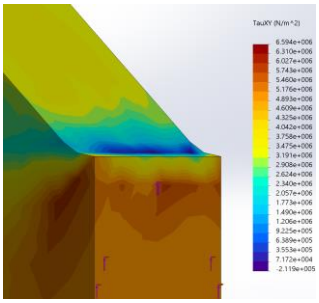

Figure 4.23 - Through Thickness Strain

Digital Image Correlation was the measurement tool used for determining the strain within a specimen. As discussed in Chapter 3, specimen surface preparation was very important in creating a surface which provided a complete and clear picture of the strain distribution. Figure 4.24 shows a comparison of glare and loss of data when the surface of each specimen was left untreated compared to a lightly wet-sanded specimen. All subsequent specimens were lightly sanded with a 350-grit sand paper to improve the quality of results.

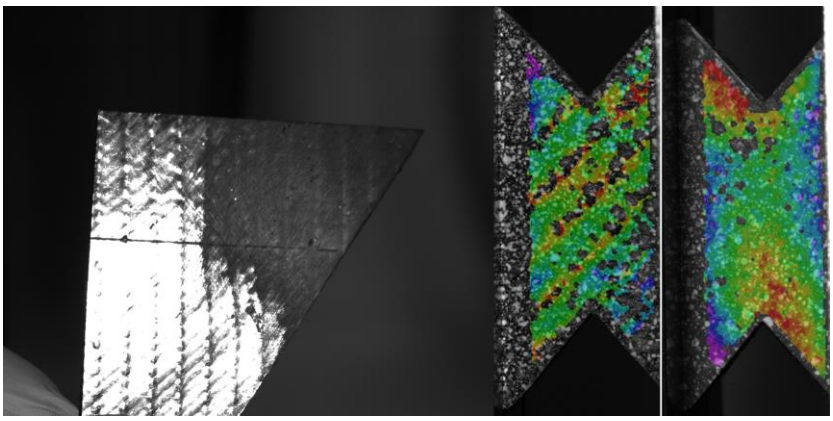

Figure 4.24 - Comparison of un-sanded (glossy) and sanded (matte) surface finishes.

Initial analysis of the images obtained through DIC show the very different strain field between the 0/90-degree layup specimen shown in Figure 4.25(a) and the strain field in

Figure 4.25(b). The strain fields obtained through DIC had a slight offset to them which could have been caused by the geometric non-linearity in the fixture.

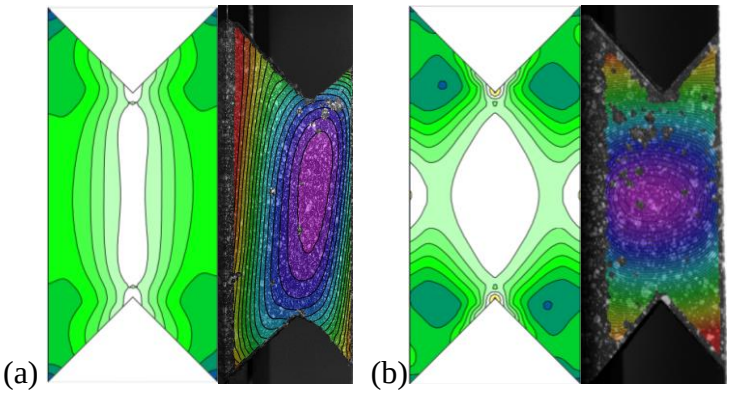

Figure 4.25 – Strain field shape comparison for (a) 0/90 layup and (b) ±45 layup. FEA Results from (Adams, Moriarty, Gallegos, & Adams, 2003).

Similarly, the strain fields were different between the Iosipescu specimen layups. The 0/90-degree layup contour is shown in Figure 4.26. It has a uniform pattern radiating out from between the notch tips. This pattern is different from the pattern seen in Figure 4.27 for the ±45 layup where the largest stress occurs between the two loaded points on the fixture along the 45-degree axis, and radiating outwards linearly.

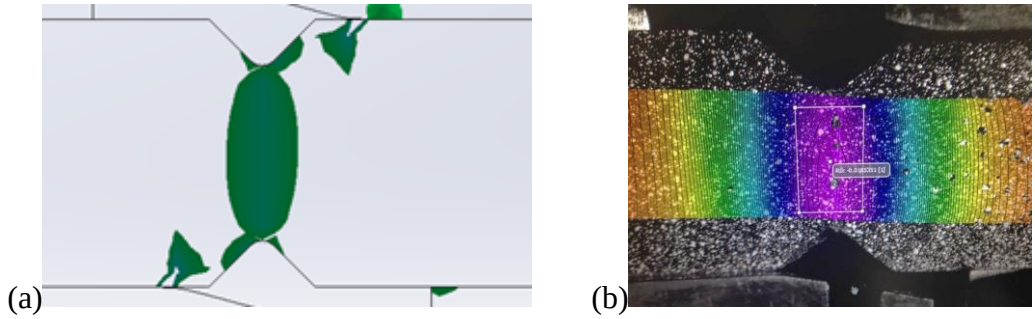

Figure 4.26 – FEA results of a 0/90 layup between 80% and 120% of expected Average shear stress and corresponding DIC strain contour

(a) 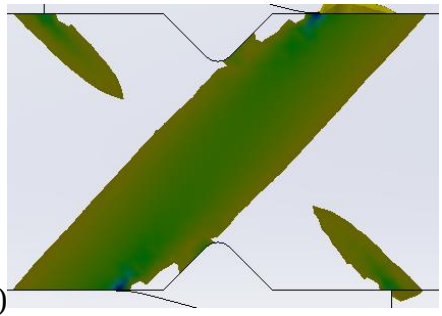 (b) 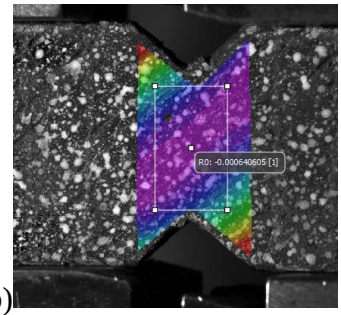

Figure 4.27 – (a) FEA results of ±45 layup between 80% and 120% of expected average shear stress and DIC Results, and corresponding DIC strain contour

A primary objective of the FEA studies was to determine the purity and uniformity of the shear stress in the specimens. Figure 4.28 shows that the von Mises stress was much greater than the shear stress. This means that the stress in the specimen was not pure shear, and therefore ultimate strength results could have been skewed because of the effect of axial and transverse stresses as predicted in Chapter 2.

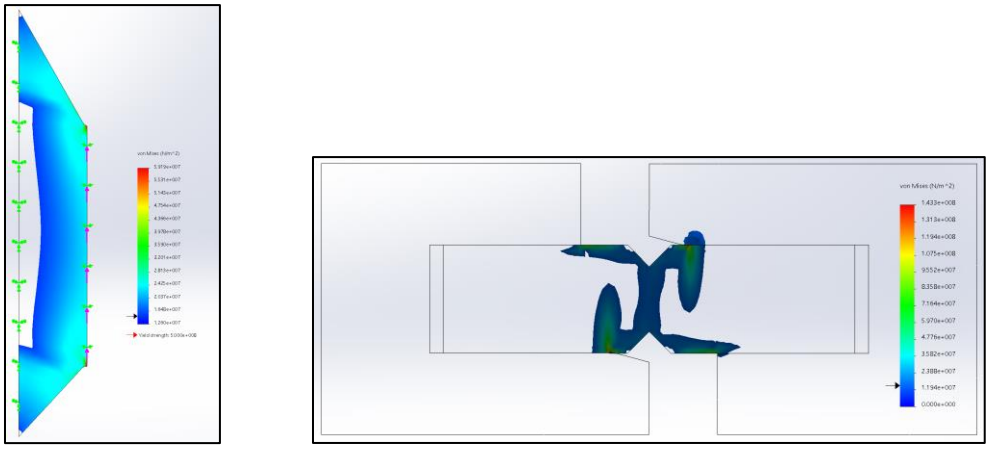

Figure 4.28 - FEA of V-Notch and Iosipescu areas above 150% nominal shear stress

Although stress concentrations could reduce the apparent shear strength of the material, shear modulus may still be accurate. FEA was carried out to see what areas of the specimen would produce accurate shear modulus results through DIC analysis. Using a 10 mm wide AoI which spanned the entire gauge length, produced a shear stress value

with 0.92% error when compared to the nominal shear stress value. It provided an appropriate measurement area with a balance between accuracy and practicality.

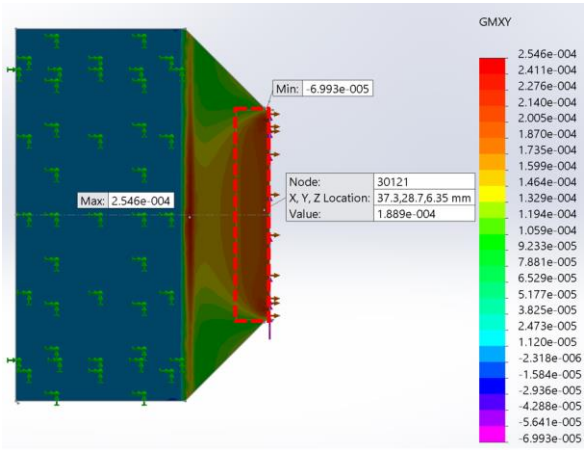

Figure 4.29 - 10mm wide area of interest box to compare with DIC Area of Interest

4.2.3 Microscopy and CT Scans

Fiber orientation after manufacturing was investigated as a potential source of error and variability in the test specimen. Microscopic analysis was initially done at Western University and used to identify and determine any error in fiber orientation of inner plies. For the simple case of a cylindrical fiber, the fiber orientation can be determined by the cross-sectional shape of the fiber when cut. The minor axis of the ellipse is two times the radius b = 2R. The major axis of the ellipse is the radius times the secant of the cut angle, a = R(sec θ). Therefore, the free surface of a fiber can show the ply angle of a lamina.

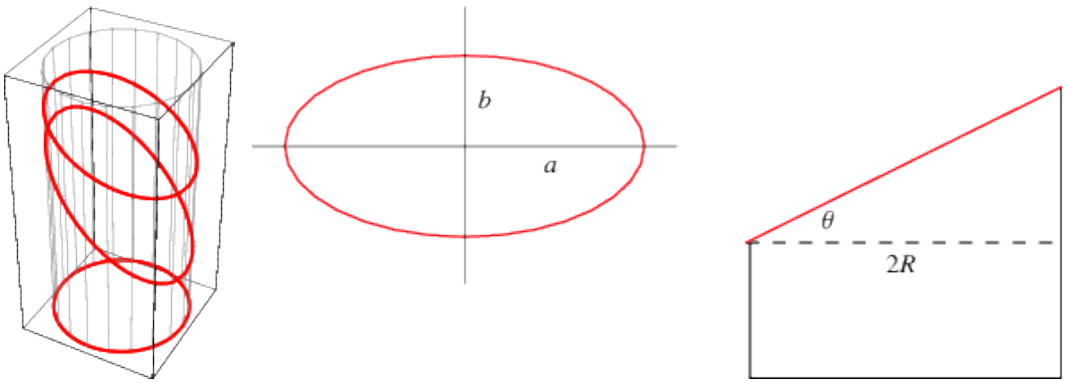

Figure 4.30 - Cylindrical Segment (Weisstein)

However, because of the irregular shape of the carbon fibres, it was impossible to determine the interlaminar ply angles using the cross-sectional geometry of the fibers with microscopy. CT Scans were used as an alternative method to determine ply angle. Scans were done by Robarts Imaging at Western University using a micro-CT system. CT Scans were performed on a V-Notched Shear specimen after it was brought to failure. The scans can distinguish between the fibers and surrounding matrix, based on differing amounts of x-ray absorption, allowing the fiber orientations in each ply to be seen. Layer by layer analysis showed that the variability between layers was very small, ±0.5-degrees. Angle measurement examples are shown in Figure 4.31.

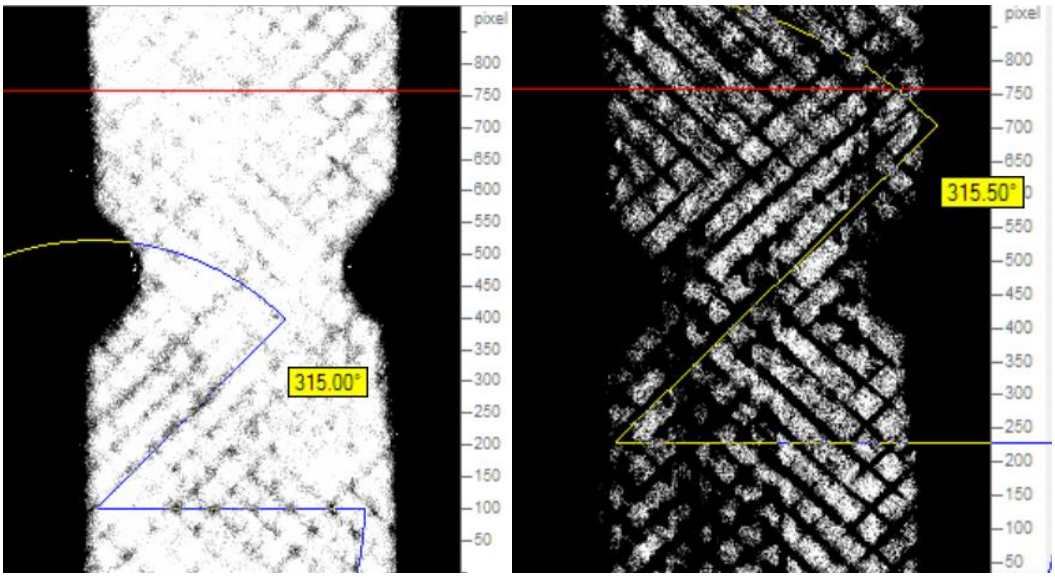

Figure 4.31 - MicroCT Image validates layup fiber angles within ±0.5º of error

Having already obtained CT Scan images, an attempt was made to look for voids or determine fiber volume fractions, but these values were beyond the ability of the software. The obtained 3D images are included in Figure 4.32 for reference. CT Scans of the specimen provided an accurate method of confirming relative ply orientation angles for fibers such as carbon fiber which have irregular shapes.

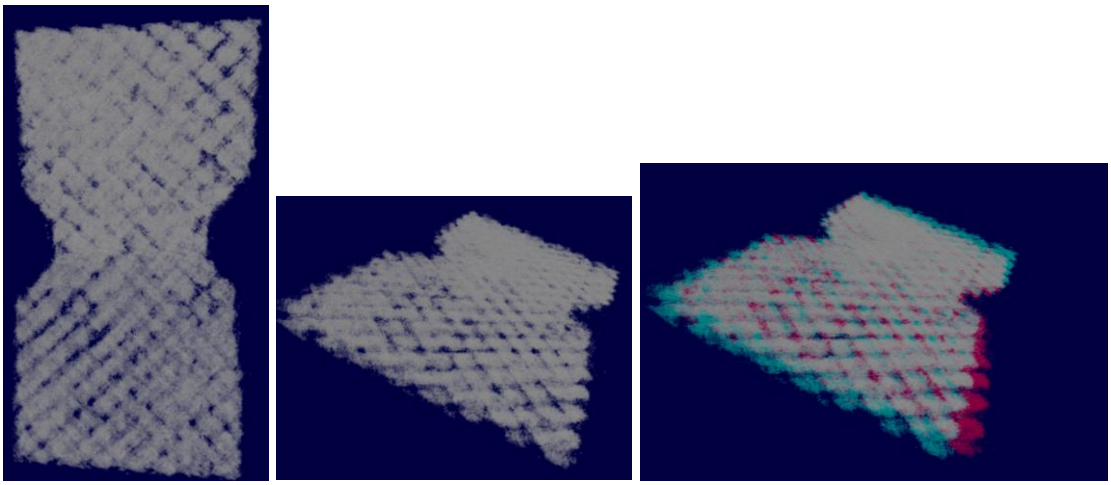

Figure 4.32 - 3D Images obtained from the MicroCT scans used to look for voids in the material

Chapter 5

5 Conclusions and Future Work

This study was carried out to evaluate methods for determining the mechanical properties of composite materials. The study included investigating a more suitable method for shear testing of high-strength composites rather than using the Iosipescu Shear test. Analytical and numerical methods showed that predicted experimental values under the conditions used throughout this thesis can be relied on for estimations. Elastic material properties are overall more reliable as the mechanisms are more well understood in comparison to material properties at failure. Beyond the materials used, including volume fraction, specific manufacturing methods, and test conditions, the analytical and numerical methods may not provide accurate estimations as any deviations may result in different mechanisms occurring throughout specimen loading.

Shear testing evaluation was accomplished by investigating the ASTM Standard 7078: V-Notched Rail Shear test method. Digital Image Correlation of the strain fields present during mechanical testing as well as Finite Element Models, were used to provide confidence in the obtained properties and learn more about failure mechanisms. Part of the investigation was to determine whether the V-Notched Shear test could break a high-strain-to-failure specimen. Problems arose because the end constraints in the Iosipescu and V-Notched tests differ. The V-Notched test required that the fibers fail for the specimen to fail, while in the Iosipescu test, failure of the specimen can occur while the fibers remain unbroken. The V-Notched Rail Shear test provided a much more linear response for the +/-45-degree layup than produced by the Iosipescu Shear test. Whereas the Iosipescu shear test produced much more consistent results for the 0/90-degree test.

The difference between the real loads seen by the specimen in both tests does not necessarily mean that one test is better than the other, as one test may more accurately reflect the application. If the material has free edges in the application, then the Iosipescu Standard may be more suitable as the structure in the application would fail from matrix

failure. If the structure is bounded at its edges, ultimate shear failure could only occur if the fibers failed, and therefore the V-Notched Shear test would be more suitable.

One of the major issues that was proposed with shear testing was the purity and uniformity in the specimen. Additional axial and transverse loading, stress concentrations, as well as other possible sources of error discussed in this report, contributed to an error in obtained material properties. Although error percentages between analytical and experimental methods were low for some results, it is possible that errors balance each other out, or that the analytical methods only work for these very specific experimental conditions. Caution and critical thinking should therefore be used if applying this research to future work.

The V-Notched Rail Shear test provided some benefits over the Iosipescu shear test, but still had some drawbacks. An even newer test fixture has been proposed by Wyoming Test Fixtures as an evolution to the V-Notched Rail Shear test. This new test is called Combined Loading Shear (CLS) and combines the advantages of the V-Notched Rail Shear test with a partial edge loading taken from the Iosipescu Shear test. Edge Loading helps to reduce slippage and reduce stresses caused by bolt torques. Another avenue for future work is to investigate test fixtures which provide a pure shear load case rather than simple shear. One such example is the Picture Frame Shear test DIN 4885 as mentioned in Section 2.6.1. This fixture retains the test specimen on all edges rather than just the two sides retained in the V-Notched Shear test, and keeps the specimen gauge area the same by using pivots about the material corners.

The purpose of this thesis was to improve upon composite material characterisation techniques. It is imperative to understand the underlying load cases that a structure will be subjected to. Only then can appropriate analysis methods be applied to aid in predicting the stress and strain levels in the material. An understanding of the application coupled with analysis tools such as Finite Element Analysis and Digital Image Correlation, can ultimately improve the efficiency of the material for the application. An efficient use of material opens many possibilities, whether in weight savings, cost savings, or performance.

References or Bibliography

Adams, D. (2017, March 31). *Best Practices for V-notched Shear Testing of Composites*. Retrieved from CompositesWorld: http://www.compositesworld.com/articles/best-practices-for-v-notched-shear-testing-of-composites

Adams, D. D. (2009, December 2). *A Comparison of Shear Test Methods*. Retrieved from Composites World: http://www.compositesworld.com/articles/a-comparison-of-shear-test-methods

Adams, D. D. (2009, December 2). *V-Notch Rail Shear test (ASTM D 7078-05).* Retrieved from CompositesWorld: http://www.compositesworld.com/articles/v-notch-rail-shear-test-astm-d-7078-05

Adams, D. O., Moriarty, J. M., Gallegos, A. M., & Adams, D. F. (2003). *Development and Evaluation of the V-Notched Rail Shear Test for Composite Laminates.* Washington: U.S. Department of Transportation, Federal Aviation Administration, Office of Aviation.

Chamis, C. C., & Sinclair, J. H. (1976, April). 10 Degree Off-Axis Tensile Test for Intralaminar Shear Characterization of Fiber Composites. *NASA Technical Note*.

DowAksa. (2016, February). 24K A-42 Technical Data Sheet. *AKSACA*. Istanbul, Turkey. Retrieved from http://www.dowaksa.com/wp-content/uploads/2016/03/24K-A-42.pdf

Engineering Archives. (2012). *Tensile Test*. Retrieved from Engineering Archives.

Epsilon Technology. (2017). *Products*. Retrieved from Epsilon Tech: https://www.epsilontech.com/

Gibson, L. J. (2012). *The Hierarchical structure and mechanics of plant materials.* Journal of the Royal Society Interface.

Gorss, J. (2003, September 17). High Performance Carbon FIbers. *National Historic Chemical Landmarks Program*, 4. Washington, DC, USA: American Chemical Society, Office of Communications. Retrieved from www.chemistry.org/landmarks

GRASSE ZUR INGENIEURGESELLSCHAFT. (2015, 10 02). *Improved Method for Testing Composite Materials*. Retrieved from Berlin Innovation: https://www.berlin-innovation.de/en/start/overview/innovation/innovation/260.html

Halverson, L., & Tuttle, M. (2000). Effect of Stacking Sequence on the Compressive Strength of Composite Laminates. *SNAME: The International Commnity for Maritime and Ocean Professionals*, 197-212.

Hansen. (2014). Retrieved from https://pages.shanti.virginia.edu/dharris/2014/09/24/devin-harris-presents-at-the-1st-international-digital-image-correlation-conference-workshop/

Hexion. (2017). EPIKOTE Resin MGS RIMR235. EPIKURE Curing Agent MGS RIMH233, RIMH235-237. *Technical Data Sheet*. Retrieved from http://www.hexion.com/Products/ShowTechnicalDataSheet.aspx?id=8257&Rev

Howard University. (2017, February 26). *General Chemistry: An Atoms First Approach. Chapter 12.9: modern Materials.* Retrieved from LibreTexts: Chemistry: https://chem.libretexts.org/LibreTexts/Howard_University/General_Chemistry%3A_An_Atoms_First_Approach/Unit_5%3A_States_of_Matter/Chapter_12%3A_Solids/Chapter_12.09%3A_Modern_Materials

Hull, D., & Clyne, T. W. (1996). *An Introduction to Composite Materials* (2nd Edition ed.). Cambridge: Press Syndicate of the University of Cambridge.

Jeong, C. (2010, 11 19). *Basic Stress Theory*. Retrieved from Tistory: http://charliestory.tistory.com/?page=43

Krishnavedala. (2012, January 12). *Shear Stress*. Retrieved from Wikipedia Commons: https://commons.wikimedia.org/wiki/File:Shear_stress_simple.svg

Kurowski, P. (2012). Finite Element Methods for Mechanical Engineering. 50. London, Ontario, Canada: Western University. Retrieved from http://slideplayer.com/slide/6403236/

Odegard, G., & Kumosa, M. (2000, June 15). Determination of shear strength of unidirectional composite materials with the Iosipescu and 10 degree off-axis shear tests. (D. o. Center for Advanced Materials and Structures, Ed.) *Composites Scient and Technology*, 27.

Reviews, C. (2016). *Materials Science and Engineering Properties: Chemistry, Materials science.* Cram101 Textbook Reviews.

Rickhey, F., Kim, M., Lee, H., & Kim, N. (2014). Evaluation of Combined Hardening Coefficients of Zircaloy-4 sheets by simple shear test. *Materials and Design*.

SAE International. (2008, June 19). *3-D Fibers Improve Thermal Conductivity of Composites*. Retrieved from SAE International: http://articles.sae.org/2331/

Sanpaz. (2016, December). *Plane Stress*. Retrieved from Wikipedia: https://en.wikipedia.org/wiki/Plane_stress

STAFF. (2015, January 1). *The Matrix*. Retrieved 2017, from Composites World: http://www.compositesworld.com/articles/the-matrix

Such, M., Ward, C., & Potter, K. (2014). Aligned Discontinuous Fibre Composites: A Short History. *Journal of Multifunctional Composites*, 155-168.

Tan, W., & Flazon, B. (2016, February). Modelling the Nonlinear Behaviour and Fracture Process of AS4/PEKK Thermoplastic Composite under Shear Loading. *Composites Science and Technology*, 19. Retrieved from https://www.researchgate.net/publication/294423187_Modelling_the_nonlinear_b

ehaviour_and_fracture_process_of_AS4PEKK_thermoplastic_composite_under_shear_loading

Toray Group. (n.d.). Technical Data Sheet. ZOLTEK PX35 Multi-Directional Fabrics. Bridgeton, Montana, USA. Retrieved from http://zoltek.com/wp-content/uploads/2015/09/PX35-MD-Fabrics.pdf

University of Cambridge. (2008, January). *Mechanics of Fibbre-Reinforced Composites*. Retrieved from Dissemination of IT for the Promotion of Materials Science (DoITPoMS): https://www.doitpoms.ac.uk/tlplib/fibre_composites/index.php

University of Cambridge. (2017). *Notes on Tensile Testing*. Retrieved from Dissemination of IT for the Promotion of Materials Science: https://www.doitpoms.ac.uk/

Veryst. (2017). *Digital Image Correlation (DIC)*. (Veryst Engineering LLC) Retrieved from Veryst Engineering: Engineering Through the Fundamentals: http://www.veryst.com/what-we-offer/mechanical-testing-modeling-validation/Testing-Library/digital-image-correlation

Weisstein, E. W. (n.d.). *Cylindrical Segment*. Retrieved from WolframMathWorld: http://mathworld.wolfram.com/CylindricalSegment.html

Appendices

Appendix A: - Product Datasheets

The following data sheets have been obtained from the manufacturer's websites for the materials tested. In order:

1. Carbon Fiber: DOWAKSA 24K A-42
2. Carbon Fiber: Toray Group, ZOLTEK PX35 Multi-Directional Fabrics
3. Resin: Hexion Epikote MGS RIMR 235 and curing agent (hardener): RIMH235

(DowAksa, 2016)

AKSACA

DOWAKSA

Revision Nr: 1
Revision Date: Feb/2016

24K A-42
TECHNICAL DATA SHEET

FIBER PROPERTIES

	English		Metric		Test Method
Tensile Strength	610	ksi	4200	MPa	ISO 10618
Tensile Modulus	34,8	Msi	240	GPa	ISO 10618
Strain	1,8	%	1,8	%	ISO 10618
Density	0,064	lbs/in³	1,78	g/cm³	ISO 10119
Yield	0,931	ft/lbs	1600	g/1000m	ISO 1889
Sizing Type & Amount	D012		1,0-1,5	%	ISO 10548
Twist	Never twisted				

PACKAGING

The table below summarizes the standard packaging; other bobbin sizes can be supplied to satisfy special needs.

Tow Sizes	Bobbin Net Weight (kg)	Bobbin Size (mm)					Spools per Case	Case Net Weight (kg)
		a	b	c	d	e		
24K	4	76	83	280	170	250	6	24

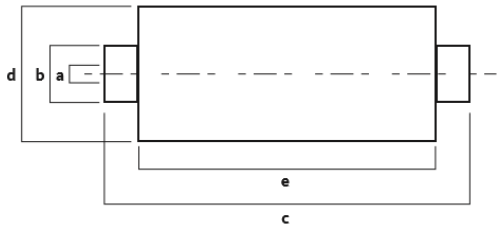

DowAksa İleri Kompozit Malzemeler Sanayi LTD. ŞTİ.

Miralay Şefik Bey Sok. Akhan No: 15 34437 Gümüşsuyu - İstanbul / TÜRKİYE
T: +90(212) 251 45 00 • **F:** +90(212) 249 35 99

www.dowaksa.com • cfsales@dowaksa.com

(Toray Group)

Technical Datasheet

ZOLTEK™ PX35 Multi-Directional Fabrics

ZOLTEK Toray Group

Stitch-Bonded Multi-Axial Carbon Fabrics

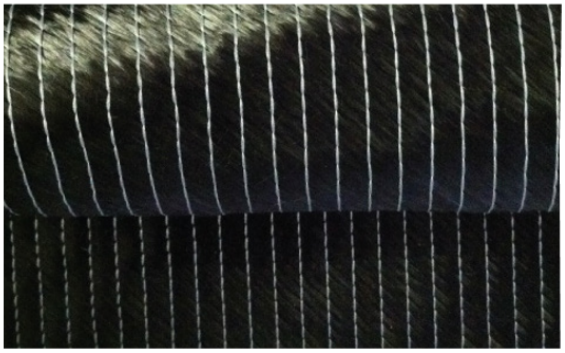

DESCRIPTION

ZOLTEK's Multi-Axial Fabric is produced from our ZOLTEK PX35 continuous carbon fiber tow. Unique fiber spreading techniques are utilized to obtain a wide range of MD fabric weights for a varied set of composite part applications. Quick composite part build-up is cost effectively achieved with our diverse weight range of low-cost carbon fabric products. Drapable fabric construction, ideal for complex shape preforms. Pillar and Tricot stitching patterns available.

APPLICATIONS

- Automotive
- Marine
- Aircraft
- Infrastructure

RECOMMENDED USE

- Body Panels (Interior / Exterior)
- Components / Undercarriage
- Reinforcement

+/- 45° FABRIC ARCHITECTURE

Material	Fiber Orientation	Nominal Weights g/m² (oz)			
		MD 300	**MD 400**	**MD 500**	**MD 600**
ZOLTEK PX35 50K	+45°	150 (4.42)	200 (5.90)	250 (7.37)	300 (8.85)
ZOLTEK PX35 50K	-45°	150 (4.42)	200 (5.90)	250 (7.37)	300 (8.85)
Polyester Stitch	—	4 (.12)	5 (.15)	7 (.21)	8 (.24)
Total	**—**	**304 (9.00)**	**405 (11.94)**	**507 (14.95)**	**608 (17.93)**

0/90° FABRIC ARCHITECTURE

Material	Fiber Orientation	Nominal Weights g/m² (oz)			
		MD 300	**MD 400**	**MD 500**	**MD 600**
ZOLTEK PX35 50K	0°	150 (4.42)	200 (5.90)	250 (7.37)	300 (8.85)
ZOLTEK PX35 50K	90°	150 (4.42)	200 (5.90)	250 (7.37)	300 (8.85)
Polyester Stitch	—	4 (.12)	5 (.15)	7 (.21)	8 (.24)
Total	**—**	**304 (9.00)**	**405 (11.94)**	**507 (14.95)**	**608 (17.93)**

ZOLTEK Corporation | 3101 McKelvey Road | Bridgeton, MO 63044
P: 314-291-5110 | F: 314-291-8536 | www.zoltek.com

Technical Datasheet

ZOLTEK™ PX35 Multi-Directional Fabrics

Stitch-Bonded Multi-Axial Carbon Fabrics

MATERIAL FIBER PROPERTIES	SI	US
Tensile Strength	4,137 MPa	600 ksi
Tensile Modulus	242 GPa	35 msi
Electrical Conductivity	0.00155 ohm-cm	0.00061 ohm-in
Density	1.81 g/cc	0.065 lb/in^3
Fiber Diameter	7.2 microns	0.283
Carbon Content	95%	

The properties listed in this datasheet do not constitute any warranty or guarantee of values. This information should only be used for the purposes of material selection. Please contact us for more details.

TYPICAL MULTI-AXIAL LAYUP

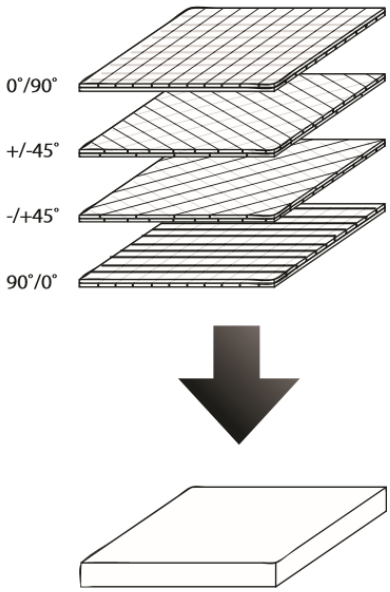

TYPICAL PACKAGING

Wound on cardboard core, sealed in polyethylene bag, and placed in cardboard box. Rolls stacked horizontally on pallets when shipping.

Standard Width: 1,270 mm +/- 20

Standard Roll Length: 50 m

+ Custom widths and roll lengths may be available upon request.

CERTIFICATION

ZOLTEK PX35 Fabrics are manufactured in accordance with ZOLTEK's written and published data. A Certificate of Conformance is provided with each shipment.

SAFETY

Obtain, read, and understand the Material Safety Data Sheet (SDS) before use of this or any other ZOLTEK product.

ZOLTEK Corporation | 3101 McKelvey Road | Bridgeton, MO 63044
P: 314-291-5110 | F: 314-291-8536 | www.zoltek.com

(Hexion, 2017)

HEXION
Technical Data Sheet

EPIKOTE™ Resin MGS™ RIMR235
EPIKURE™ Curing Agent MGS™ RIMH233, RIMH235 - 237

CHARACTERISTICS

Approval	DNV-GL Germanischer Lloyd (RIMH235 – RIMH237)
Application	Rotor blades for wind turbines, boat and shipbuilding, sports equipment, model construction, tooling and moulding
Operational temperature	-60 °C up to +50 °C without heat treatment -60 °C up to +80 °C after heat treatment
Processing	at temperatures between 15 °C and 50 °C
Features	very low viscosity pot life from approx. 10 minutes to approx. 4,5h
Storage	shelf life of 24 months in originally sealed containers

APPLICATION

RIMR235 is a low-viscous infusion resin system with different pot lives for processing of glass, carbon and aramide fibers. Due to its excellent mechanical properties, this system is suitable for the production of components featuring high static and dynamic loadability.
The range of pot lives is between approx. 10min and more than 4h depending on the choice of curing agent.
RIMR235 features an extraordinary low mixed visosity, resulting in fast and complete fibre wetting at a high transportation rate in infusion processes. The infusion resin system does not contain any unreactive components. The raw materials used feature a very low vapour pressure which permits processing of the material under vacuum even at elevated temperatures.

Optimum processing temperatures are in the range of 15 - 40°C. As the initial cure at room temperature is very slow as for the low reactive hardeners, some heat treatment should be performed at minimum 40 - 50 °C before demoulding.
Curing at higher temperatures (up to approx. 80 - 100°C) is possible, depending on layer thickness, geometry of the parts and choice of curing agent.
Full mechanical properties will only be obtained after a suitable post cure cycle. Especially for operations at elevated temperatures such a post cure cycle is required to obtain the required thermal stability. For optimum mechanical properties a heat treatment of minimum 50°C is required.

The infusion resin system RIMR235 remains practically free of crystallisation, even if it is stored at low temperatures (<15 °C). In an early stage, crystallisation is visible as a clouding, and can progress to a stage, where the resin becomes a wax- like solid. Crystallisation can be reversed by slow heating of the product to approx. 40 - 60 °C while stirring. This physical phenomenon is reversible and is no restriction to quality after removal, in fact a high purity of material will increase a tendency for crystallisation.

After dispensing material, the containers must again be closed carefully, to avoid contamination or absorption of water. All amine curing agents show a chemical reaction when exposed to air, known as „blushing“. This reaction is visible as white carbamide crystals, which could make the materials unusable.

Curing agents can be coloured to distinguish between resin and curing agents, and for easier identification of a correct mixing process. Although unlikely, deviations in colour are possible (e.g. due to UV radiation after longer exposure to sun light), but however have no effect on the processing and final properties of the material

The materials have a shelf life of minimum 2 years, when stored in their originally sealed containers.

EPIKOTE Resin MGS RIMR 235 and EPIKURE Curing Agent RIMH 235-237

The relevant industrial safety regulations for the handling of epoxy resins and hardeners for safe processing are to be observed.

SPECIFICATIONS

		Infusion resin RIMR235
Density [1)]	[g/cm³]	1,14 – 1,18
Viscosity [1)]	[mPa·s]	1.000 – 1.300
Refractory index [1)]	[-]	1,550 – 1,560

		Curing agents without GL-Approval
		RIMH233
Density [1)]	[g/cm³]	0,96 – 1,00
Viscosity [1)]	[mPa·s]	50 – 100
Refractory index [1)]	[-]	1,505 – 1,515
Potlife [2)]	[min]	Approx. 10 min
$Tg_{mid,pot}$	[°C]	90 – 95°C unconditioned

		Curing agents with GL-Approval		
		RIMH235	RIMH236	RIMH237
Density [1)]	[g/cm³]	0,92 – 0,96	0,93 – 0,96	0,92 – 0,96
Viscosity [1)]	[mPa·s]	10 – 30	10 – 30	10 – 30
Refractory index [1)]	[-]	1,465 – 1,469	1,460 – 1,469	1,457 – 1,460
Potlife [2)]	[min]	Approx. 80 min.	Approx. 3h	Approx. 4,5h
$Tg_{mid,pot}$	[°C]	90 – 95°C unconditioned		

Measuring conditions:

1) measured at 25°C

2) measured at 30°C

MIXING RATIOS

	RIMR235 : All curing agents
Parts by weight	100 : 34 ± 2
Parts by volume	100 : 41 ± 2

The mixing ratio stated must be observed very carefully. Adding more or less curing agent will not influence reaction speed – but in incomplete curing which cannot be corrected in any way. Resin and curing agent must be mixed very thoroughly, mix until no clouding is visible in the mixing container.

TEMPERATURE DEVELOPMENT

EPIKOTE Resin MGS RIMR 235 and EPIKURE Curing Agent RIMH 235-237

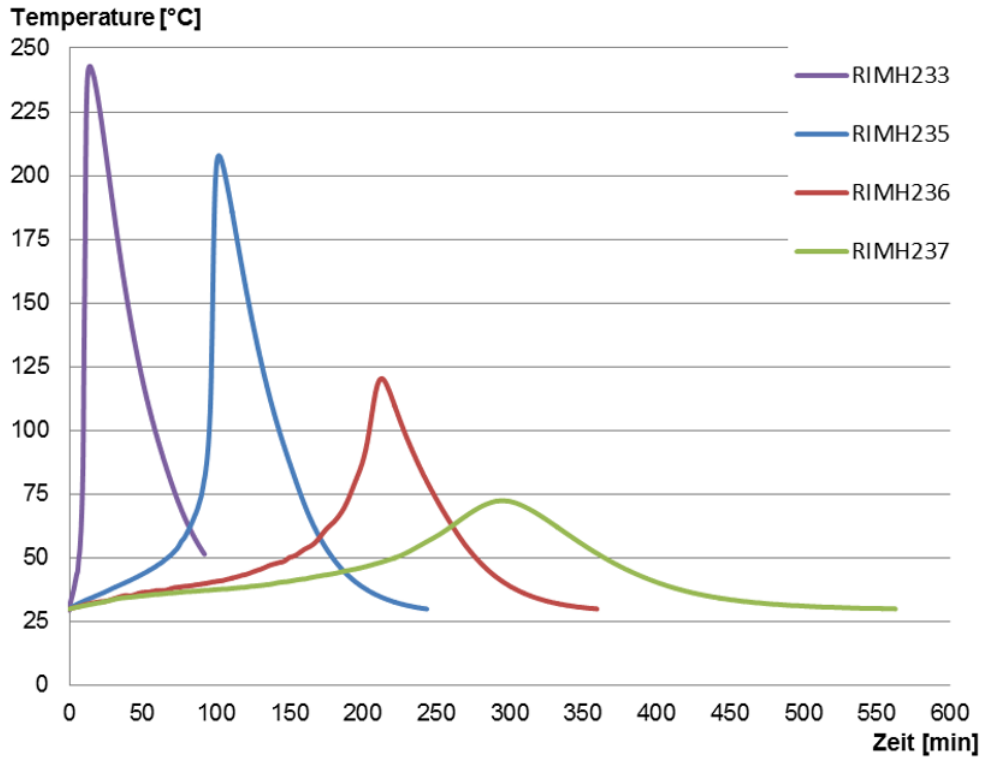

Measuring conditions: 100g mixture in a water bath at 30°C

Optimum processing temperature is in the range of 20 to 35 °C. Higher temperatures are possible, but will shorten pot life. A temperature increase of 10 °C will halve the pot life. Water (e.g. high humidity or contained in additional fillers) causes an acceleration of the resin/curing agent reaction. Different temperatures during processing are not known to have significant impact on the mechanical properties of the cured product.

Do not mix large quantities – particularly of highly reactive systems – at elevated processing temperatures. As the heat dissipation in the mixing container is very slow, the contents will be heated up by the reaction heat rapidly. This can result in temperatures of more than 200 °C in the mixing container, which may cause smoke-intensive burning of the resin mass.

VISCOSITY OF MIXTURE

EPIKOTE Resin MGS RIMR 235 and EPIKURE Curing Agent RIMH 235-237

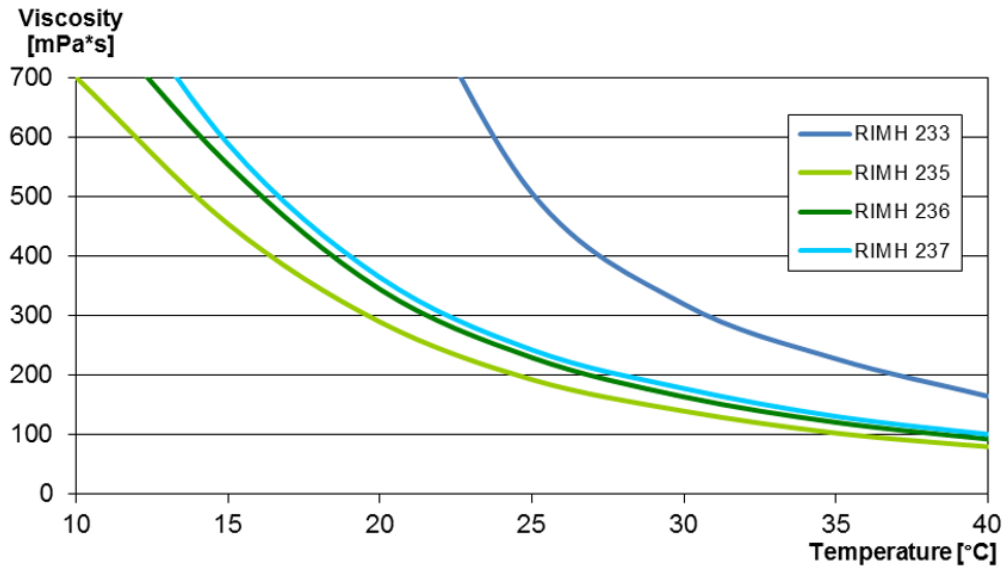

Measuring conditions: Rotation viscosimeter, plate-plate configuration, measuring gap 0.2 mm

VISCOSITY DEVELOPMENT

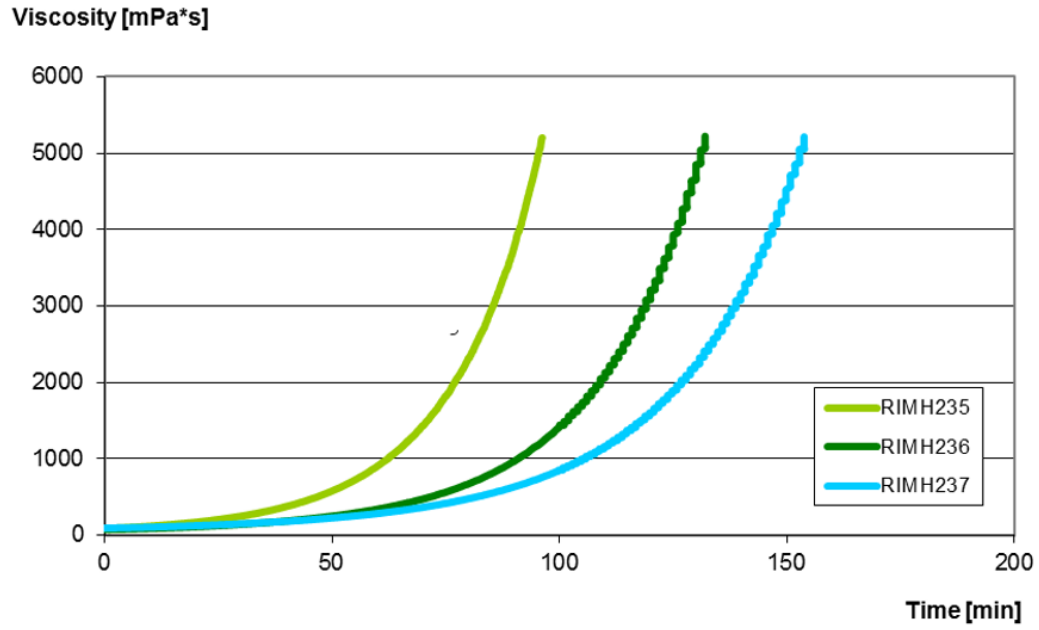

Measuring conditions: Rotation viscosimeter, plate-plate configuration, measuring gap 0.2 mm, Temperature 40°C

T_G DEVELOPMENT

EPIKOTE Resin MGS RIMR 235 and EPIKURE Curing Agent RIMH 235-237

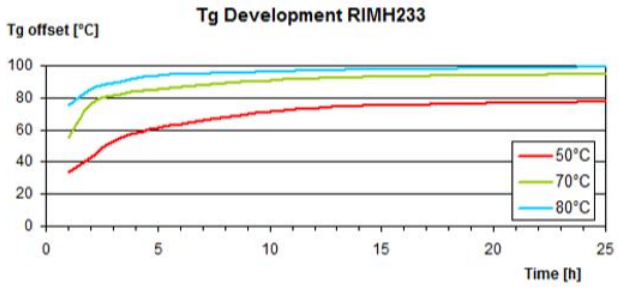

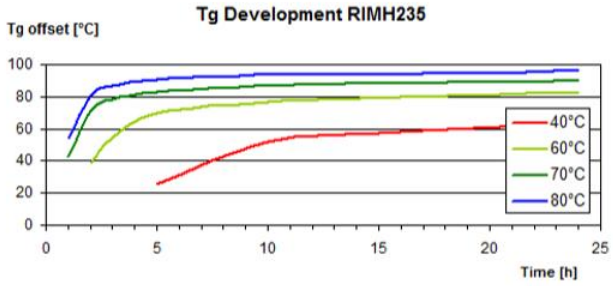

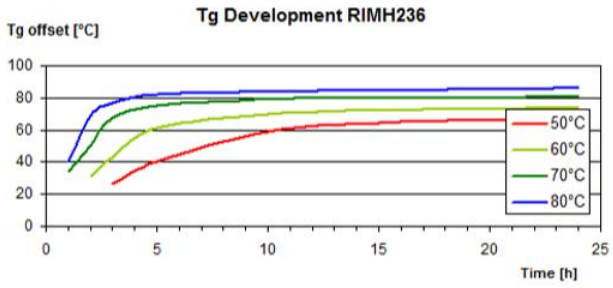

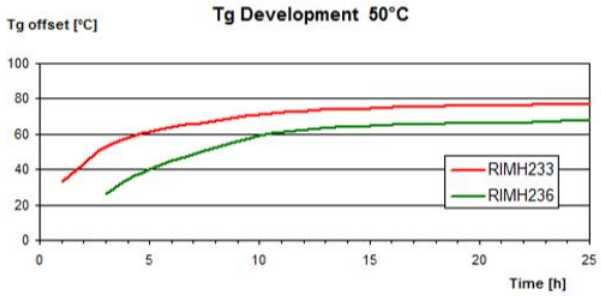

EPIKOTE Resin MGS RIMR 235 and EPIKURE Curing Agent RIMH 235-237

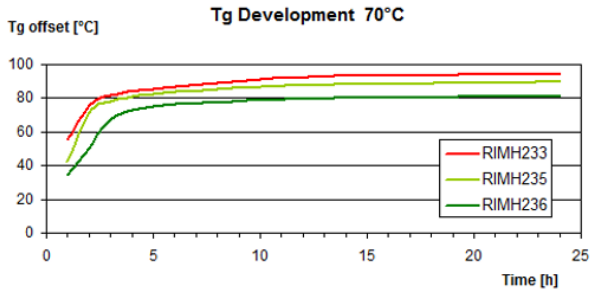

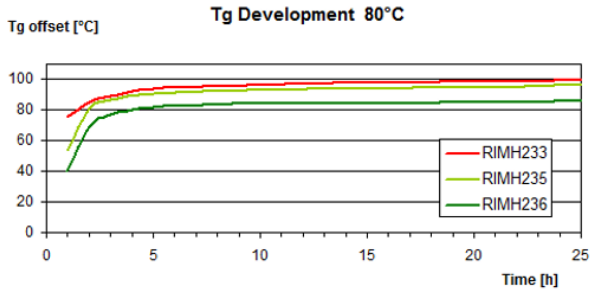

MECHANICAL DATA OF NEAT RESIN

Mechanical data, typical for curing of 10hrs at 70°C		
Density DIN EN ISO 1183-1	[g/cm³]	1,12 – 1,18
Flexural strength DIN EN ISO 178	[MPa]	95 – 115
Tensile modulus DIN EN ISO 527-2	[GPa]	3,0 – 3,2
Tensile strength DIN EN ISO 527-2	[MPa]	65 – 70
Elongation at break DIN EN ISO 527-2	[%]	6 – 8
Water absorption at 23°C DIN EN ISO 175	24h [%] 7d [%]	0,10 – 0,30 0,40 – 0,60

Advice:
Mechanical data are typical for the combination of infusion resin RIMR235 with curing agent RIMH237. Data can differ in other applications.

Appendix B – Full Material Property Cards

Fabric QI

Properties from experiment	Theoretical	Actual	Error	Standard Deviation	Coefficient of Variation
Young's modulus (11) (0º) (Gpa)	40.39	37.96	-6%	2.40	6.32
Young's modulus (22) (90°) (Gpa)	40.39	39.77	-2%	1.91	5.03
Young's modulus (22.5°) (Gpa)	40.39	29.68	-27%	1.41	3.54
Young's modulus (45°) (Gpa)	40.39	26.97	-33%	1.15	4.28
Poisson's ratio (0°)	0.317	0.255	-20%	0.008	3.259
Poisson's ratio (22.5°)	0.317	0.303	-4%	0.020	6.439
Poisson's ratio (45°)	0.317	0.470		0.025	5.238
Poisson's ratio (90°)	0.317	0.340	7%	0.016	4.845
Failure Strain (0°) (%)	1.12%	1.36%	22%	0.05	3.45
Failure Strain (45°) (%)	1.12%	1.18%	6%	0.11	9.48
Failure Strain (90°) (%)	1.12%	1.39%	24%	0.14	9.88
Longitudinal tensile strength (11) (Mpa)	451.50	505.68	12%	13.57	2.68
Transverse tensile strength (22) (Mpa)	451.50	518.10	15%	25.24	4.87
UTS 22.5	451.50	241.98		18.98	7.84
UTS 45	451.50	292.13		14.67	5.02
Longitudinal compressive strength (1) (Mpa)		201.96		39.16	19.39
UCS 22.5		292.48		23.97	8.20
UCS 45		187.20		20.83	11.13
Transverse compressive strength (2) (Mpa)		183.80		19.82	10.78
Shear modulus (12) (Gpa)	14.53	19.80	36%	0.42	2.14
Shear modulus (21) (Gpa)	14.53	19.09	31%	0.01	0.04
Shear modulus (45°) (Gpa)	14.53	18.08	24%	0.97	5.36
Shear Strength (12 plane) (Mpa)	97.50	97.91	0%	22.22	22.69
Strength 45	97.50	89.83	-8%	1.01	1.13
Shear Strength (21 plane) (Mpa)	97.50	112.13	15%	2.06	1.84
Flexure strength (0°) (Mpa)		313.07		14.20	4.54
Flexure strength (22.5°) (Mpa)		333.98		25.45	7.62
Flexure strength (45°) (Mpa)		480.00		4.91	1.02
Flexure strength (90°) (Mpa)		667.11		18.51	2.77
Flexure modulus (0°) (Gpa)		16.31		0.23	13.92
Flexure modulus (22.5°) (Gpa)		23.43		1.01	3.62
Flexure modulus (45°) (Gpa)		33.89		0.08	2.13
Flexure modulus (90°) (Gpa)		41.15		0.05	5.95

Fabric OR

Properties from experiment	Theoretical	Actual	Error	Standard Deviation	Coefficient of Variation
Young's modulus (11) (0º) (Gpa)	44.71	43.20	-3%	0.76	1.75
Young's modulus (22) (90°) (Gpa)	64.48	60.14	-7%	6.95	16.08
Young's modulus (22.5°) (Gpa)	15.59	16.43	5%	0.42	0.69
Young's modulus (45°) (Gpa)	8.84	10.72	21%	0.15	1.39
Poisson's ratio (0°)	0.120	0.115	-4%	0.008	6.957
Poisson's ratio (22.5°)		0.310		0.013	4.056
Poisson's ratio (45°)	0.835	0.761	-9%	0.012	1.616
Poisson's ratio (90°)	0.021	0.024	14%	0.001	2.357
Failure Strain (0°) (%)	0.81%	0.90%	11%	0.05	5.46
Failure Strain (45°) (%)	3.01%	3.90%	30%	0.82	20.99
Failure Strain (90°) (%)	0.84%	1.22%	45%	0.13	10.41
Longitudinal tensile strength (11) (Mpa)	361.20	366.98	2%	19.66	5.36
Transverse tensile strength (22) (Mpa)	541.80	582.73	8%	16.76	2.88
UTS 22.5	105.53	129.10	22%	7.16	5.54
UTS 45	97.50	90.25	-7%	3.86	4.28
Longitudinal compressive strength (1) (Mpa)		212.48		13.41	6.31
UCS 22.5		251.52		34.99	13.91
UCS 45		158.88		5.39	3.39
Transverse compressive strength (2) (Mpa)		119.23		6.46	5.42
Shear modulus (12) (Gpa)	4.81	5.52	15%	0.54	9.74
Shear modulus (21) (Gpa)	4.81	5.87	22%	1.39	23.61
Shear modulus (45°) (Gpa)	51.55	40.97	-21%	1.29	3.14
Shear Strength (12 plane) (Mpa)	97.50	82.50	-15%	0.88	1.06
Strength 45	97.50	88.61	-9%	1.94	2.19
Shear Strength (21 plane) (Mpa)	97.50	109.90	13%	1.44	1.31
Flexure strength (0°) (Mpa)		514.05		15.92	3.10
Flexure strength (22.5°) (Mpa)		417.60		6.56	1.57
Flexure strength (45°) (Mpa)		285.90		35.91	12.56
Flexure strength (90°) (Mpa)		573.43		34.02	5.93
Flexure modulus (0°) (Gpa)		57.31		2.27	3.96
Flexure modulus (22.5°) (Gpa)		39.77		0.85	2.13
Flexure modulus (45°) (Gpa)		19.61		0.72	3.68
Flexure modulus (90°) (Gpa)		45.39		2.45	5.39

Curriculum Vitae

Name:	Matthew Crossan
Post-secondary Education and Degrees:	Western University Western, Ontario, Canada 2011-2015 B.Eng.
Honours and Awards:	Dean's Honour List 2012-2013
Related Work Experience	Teaching Assistant The University of Western Ontario 2015-2017